Diss. ETH No. 7632

MAGNETO-OPTICAL KERR-EFFECT OF URANIUM-COMPOUNDS:
A STUDY OF THE ELECTRONIC AND MAGNETIC STRUCTURE

A dissertation submitted to the
SWISS FEDERAL INSTITUTE OF TECHNOLOGY ZUERICH

for the degree of
Doctor of Natural Sciences

presented by

WOLFGANG REIM
Dipl. Phys. ETH
born Nov. 12th, 1956
citizen of West-Germany

accepted on the recommendation of
Prof. Dr. P. Wachter, examiner
PD Dr. J. Schoenes, co-examiner

1984

ABSTRACT

KURZFASSUNG

ABSTRACT

A comprehensive study of the magneto-optical properties of metallic ura-
nium compounds is presented in the 0.5 - 6 eV photon energy range. New
results about the electronic and the magnetic structure of these mate-
rials are derived.

The f states are best described in an itinerant model with an occupation
of nearly 3 for all investigated materials except the Th_3P_4-structure
compounds, although correlation effects are shown to play a dominant role
in UTe. A spin-polarized band structure of f and d states in the system
UTe-USb-YSb is derived and the competition of f-d and f-p hybridization
in this system is discussed. The maintenance of a f^3-f^2 valence transi-
tion in the USb-YSb pseudo-binary system is challenged.

The magnetic f-d exchange energy is established to be negative for all
investigated materials i.e. the f and d moments allign antiparallel upon
magnetic ordering. This property manifests itself in two magneto-optical
effects: First, the conduction electron spin-polarization displays a ne-
gative sign and its size is observed to range up to -100% for certain
compounds, which is an extraordinary value for magnetic metals. Second,
the f→d transition energy displays a magnetic red-shift in the order of
200meV due to the formation of spin-polarized subbands of the d states
which are energetically split by the exchange energy. The size of the
magnetic shift is found to depend on the sublattice magnetization rather
than on the net moment which results in similar magnitudes for some fer-
ro- and antiferromagnets. This behavior completely differs from the one
known up to now for antiferromagnetic semiconductors, but is well under-
stood in terms of the magnetic structure of the uranium pnictides.

For most of the materials, the value of the f polarization is calculated.
The f moment itself is evidenced to consist of antiparallel spin and or-
bital contributions with a predominant orbital part in most of the inves-
tigated NaCl-structure compounds.

Some of the investigated uranium systems seem to be very promising candi-
dates for technical applications due to the by far largest Kerr-rotaton
ever observed for metals, reaching up to $\approx 9.2^o$ at 65% reflectivity.

KURZFASSUNG

In dieser Arbeit wird über eine umfassende Untersuchung der magneto-opti-
schen Eigenschaften metallischer Uran-Verbindungen im Energiebereich zwi-
schen 0.5 und 6 eV berichtet. Neue Erkenntnisse sowohl über die elektro-
nische als auch die magnetische Struktur dieser Substanzen, die sich aus
der Analyse der magneto-optischen Daten ergeben, werden diskutiert.
Wir finden, dass die 5f-Elektronen in allen untersuchten Materialien aus-
ser denen mit Th_3P_4-Struktur am geeignetsten in einem Bandmodell be-
schrieben werden. Für UTe hat sich allerdings gezeigt, dass Korrelations-
effekte eine wichtige Rolle spielen. Für das Mischsystem UTe–USb–YSb war
es möglich, ein spin-polarisiertes Bandstrukturmodell aufzustellen und es
konnte zudem das Wechselspiel von f-d und f-p Hybridisierung studiert
werden. Das Auftreten einer f^3-f^2 Valenzänderung im Teilsystem USb–YSb
wird allerdings in Frage gestellt.
Wir zeigen in dieser Arbeit, dass die f-d Austauschenergie für alle un-
tersuchten Materialien ein negatives Vorzeichen aufweist, d.h. die Momen-
te der f- und d-Elektronen koppeln antiparallel. Diese Tatsache manifes-
tiert sich in zwei verschiedenen Ergebnissen der Magneto-Optik: Zum einen
finden wir eine negative Spin-Polarisation der Leitungselektronen in al-
len Substanzen, die bei einigen sogar eine Grössenordnung von bis zu
–100% erreicht. Zum anderen äussert sich die antiparallele f-d Kopplung
in einer magnetischen Rotverschiebung der f→d Uebergangsenergie von
200meV, verursacht durch die Austausch-induzierte Aufspaltung des d-Ban-
des in spin-polarisierte Teilbänder. Ueberraschenderweise finden wir Ver-
schiebungen ähnlicher Grösse in gewissen Antiferro- und Ferromagneten und
eine Proportionalität zur Untergittermagnetisierung. Dies ist zwar ein
völlig anderes Verhalten als bisher von magnetischen Halbleitern her be-
kannt ist, kann aber im Rahmen der magnetischen Struktur der Uran-Pnik-
tide gut verstanden werden.
Für die meisten Materialien geben wir eine Abschätzung der Polarisation
der f-Elektronen an. Zudem wird gezeigt, dass für bestimmte Verbindungen
das totale f-Moment vorwiegend durch den Bahndrehimpuls gegeben ist und
das f-Spinmoment antiparallel dazu steht, obwohl die f-Elektronen itine-
ranten Charakter zeigen.
Einige der untersuchten Materialien bieten vielversprechende Vorausset-
zungen für technische Anwendungen, ist doch die maximale beobachtete
Kerr-Drehung von ≈9.2° bei 65% Reflexion um mindestens eine Grössenord-
nung grösser als in allen bekannten nicht-5f Metallen.

1. INTRODUCTION

It is well known, that with a few exceptions only in compounds of 3d, 4f and 5f elements magnetic long range order appears. In most of the 4f systems, the f electrons are localized and form a Hund's rule ground state. The magnetic properties of these materials are in fact well understood in terms of the Heisenberg exchange model. On the other hand, the 3d electrons in most of the metallic transition metal compounds form relatively wide bands with a totally quenched orbital momentum. A qualitative idea about the origin of magnetism in these materials may be obtained in the Stoner picture of exchange-split spin-polarized subbands. However, this description is certainly far from reality because it predicts e.g. for the magnetic susceptibility a wrong temperature dependence. Recent experiments, however, indicate Stoner-like behavior at certain points in the Brillouin-zone but a temperature independent exchange splitting at other symmetry points [1]. A more quantitative description of band magnetism than the Stoner model has been attempted by some sort of 'unified' theory which combines aspects of both the itinerant and localized models [2-5], but a complete theory is still lacking.

In view of this dilemma in theory it appears promising to study magnetic 5f compounds, which are expected to bridge the gap between itinerant and localized behavior of magnetic electrons. In particular, the 5f systems may provide the opportunity of a gradual localization with increasing separation of the magnetic ions.

Yet, an intensive experimental and theoretical study in the last decade [6] has revealed that 5f magnetism is more complex than expected, because Coulomb, spin-orbit, crystalline field and exchange energies are in the same order of magnitude. In addition, for certain compounds strong f-d and f-p hybridization result in a f bandwidth, which is nearly independent of the lattice constant and this hybridization is often the reason for the metallic behavior of these compounds. The intermediate magnetic behavior of certain 5f materials is elucidated by a recent theoretical work [7] which predicts a substantial orbital contribution to the uranium moment for the itinerant antiferromagnet UN. Hence, electronic structure and magnetism are strongly related in these materials and a knowledge of the spin-polarized band structure is desirable.

The bearing of magneto-optics for the study of spin-polarized electrons comes of the proportionality of the polar magneto-optical effects (Fara-

day- and polar Kerr-effect) to the spin-polarization of the involved
electronic states. By a combination of optics and magneto-optics these
states may therefore be identified and analyzed in respect to their spin-
polarization, symmetry character and energy. It is noteworthy to mention
in this context, that compared to spin-polarized photoemission experi-
ments, the polar Kerr-effect is known to be much less sensitive to sur-
face effects.

Unfortunately, this experimental potential to study itinerant magnetism
could not be applied much to the 3d metals because no dipole allowed op-
tical transitions occur at energies up to 5 eV. In the case of metallic
5f compounds, on the other hand, dipole allowed excitations of f and d
electrons are expected at low energies allowing the study of spin-pola-
rized d and f bands a few eV around E_F. For the same reasons, a direct
determination of magnetic exchange energies may be possible similar to
the situation in the Eu-chalcogenides [8,9].

The magneto-optical properties of 5f compounds have not been investigated
up to now with the exception of UO_2, which is the only cubic 5f magnetic
semiconductor based on uranium. It has been shown, that the magneto-opti-
cal response of the localized $5f^2$ ground state of UO_2 displays large si-
milarities to the Eu-chalcogenides and that it is governed by a final
state splitting of the $f^2 \rightarrow f^1 d^1$ transition [10]. The magneto-optical sig-
nal can be understood perfectly in terms of atomic theory, treating the
$f^1 d^1$ final state as a whole. In this work, the complex magneto-optical
polar Kerr-effect of various metallic uranium compounds is presented and
discussed.

In section 4, the electronic structure of uranium chalcogenides and pnic-
tides will be compared and trends along these series are discussed. For
these materials, a direct examination of the magnetic f-d exchange is
possible. In section 5, the effect of dilution of the magnetic ion is
studied in $U_x Y_{1-x} Sb$ with special emphazis on the claimed $f^3 - f^2$ va-
lence transition [11] in this system. In sections 6 and 7, the f,d ground
state of uranium in different crystallographic structures is examined. In
section 8 finally, some aspects of the technical application of magneto-
optics are discussed in the light of the extraordinary magneto-optical
response of the present materials.

During the course of this work, also some intermetallics like UPd_3, UPt_3
and UIr have been investigated. However, the magneto-optical response
even of ferromagnetic UIr was found to be less than 0.05°. Up to now,
these compounds have not been studied further.

2. EXPERIMENTAL DETAILS

2.1 Samples

All experiments to be discussed in this work have been performed on sin-
gle crystals. In general, the crystals have been cleaved in air followed
by a quick transfer into the cryostat. Some USb_xTe_{1-x} and
$U_xY_{1-x}Sb$ crystals have either been cleaved in the argon chamber and
were transfered subsequently without contact to air into the cryostat or
they have been cleaved in the cryostat in helium atmosphere a few minutes
before measurement. We found no differences in the magneto-optical spec-
tra obtained from surfaces prepared by these three methods apart from
slight changes of the size of the magnetooptical response by less than
5%. Deviations in the same order of magnitude have been observed between
spectra obtained from cleaved crystals with different surface roughness.
It is interesting to note, that the magneto-optical response of a cleaved
crystal remains nearly unchanged even if the optical reflectivity is re-
duced by a factor of three due to an imperfect surface. In general it is
to state, that the magneto-optical Kerr-effect is very insensitive on
surface preparation for the investigated uranium compounds.
In contrast to the cleaved samples, tremendous changes of the spectra
have been observed for polished samples. Due to this surface treatment,
several effects are found to occur. A first observation is, that the size
of θ_K and ε_K deviates at $\hbar\omega > 3eV$ from those spectra obtained for clea-
ved samples, which is illustrated for US-(100) in fig.1. This effect may
have the same reasons as the difference of the reflectivities at high
energies for cleaved and polished samples [12].
In the case of $USb_{0.8}Te_{0.2}$ we have observed a complete change of the
magneto-optical f→d transition signal due to polishing. On the one hand,
this behavior gives new insight into the physical properties of this spe-
cial material (discussed in sec. 4.4.2.2) but on the other hand shows,
that the measurement of a polished sample can lead to misinterpretations.
Finally, the polishing treatment may influence the magnetic structure of
the sample. This effect has been observed for UAs [13] and is discussed
in detail in sec. 4.5.
The magneto-optical results, presented in the following chapters have
therefore been obtained on cleaved samples as far as possible. The inves-

tigation of Th_3P_4-structure compounds, which are not cleavable, and of course the measurements on (111)- and (110)-oriented surfaces of cubic compounds have been performed on polished samples.
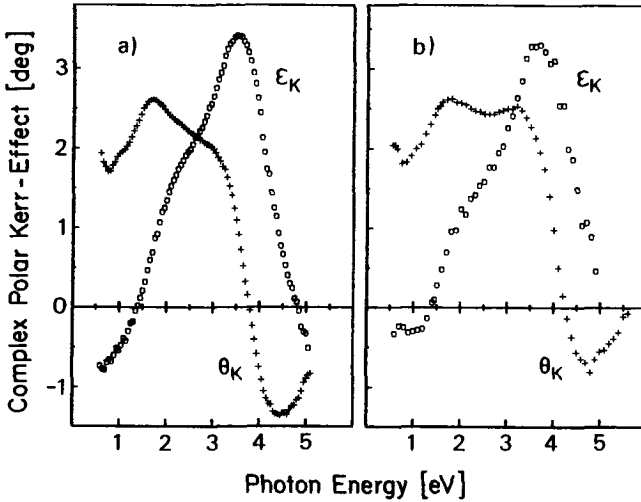

Fig. 1: Polar Kerr-rotation θ_K and -ellipticity ϵ_K of uranium-mono-sulfide at magnetic saturation (B=4T, T=15K). a) (100)-cleaved. b) (100)-polished.

2.2 Magneto-optical measurements

Fig. 2 shows the principal components of the equipment for the determination of θ_K and ϵ_K in the photon energy range between 0.5 eV and 5.7 eV. To achieve high light intensities I_0, we have used a 50W halogen lamp below ≈2.5 eV and a 450W Xenon arc light source above ≈2.5 eV. The light is polarized by an air gap Glan-Thomson polarizer. The sample and the reference mirror are mounted in a gas flow cryostat which allows measurements in the 1.5-300 K temperature range. Magnetic fields up to 10 T are generated by a split coil superconducting magnet. The angle of incidence is kept less than 3° to avoid mixing of the polar Kerr-signal with quadratic magneto-optical effects. In fact, a calculation of the Kerr-
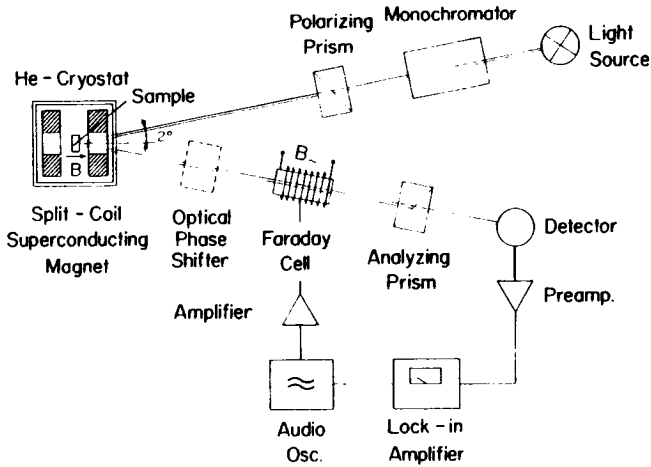
Fig. 2: Experimental set-up for the polar Kerr-measurement in the 0.5-
5.7eV photon energy range.

effect as function of the angle of incidence has proved, that the devia-
tion from the result at normal incidence is negligible at such small an-
gles of incidence [14].
The reflected light is modulated by a Faraday modulator, using a SCHOTT
SF-59 glas or a quartz rod of 10cm length for wavelengths below and above
≈2.5 eV, respectively. With an analyzer setting of 90±δ relative to the
polarizer setting (nearly crossed) and a modulation $\phi=\phi_0\sin\omega t$, one ob-
tains as a function of the Kerr-rotation θ_K at the detector an intensi-
ty of the form

$$I=\frac{I_0}{2}\left[(1-J_0(2\phi_0)\cos(2(\theta_K-\delta)))+2\sin(2(\theta_K-\delta))J_1(2\phi_0)\sin\omega t-..\cos\omega t..\right] \quad (1)$$

with the n-th order Bessel functions $J_n(x)$. Thus, the difference of the
analyzer settings for vanishing ω-signal for light, reflected from the
reference mirror and from the sample gives the Kerr-rotation θ_K of the
sample. The reference mirror was an evaporated gold film, which in a
field of 10T shows a Kerr-rotation and ellipticity of less than 0.02° in

the whole energy range [15].

The Kerr-ellipticity ϵ_K has been measured in the same way as the rotation but with a Soleil Babinet compensator introduced between sample and modulator. Keeping the fast axis of the compensator with $\lambda/4$-retardation parallel to the major axis of the light ellipse, the light becomes linearly polarized with a rotation of ϵ_K after passing the compensator (Senarmont principle) [16]. The difference of the analyzer settings - nulling the ω-signal for sample and reference - gives the Kerr-ellipticity ϵ_K. The Kerr-rotation of the sample has to be compensated by setting the polarizer at $-\theta_K(\hbar\omega)$.

The absolute error of this method depends on the adjustment of the light path and amounts to less than a few hundredth of a degree. It originates in the difference in Faraday-rotation of the lenses, if the reference and sample light beams are slightly misalligned. The relative error of adjacent points, however, is certainly less than 1%. The sensitivity is 0.001^o at all photon energies except those at both ends of the spectrum, where it increases to a few hundredth degree.

3. THEORETICAL BACKGROUND

3.1 Optical Constants and the Polar Magneto-Optical Kerr-Effect

In the geometry of the polar Kerr-effect, i.e. the vector of light propagation $\vec{q}$ as well as the applied magnetic field $\vec{H}$ are perpendicular to the sample surface, the eigenstates of light are right (+) and left(-) hand circular polarizations. In general, the coefficients of reflection $r_\pm = |r_\pm| e^{i\phi_\pm}$ of these modes are different, resulting in a Kerr-rotation $\theta_K = (|r_+| - |r_-|)/(|r_+| + |r_-|)$ and a Kerr-ellipticity $\epsilon_K = (\phi_+ - \phi_-)/2$.

To obtain information about the electronic structure, one needs a relation between the measured values θ_K and ϵ_K and microscopic quantities like the electronic density of states, spin-polarization, transition probability etc. Unfortunately, there is no direct connection of these microscopic quantities to θ_K and ϵ_K, but they are related to the conductivity tensor σ_{ij} (or the dielectric tensor $\epsilon_{ij} = \delta_{ij} - i4\pi\sigma_{ij}/\omega$) as will be shown in sec. 3.2.

For crystals with cubic symmetry and $\vec{q}$, $\vec{H}$ parallel to the z-axis, the conductivity tensor $\underline{\sigma}$ has the following form:

$$\underline{\sigma} = \begin{pmatrix} \sigma_{xx} & \sigma_{xy} & 0 \\ -\sigma_{xy} & \sigma_{xx} & 0 \\ 0 & 0 & \sigma_{zz} \end{pmatrix} . \tag{2}$$

The absorptive parts of the complex tensor elements $\sigma_{ij}=\sigma_{1ij}+i\sigma_{2ij}$ are σ_{1xx} and σ_{2xy} as can be shown by a decomposition of $\underline{\sigma}$ into the hermitian and antihermitian contribution [17]. From the Onsager relation $\sigma_{ij}(H)=\sigma_{ji}(-H)$ and the antisymmetry $\sigma_{ij}=-\sigma_{ji}$ it follows, that σ_{xx} and σ_{xy} are even and odd in H, respectively. Thus, to first order in H, the diagonal element σ_{xx} is independent of the applied field and σ_{xy} is a linear function in H.

For the off-diagonal conductivity, one finds in a straightforward calculation the following relation to the polar Kerr quantities θ_K and ϵ_K:

$$\sigma_{1xy} = \frac{\omega}{4\pi}\left[-\theta_K(3n^2k-k^3-k)-\epsilon_K(n^3-3nk^2-n)\right]$$

$$\sigma_{2xy} = \frac{\omega}{4\pi}\left[-\theta_K(n^3-3nk^2-n)+\epsilon_K(3n^2k-k^3-k)\right] \quad . \tag{3}$$

In these equations, n and k are the refractive and absorption index, respectively. They are related to the diagonal conductivity σ_{xx} by:

$$\sigma_{1xx} = 2nk\omega/4\pi$$

$$\sigma_{2xx} = (n^2-k^2-1)\omega/4\pi . \tag{4}$$

The real and imaginary part of σ_{xy} obey the well known Kramers-Kronig formula [18]

$$\sigma_{1xy}(\omega) = -\frac{2}{\pi} P\int_0^\infty \frac{\omega'}{\omega'^2-\omega^2} \sigma_{2xy}(\omega')d\omega'$$

$$\sigma_{2xy}(\omega) = \frac{2\omega}{\pi} P\int_0^\infty \frac{1}{\omega'^2-\omega^2} \sigma_{1xy}(\omega')d\omega' \quad . \tag{5}$$

This relation can be used for a rough extrapolation of σ_{xy} below the lower energy limit of the measurement. For this purpose, an extrapolation of σ_{1xy} below 0.5eV is chosen in such a way, that eq.(5) reproduces the measured $\sigma_{2xy}(\omega)$ in the energy range above 0.5eV, and vice versa. We

have found that, in the case of the present materials, the calculated σ_{xy} in the energy range from 0.5eV to 2.5eV depends quite strongly on the chosen extrapolation.

At zero frequency, $\sigma_{2xx}=\sigma_{2xy}=0$ [19] and σ_{1xx} and σ_{1xy} are related to the DC-resistivity ρ_{xx} and the Hall-resistivity ρ_{xy} to first order in H by

$$\sigma_{1xx}(0) = 1/\rho_{xx}$$

$$\sigma_{1xy}(0) = -\rho_{xy}/\rho^2_{xx} \quad .$$

(6)

These relations may give additional hints how to extrapolate σ_{xy} below the lower energy limit of the measurement.

It should be mentioned, that the coefficients of θ_K and ϵ_K in eq.(3) are quite complicated functions of n and k. In contrast to remarks in refs.[20] and [21] it is not possible to make any statement about a dominant contribution of either θ_K or ϵ_K to σ_{1xy} or σ_{2xy}. This can easily be seen from fig.3, which shows a plot of n^3-3nk^2-n and $3n^2k-k^3-k$
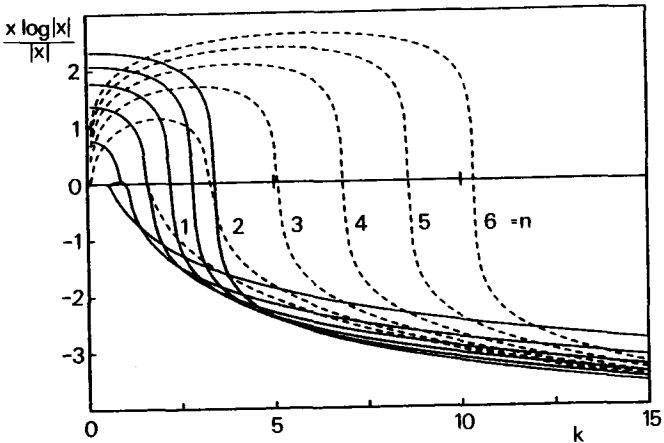
Fig. 3: Coefficients of θ_K and ϵ_K in the calculation of σ_{xy} (eq.(3)) as a function of n and k. Solid lines: $x=3n^2k-k^3-k$. Dashed lines: $x=n^3-3nk^2-n$.

versus k for different values of n. Even for $n \gg k$ or $n \ll k$, none of the functions becomes dominant.

With these complications in mind it becomes clear, that a direct inter-pretation of θ_K and ε_K may lead to faulty results. This fact shall be illustrated by a comparison of two materials, both showing a strong f→d interband transition at 0.8 eV. This transition displays a diamagnetic line shape in σ_{xy} and a similar width for both compounds which is visu-alized by the comparison of $\sigma_{xy}(\omega)$ for UAs and UAsSe in figs.4a and 4b. Due to different $n(\omega)$ and $k(\omega)$, the measured Kerr-rotaion and -elliptici-ty no longer exhibit these similarities for the two materials (figs. 4c and 4d).
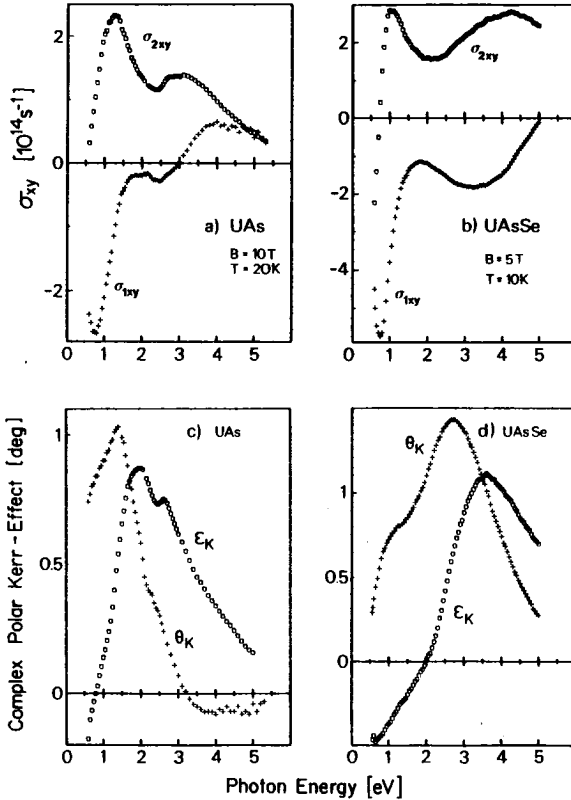

Fig. 4: Off-diagonal conductivity (a,b) and complex polar Kerr-effect (c,d) of UAs and UAsSe single crystals at B=10T, T=20K and B=5T, T=10K, respectively. An analysis of these data is given in secs. 4.2.2 and 6.

3.2 Microscopic Theory

After the enormous progress in theoretical work about the magneto-optical response of magnetically ordered materials in the 60's and early 70's, there has been a stagnation in the development of theoretical concepts in the last ten years. Therefore, only the basic ideas of theoretical models which are necessary to interpret the magneto-optical response of uranium compounds are presented in the following and appropriate references will be given.

It has been shown by several authors [22-27] that the large magneto-optical effects observed for ferromagnets can not be explained simply considering the Zeeman perturbation on the initial and final states as it is generally done for nonmagnetic materials [28] but needs the introduction of spin-orbit coupling. The influence of spin-orbit coupling has been considered as a perturbation of either the initial [23] or the final [22] state energies of an interband transition or as a modification of the initial state wavefunctions [29] which is of importance if the ground-state orbital momentum is quenched.

It has been pointed out that in general the magneto-optical effects will be proportional to

$$\sum_i \vec{s}_i \times \nabla V \; \vec{p}_i \qquad (7)$$

which is the spin-orbit energy of an electron with spin $\vec{s}$ and momentum $\vec{p}$ moving through the electrical field $-\nabla V$. This vector sum clearly evidences, that the magneto-optical effects are proportional to the product of magnetization $\sum \vec{s}_i$ and spin-orbit energy, i.e. apart from a sufficient spin-orbit splitting, a high spin polarization is required to obtain a large magneto-optical response.

Based on these ideas, Erskine and Stern [27] have developed expressions for σ_{xy} which allow quantitative calculations for interband and intraband transitions

3.2.1 Conduction Electrons

It has been shown [27,30], that intraband transitions may contribute to σ_{xy} with two different frequency dependences, $\sigma_{2xy} \approx \omega^{-1}$ and $\approx \omega^{-3}$. The theory gives a proportionality of σ_{xy} to the conduction electron con-

centration via the plasma frequency $\omega^2_p = 4\pi Ne^2/m^*$ and to their spin po-larization $\sigma_d = (n_\uparrow - n_\downarrow)/(n_\uparrow + n_\downarrow)$. $n_\uparrow$ and $n_\downarrow$ are the number of conduction electrons with spin moment parallel and antiparallel to the total moment, respectively. In addition, the second term of σ_{xy} is proportional to the strength of the spin-orbit coupling via P_0/ev_0 [27]:

$$\sigma_{xy}(\omega) = \frac{\omega_p^2}{4\pi} \sigma_d \left[\frac{-\Omega}{\Omega^2 + (1/\tau + i\omega)^2} + \frac{P_0}{ev_0} \left[1 - \frac{i\omega(1/\tau + i\omega)}{\Omega^2 + (1/\tau + i\omega)^2} \right] \right] . \tag{8}$$

In this equation, $\gamma = 1/\tau$ and Ω are the relaxation and the skew-scattering frequency, respectively. Consequently, the absorptive part of the free electron contribution is given by

$$\sigma_{2xy}(\omega) = \frac{\omega_p^2}{4\pi} \sigma_d \left[\frac{2\gamma\Omega\omega}{(\Omega^2 + \gamma^2 - i\omega^2)^2 + 4\gamma^2\omega^2} - \frac{P_0}{ev_0} \frac{\omega\gamma(\Omega^2 + \gamma^2 + \omega^2)}{(\Omega^2 + \gamma^2 - \omega^2)^2 + 4\gamma^2\omega^2} \right]. \tag{9}$$

It is interesting to note, that the first term on the right side corres-ponds to the classical Drude theory if $\sigma_d \cdot \Omega$ is replaced by the cyclo-tron frequency ω_c. This first term manifests itself by different plasma frequencies for right and left circularly polarized light. The skew-scat-tering frequency Ω has been shown to coincidence with the spin-orbit parameter ζ_{so} [30].

The decisive number for the dominance of the first or the second term in eq.(9) at a frequency ω is the ratio $(|P_0|/ev_0)/(\Omega/\omega^2)$. This ratio can be estimated using the relation

$$P_0/ev_0 \simeq (ma^2\omega_{so})/(\hbar\omega_{ab}) . \tag{10}$$

Here, a is the lattice constant and $\hbar\omega_{so}$ and $\hbar\omega_{ab}$ are typical spin-orbit and interband energies, respectively [31].

In conclusion, the analysis of the free electron part enables the deter-mination of the sign of the conduction electron spin-polarization σ_d from the sign of σ_{xy} and it gives information on the size of σ_d, the number of conduction electrons N and the magnitude of the relaxation fre-quency γ.

3.2.2 Interband Transitions

The modified atomic model of Erskine and Stern [27] for an interband

transition a→b introduces the total weight

$$\langle \sigma_{xy} \rangle = \int\limits_{a \to b} |\sigma_{2xy}| d\omega \tag{11}$$

of this transition, which is given in atomic theory by:

$$\langle \sigma_{xy} \rangle = \frac{\pi N e^2}{2\hbar} \sum_{\alpha\beta} (\omega_{\alpha\beta}^+ |\langle \beta | x - iy | \alpha \rangle|^2 - \omega_{\alpha\beta}^- |\langle \beta | x + iy | \alpha \rangle|^2) \sigma_j n_\alpha n_\beta. \tag{12}$$

In this equation, α and β are the spin-orbit split sublevels of a and b, respectively, and σ_j is the joint spin polarization of the initial and final state.

The dipole matrix elements are nonzero only for transitions with $\Delta m = \pm 1$. Assuming a fixed spin moment m_s due to strong exchange forces, the spin-orbit coupling lifts the degeneracy of the orbital quantum number m_l:

$$E^m_{so} = \zeta_{so} \cdot m_l \; . \tag{13}$$

The calculation of the dipole matrix elements for right and left hand circularly polarized light in eq.(12) is performed within the approximation, that the atomic oscillator strength of the transition a→b is unchanged in the solid, but smeared out over the band-width E_B. In this approximation the initial and final state wavefunctions are spherical harmonics Y_l^m for the orbital part, multiplied by a radial contribution $u(r)$ and it follows:

$$\sum_{\alpha\beta} |\langle \beta | x - iy | \alpha \rangle|^2 - |\langle \beta | x + iy | \alpha \rangle|^2 = \sum_m (|\langle Y^{m-1}_{l\pm1} | x - iy | Y^m_l \rangle|^2 - |\langle Y^{m+1}_{l\pm1} | x + iy | Y^m_l \rangle|^2) \cdot R^2_{ab} \; . \tag{14}$$

Here, R^2_{ab} is the radial overlap integral

$$R^2_{ab} = \left| \int u_a u_b r^2 dr \right|^2 \; . \tag{15}$$

The comparison of the off-diagonal weight $\langle \sigma_{xy} \rangle$ with the total diagonal weight $\langle \sigma_{xx} \rangle$ of the interband transition a→b, which is given by

$$\langle \sigma_{xx} \rangle = \frac{\pi N e^2}{\hbar} \omega_{ab} \left| \langle b | \bar{r} | a \rangle \right|^2 n_a n_b \qquad (16)$$

shows up, why the combination of optics and magneto-optics is a powerful method for the investigation of the electronic structure of magnetic solids: while all electronic states contribute to eq.(16), only those states showing a net spin-polarization contribute to eq.(12). However, also unpolarized but exchange split states may contribute to the magneto-optical response but with a much smaller signal [8, 27].

It is noteworthy to mention, that the maximum value of $\langle \sigma_{xy} \rangle / \langle \sigma_{xx} \rangle$ is 2/3. This fact can easily be seen, writing $\left| \bar{r} \right|^2 = \left| (\bar{x} + i\bar{y})/\sqrt{2} \right|^2 + \left| (\bar{x} - i\bar{y})/\sqrt{2} \right|^2 + \left| \bar{z} \right|^2$ in eq.(16). In the presented modified atomic model, maximum $\langle \sigma_{xy} \rangle$ is reached for $\sigma_j = 1$ and $E^m_{so}/E_B = 1$ [27].

Finally, the diagonal and off-diagonal oscillator strengths f_{xx} and f_{xy}, respectively, are defined by

$$f_{xx} \approx \langle \sigma_{xx} \rangle / N$$

$$\qquad (17)$$

$$f_{xy} \approx \langle \sigma_{xy} \rangle / N \quad .$$

This characteristic quantity of an interband transition is independent of the density of molecules N in the crystal and therefore it is more suitable than the total weight for a comparison of the same transition in different materials.

4. BINARY AND PSEUDO-BINARY COMPOUNDS $UX_x Z_{1-x}$
(X = S, Se, Te; Z = P, As, Sb; 0<x<1)

4.1 Introduction

The face centered cubic uranium-monochalcogenides and -monopnictides are certainly the most investigated class of actinide compounds. This fact reflects on one hand the relative easy handling of these materials from both the experimental and theoretical point of view, and on the other hand the large variety of physical effects encountered in these systems. In some way, this class of materials can be thought of as a model system

for the understanding of uranium compounds at all.

The uraniumchalcogenides as well as a great variety of mixed crystals UX_xZ_{1-x} are ferromagnets [32]. The magnetic moments are strictly con-fined to the (111)-easy axis and the total moment increases going from US to UTe. The moment obtained from magnetization measurements is found to be smaller than the neutron moment, which has been interpreted by antipa-rallel d and f contributions [33].

The uraniumpnictides and some other mixed crystals, on the other hand, order antiferromagnetically [32]. In general, they exhibit a very complex magnetization-field-temperature phase diagram, showing various multiple-k antiferro- and ferrimagnetic phases. Especially the phase diagram of UAs has been intensively studied by neutron scattering [34]. The magnetic pa-rameters of the UX and UZ compounds are summarized in fig.5.
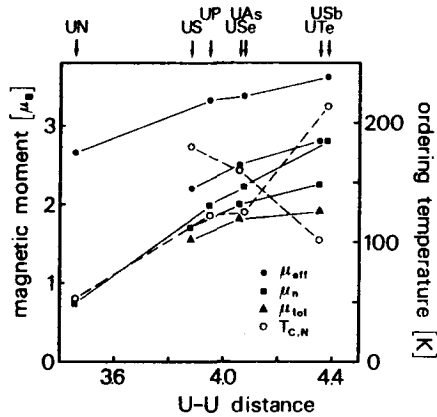

Fig. 5: Ordering temperature T_C, T_N, paramagnetic moment μ_{eff}, mag-netization moment μ_{tot} and neutron moment μ_n of uranium-chal-cogenides and pnictides [32, 34-42].

The complex magnetic behavior of UX_xZ_{1-x} goes along with an unusual electronic structure. One characteristic feature is the spatially exten-ded nature of the uranium f wavefunctions and their proximity to the Fer-mi level [43]. The metallic conductivity, however, is predominantely due to occupied d states. A cluster calculation for US has indicated the for-mation of a dip in the d density of states near E_F [44] due to a strong

fd hybridization. Recently, this theoretical prediction has been con-
firmed by a spin-polarized APW band structure calculation for UN [45]. In
addition a large fp hybridization is expected for the pnictides (x=1),
decreasing with decreasing x because of a shift of the p band center to
higher binding energies with decreasing covalency [46,47].

While for the compounds with small anions, i.e. US and UP, this view of
the electronic structure seems to be well established, there are large
discrepancies in the interpretations of different experimental results
for compounds with heavier anions [43]. Optical [46], specific heat [48]
and some photoemission [49-53] results favour band like f states with a
decreasing width going from US to UTe and UP to USb, respectively, while
other photoemission data on USe, UTe, UAs and USb [54] have been inter-
preted in a 'quasi'-localized picture. The paramagnetic moment of all ma-
terials, derived from the Curie-Weiss law at $T \gg T_{C,N}$ can not be inter-
preted by Hund's rule localized f^2 or f^3 states, but increases continu-
ously with heavier anions (fig.5).

Regarding the electronic structure of these compounds, the aim of the
present work is i) to provide a systematic magneto-optical study of the
electronic density of states in the vicinity of E_F; ii) to shed light
on a possible localization of the f states with increasing spatial sepa-
ration of the uranium atoms; iii) to obtain results on the magnetic ex-
change and spin-polarization of d and f electrons and iv) to get informa-
tion about the strength of hybridization effects between f states and p,d
electrons.

In sec. 4.2, the optical and magneto-optical behavior of UAs_xSe_{1-x} is
discussed to point out similarities and differences in the electronic
structure of uranium chalcogenides and pnictides. In sec. 4.3, the magne-
to-optical data along the chalcogenides and pnictides series are presen-
ted and trends of the electronic structure along these series will be
examined. Magnetic exchange in uranium pnictides, but especially in the
system USb_xTe_{1-x} is studied in detail in sec. 4.4. Finally, magneto-
optics as a powerful technique for the study of magnetic phase transi-
tions is demonstrated in sec. 4.5 for UAs.

4.2 Similarities and Differences in the Electronic Structure of Uranium-
    Chalcogenides and Pnictides: UAs_xSe_{1-x}

UAs and USe form a continuous series of solid solutions crystallizing in
the rocksalt structure with a nearly constant lattice parameter $a \approx 5.75 Å$

[55]. UAs is an antiferromagnet with an Néel temperature of 124±2 K. At about $T_N/2$, it undergoes a first order phase transition from a +−+− (type I) to a ++−− (type IA) stacking of ferromagnetic (001)-planes. At this phase transition, a 10% decrease of the magnetic moment of the uranium ion has been observed [56]. Recent neutron experiments have shown, that the IA to I transition is accompanied by a transition from a $2\bar{k}$ (easy axis (110)) to a $1\bar{k}$ (easy axis (100)) collinear spin structure, explaining the change in the magnetic moment [34]. The application of magnetic fields induces intermediate spin structures like multiple-$\bar{k}$ ferrimagnetic phases [57]. The magneto-optical determination of the magnetization-field-temperature phase diagram of UAs will be presented in sec. 4.5.

USe orders ferromagnetically below T_C=160 K [58]. The easy direction is the (111)-axis. No rotation of the magnetization out of this direction could be observed by the application of fields up to 15 T. This evidences the existence of very strong anisotropy fields.

4.2.1 Optical Properties

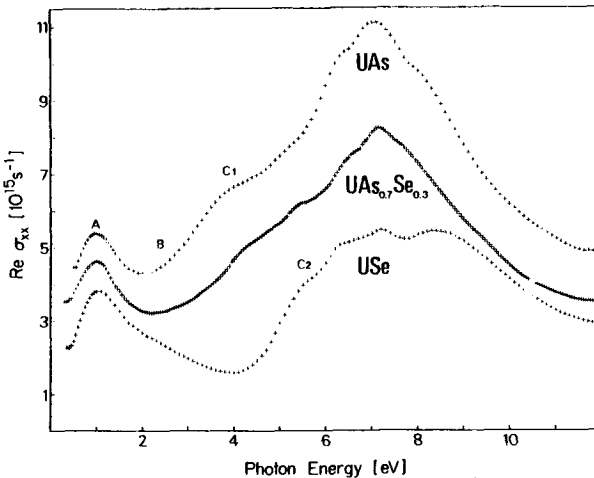The optical conductivity of $UAs_{0.7}Se_{0.3}$ (fig. 6) shows features,

Fig. 6: Absorptive part of the diagonal conductivity of UAs, $UAs_{0.7}Se_{0.3}$ and USe at room temperature and B=0. Consecutive curves are vertically shifted by one unit.

which are typical for UX and UZ compounds [46]. The free electron contribution is weak relative to the expected number of conduction electrons and is highly damped. The plasma energy lies between the values observed for UAs and USe [46]. Two strong interband transitions (peaks A and B) dominate the low energy conductivity while the broad and structured absorption band around 7.5 eV is attributed to valence-band excitations [46].

To compare with the magneto-optical data, we will focus on the low energy range (0.5 - 6 eV). A quantitative analysis including the decomposition of the diagonal condutivity into a free electron part and different Lorentzian shaped interband transitions [59] gives the following results:
i) Peak A has in all three compounds the same transition energy $\hbar\omega_A$= 1.0±0.02 eV, the same width $\hbar\gamma\approx$1.15±0.05 eV and the same oscillator strength f=0.9±0.02. This points to identical initial and final states for this excitation in the different compounds. ii) Peak B decreases in oscillator strength by about a factor of three going from USe to UAs, while its energy $\hbar\omega_B\approx$2.4±0.2 eV and its width $\hbar\gamma\approx$2±0.3 eV remain constant. iii) Substituting As by Se, peak C1 at about 4 eV in UAs weakens at constant energy and at about 5.5 eV a new peak C2 develops.

4.2.2 Magneto-Optical Properties

4.2.2.1 Experimental Results

In sec. 3.2 it has been argued, that the polar Kerr-effect is proportional to the magnetization of the sample volume, which is probed by this technique. The penetration depth of the light beam is roughly given by the absorption constant K $[\text{cm}^{-1}]$:

$$d \approx 1/K = \lambda/4\pi k \tag{18}$$

and amounts to 200-1000Å in metals. Thus it can be expected, that in general the size of the polar Kerr-effect is a measure of the bulk magnetization and, on the other hand, deviations from the bulk behavior indicate sample imperfections for the first few hundredth of Å.

Fig. 7 shows the temperature dependence of the Kerr-rotation of UAs, $UAs_{0.7}Se_{0.3}$ and USe which enlightens the complex magnetic phase diagram in the system UAs_xSe_{1-x}.

The simplest case is USe for which the temperature dependence of θ_K shows a typical ferromagnetic behavior (fig. 7a) with M(111)=1.81μ_B/U
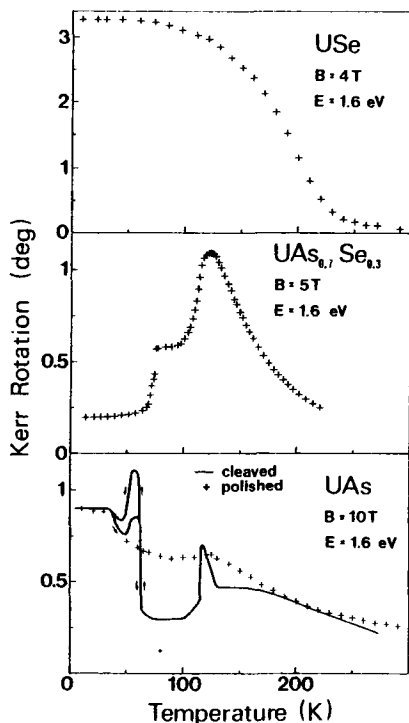
Fig. 7:

Temperature dependence of θ_K at $\hbar\omega=1.6$ eV for (a) USe, (b) $UAs_{0.7}Se_{0.3}$ and (c) UAs. The applied field is the same as in the energy-dependent measurements of θ_K and ϵ_K displayed in fig. 8.

at 15 K and 4 T [58]. UAs orders antiferromagnetically and thus only very small magneto-optical effects are found in lower fields. However, UAs undergoes a magnetic phase transition at 8.7 T (see also sec. 4.5). In the high-field induced ferrimagnetic phase, the magnetic moment reaches $M(100)=0.42$ μ_B/U at 10 T and 20 K. Consequently, the observed Kerr-rotation is about a factor of three smaller than in USe (fig. 7c). With increasing temperature different ferri- and antiferromagnetic phases can be observed which will be discussed in detail in sec. 4.5.

In a field of 5 T, the mixed compound $UAs_{0.7}Se_{0.3}$ shows four magnetic phases as a function of temperature (fig. 7b): paramagnetic behavior for $T>T_N=127$ K, a ferromagnetic phase between T_N and about 115 K and two different antiferromagnetic regions at lower temperatures [55]. The highest magnetization occurs in the ferromagnetic phase at 123 K and amounts to $M(100)=0.48\mu_B/U$.

To obtain the highest resolution the magneto-optical spectra to be repor-

ted have been measured at that temperature, which gives the largest sig-
nal. Fig. 8 displays the energy dependent complex polar Kerr-effect for
the three compounds. The spectra all look very similar, each with two
structures in θ_K and ε_K. Yet, because θ_K and ε_K are linear combi-
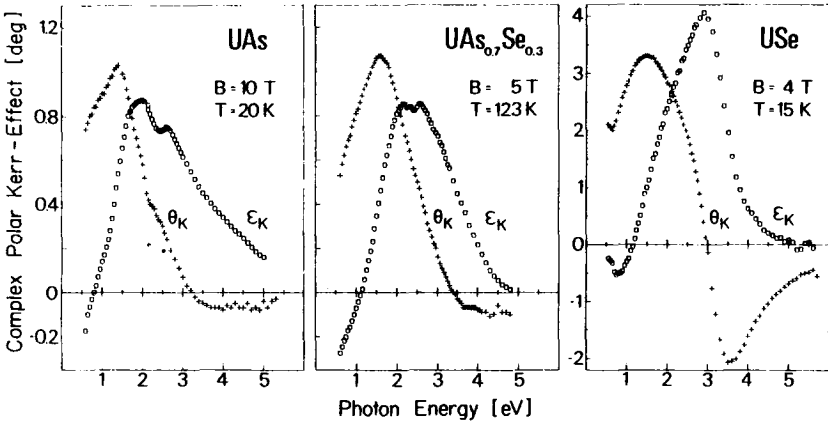nations of absorptive and dispersive quantities, the interpretation in

Fig. 8: Energy dependent polar Kerr-rotation θ_K and -ellipticity ε_K
for (100)-oriented cleaved single crystals of UAs,
$UAs_{0.7}Se_{0.3}$ and USe. Note the change of the ordinate scale
for USe.

terms of the electronic structure is not straightforward. Instead, the
real and imaginary part of the off-diagonal conductivity σ_{xy} shown in
fig. 9 should be discussed. In this figure, an extrapolation of σ_{xy} for
energies less than 0.5 eV is included taking advantage of the Kramers-
Kronig relation between $\sigma_{1xy}(\omega)$ and $\sigma_{2xy}(\omega)$ (sec. 3.1, eq. (5)).
Up to about 2.5 eV the off-diagonal conductivity of the three materials
displays large similarities. At higher energies, no magneto-optically ac-
tive excitations are observed in USe, but there appears a broad peak C1
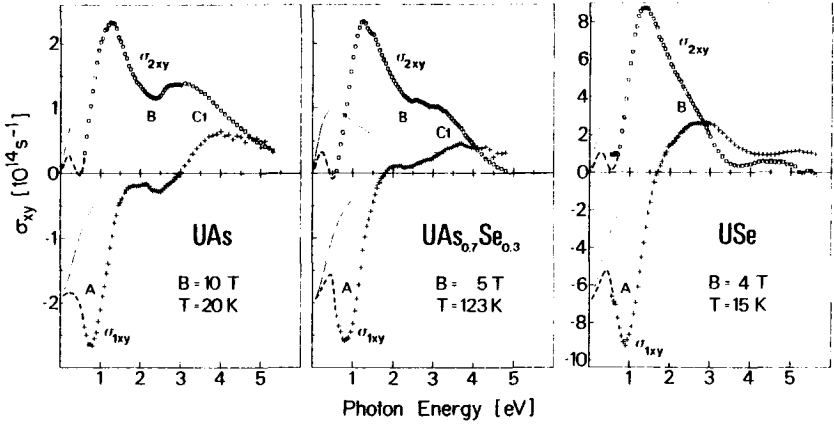around 3 eV with increasing As concentration.

Fig. 9: Absorptive (σ_{2xy}) and dispersive (σ_{1xy}) part of the off-dia-
gonal conductivity of UAs, $UAs_{0.7}Se_{0.3}$ and USe. The dashed
line displays the extrapolation of σ_{xy} for $\hbar\omega < 0.5$ eV obtained
by Kramers-Kronig inversion (see sec. 3.1). The solid and dash-
dotted curves render visible the estimated free-electron contri-
bution to σ_{2xy} and σ_{1xy}, respectively. Note the change in or-
dinate scale for USe.

4.2.2.2 Conduction Electrons

A comparison of the energy of peak A in σ_{xx} and σ_{xy} (sec. 4.2.2.3)
indicates, that the line shape of this lowest energy interband transition
A has to be 'diamagnetic', i.e. it shows a bell shaped form with a maxi-
mum in σ_{1xy} at $\hbar\omega_A$ and $\sigma_{2xy}(\hbar\omega_A)=0$. Consequently, the free elec-
tron contribution to σ_{2xy} must be positive, which is equivalent to a
negative spin-polarization of the conduction electrons (eq. 9), i.e. the
number of d electrons with spin moment antiparallel to the f moment is
larger than the number of those with parallel spin moment. This holds for
ferromagnetic USe and $UAs_{0.7}Se_{0.3}$ as well as for ferrimagnetic UAs
and it constitutes the first experimental determination of the conduction
electron spinpolarization for an uraniumpnictide. It agrees with the re-
sult of a spinpolarized band structure calculation for UP [60]. In the
case of USe, the negative polarization is in qualitative agreement with a

calculation for US [44] and with spin-polarized photoemission results [61].

To derive the size of the spin-polarization from the free-electron contribution, several parameters occuring in eq. (9) have to be estimated. First, comparing the two terms on the right side of this equation, we note that at $\hbar\omega=1$ eV their ratio [30] $(P_0/ev_0)/(\Omega/\omega^2)$ amounts to ≈10 for our compounds. Thus we neglect the first term in the following.

Using eq. (10) the spin-orbit contribution P_0/ev_0 in eq. (9) may be calculated. Taking a=1.5Å for the atomic radius [44] and 1 eV for both the spin-orbit energy $\hbar\omega_{so}$ and the lowest interband energy $\hbar\omega_{ab}$, one obtains $P_0/ev_0 \simeq 2\cdot10^{-16}$ sec. Taking for the conduction electron relaxation frequency at low temperatures $\hbar\gamma=0.5$ eV, the product of spin-polarization and conduction electron concentration is found to be -41, -13 and -12 %·electrons/formula unit for USe, $UAs_{0.7}Se_{0.3}$ and UAs, respectively. The solid and dash-dotted curve in fig. 9 display the corresponding free electron contributions to σ_{xy}. To obtain the size of the spin polarization alone, one needs to know the conduction electron concentration. Assuming for USe 1.1 electrons per formular unit (this number will be discussed in sec. 4.3.2.1), and scaling the conduction electron concentration with either the square of the plasma energy or with the intensity of the d→f transition (see sec. 4.2.2.3) within the UAs_xSe_{1-x} series, spin-polarization values of -35%, -20% and -30% are derived for the three compounds with increasing x and the magnetic fields given in fig. 7.

These numbers express very interesting physical properties of the d-conduction band and the f-d exchange. The observed macroscopic d-spin-polarization for UAs, for example, has to be viewed in the context of the low macroscopic magnetization in the ferrimagnetic phase, amounting to 0.42 μ_B/U. This means, that the local d-spin-polarization, in the vicinity of the f moment, must be ≈-100%. This idea is visualized in fig. 10, which shows a simple ferrimagnetic f-spin structure and d-electrons, which are -100% spin polarized locally. The macroscopic conduction electron spin-polarization, however, is given by summing over all d electrons, i.e. amounts to -33%.

Assuming the same hypothetical saturation magnetization for UAs, $UAs_{0.7}Se_{0.3}$ and USe of 1.8 μ_B/U, one finds a local spin polarization of -100%, -75% and -35%, respectively. Because of some ambiguity in the determination of n, σ_d and of the total moment, these values should be viewed as showing up a tendency and not as exact numbers.

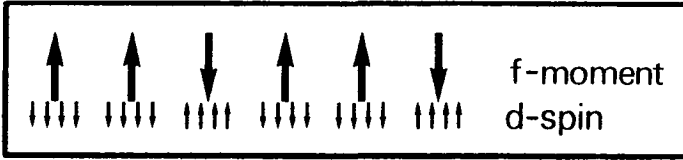In a first approach, the conduction band in a magnetized solid is split

Fig. 10: Model for the explanation of the high conduction electron spin-
polarization in uranium-monopnictides. The macroscopic d spin-
polarization for the displayed ferrimagnetic structure (UAs)
amounts to -33%, if a -100% local spin polarization is assumed.

into two subbands with opposite spin direction. Assuming a rectangular
density of states of 1 electron/eV·spin, the two subbands have to be
energetically split by at least 0.4 eV to obtain -100% spin polarization
and an occupation of ≈0.4 electrons/U (fig. 11) as it has been observed
for UAs.

Fig. 11:
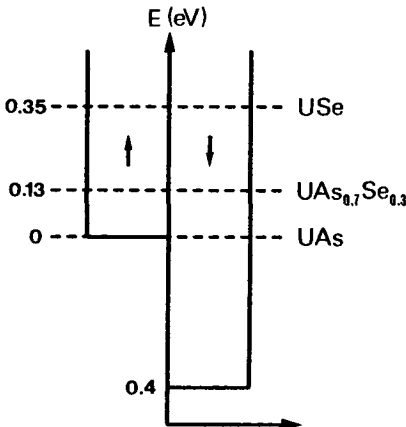Simple sketch of the spin-po-
larized conduction electron
density of states which allows
the interpretation of magneto-
optical data. The assumed
Fermi – energy for UAs,
$UAs_{0.7}Se_{0.3}$ and USe is vi-
sualized by the dashed hori-
zontal lines.

It is interesting to note, that the simple idea of the filling of a rigid
band can account for both the decrease in spin polarization and the in-

creasing occupancy in going from UAs to USe. The dashed horizontal lines in fig. 11 indicate E_F for $UAs_{0.7}Se_{0.3}$ and USe for the measured d electron numbers of 0.65 and 1.1 electrons/U, respectively. The obtained spin polarization in this model amounts to -65% and -35%, which compares favourably with the magneto-optical results.

The observed negative conduction electron spin polarization and the two subband model leads to an important prediction for the f→d transition energy. If the f-moment is mainly spin-like it follows, that the f→d transition energy should increase by 0.2 eV comparing unmagnetized UAs with magnetized UAs, i.e. a blue shift is predicted (fig. 12). However, as we will show in secs. 4.2.2.3 and 4.4, we observe a red-shift of this magnitude. Thus if follows, that the f moment is not determined by the spin, but the orbital moment, i.e. it obeys Hund's rules of antiparallel L and S for less than seven f electrons (see also sec. 4.4). This is a first direct experimental corroboration of a recent theoretical work on UN, proposing a dominant orbital moment contribution to 5f band magnetism [7].
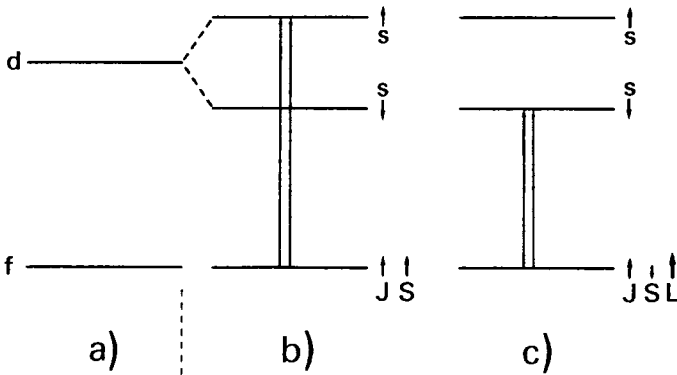

Fig. 12: Model of the atomic f and d states for an unmagnetized (a) and a magnetized (b,c) solid. A dominant f spin moment results in a blue-shift of the f→d transition energy (b) whereas a dominant orbital f moment predicts a red-shift (c).

4.2.2.3 Interband Transitions

The pure interband contribution to $\sigma_{xy}(\omega)$ is the difference of the measured $\sigma_{xy}(\omega)$ and the free electron contribution. It is dominated by a 'diamagnetic' transition A with exactly the same line width (FWHM≈0.7 eV) but different transition energies for USe, $UAs_{0.7}Se_{0.3}$ and UAs (tab. 1). The total weight (eq. 11) is about a factor of four less for UAs than for USe which corresponds approximately to the ratio of the total magnetic moments and not to the ratio of the moments along the (100)- direction as it would be expected [62].

	UAs	$UAs_{0.7}Se_{0.3}$	USe
$\hbar\omega_A$ [eV]	0.82	0.86	0.94
$\langle\sigma_{2xy}\rangle$ [10^{29} sec^{-2}]	2.3	2.3	9.0
μ_{tot} [μ_B]	0.42	0.48	1.8

Table 1: Observed transition energy $\hbar\omega_A$ in σ_{xy} and integrated weight $\langle\sigma_{2xy}\rangle$ of transition A in the magnetically ordered phases (magnetization μ_{tot}) of the three compounds. The field and temperature conditions are given in fig. 9.

In σ_{xx} as well as in σ_{xy}, we assign peak A to a transition from a narrow f band at E_F into d states. This interpretation is substantiated by the following arguments:
i) Peak A is present in the optical spectrum (σ_{xx}) of UAs as well as of USe with the same line-shape and the same oscillator strength; ii) in σ_{xy}, this transition again has the same line shape and the size of the peak is proportinal to the magnetic moments in the different compounds; iii) the large size of the magneto-optical response points to an excita-

tion of 'magnetic' electrons with large spin-polarization; iv) eqs. (12) and (16) describe the experimental oscillator strengths and line-shapes for σ_{1xx} and σ_{2xy} which will be discussed in sec. 4.3.2.2. These equations result in an f occupancy, n_f, which is by about a factor of 2 less than the expected occupancy assuming $n_f=4-n_d$ in USe and $n_f=3-n_d$ in UAs. This is a clear indication of non-negligible correlation effects [63] in the narrow f band; v) the absence of any fine structure in σ_{xy} which would be expected for strictly localized f states [8,10], on the other hand, points to an f band width in excess of typical spin-orbit energies.

We have already mentioned in the last section, that one further interes-ting feature of the f→d transition in UAs_xSe_{1-x} is the different re-sonance energy $\hbar\omega_A$ in σ_{xx}, observed at T=300K for B=0T and in σ_{xy}, observed for $T<T_{C,N}$ and B≠0. Such large magnetization induced red-shifts were up to now only observed in some ferro- and antiferromagnetic semiconductors [9]. The maximum shift is 0.3 eV in EuO. Yet, it was found for EuO doped with Gd, that the red-shift decreases with increasing con-duction electron concentration [64]. Applying a similar argument to our UAs_xSe_{1-x} system, UAs should exhibit the largest red-shift which is actually the case. Unfortunately, the evolution of the entire 0.17 eV shift in UAs as function of magnetization is hard to follow up in detail because of the complex magnetic phase diagram of UAs and the rather small magneto-optical signals in the antiferromagnetic phases. This problem is less difficult in UAs_xSe_{1-x} for x<0.7 and we have measured the Kerr-rotation maximum which corresponds to peak A in σ_{xy} as a function of magnetization. Fig. 13 displays the photon energy dependence of the Kerr-rotation at T=123 K ≈ T_N normalized to its maximum value for different magnetic fields. We observe, that the red-shift of the f→d transition sa-turates at a field of ≈5 T and amounts to about 0.14 eV. To our knowled-ge, the As-rich UAs_xSe_{1-x} compounds are the first metals showing such a striking magneto-optical effect.

The same effect, but even more pronounced, is presented for USb_xTe_{1-x} in sec. 4.4.

Moving our attention to higher photon energies, we find at ≈2.3 eV peak B with a 'paramagnetic' line shape in all materials. The total weight of this peak decreases from USe to UAs by a factor of about 6. The initial and/or final states of this transition have to possess a net spin-polari-zation, which is responsible for the observed large magneto-optical re-
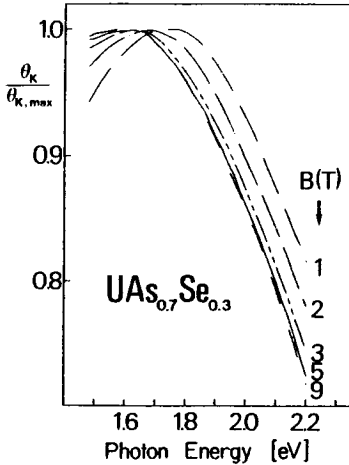
sponse. In addition, the oscillator strengths, normalized with the re-
spective magnetizations, decrease nearly proportionally to ω_p^2, i.e.
they are proportional to the number of d electrons. Both facts point to
an interpretation in terms of a d→f transition. The occurrence of a
strong d→f transition, however, can only be expected, if the f states are
not localized [63]. Consequently, the observation of this transition with
equivalent strength in UAs_xSe_{1-x} corroborates similar f delocaliza-
tion for different x. On the other hand as it will be shown in sec.
4.3.2.3, the same excitation shows a drastic decrease in oscillator
strength along the uranium-chalcogenide and pnictide series, indicating
the increase of f localization for UX and UZ compounds with heavier
anions.

Peak C1 around 3 eV in fig. 9 has also a 'paramagnetic' line shape but
it is only present in the As-rich samples. The width of this transition
increases with the As concentration. Its energy agrees roughly with the
energy of peak C1 in the diagonal conductivity (fig. 6). Peak C2, how-
ever, which is clearly resolved in σ_{1xx} for USe around 5 eV, has no
corresponding signal in σ_{xy}. At first sight the strong magneto-optical
response of this transition for UAs and its absence for USe is an unex-
pected result. To understand this behavior, let us examine somewhat clo-
ser the p valence-band in the system under discussion.

Band structure calculations [44,47,65] find the valence-band of UAs and
USe centered at binding energies of about 3 eV and 5 eV, respectively. In
addition, due to a strong admixture of some f and merely d states to the

p states, a nonuniform distribution of angular momentum throughout the band is predicted for the pnictides with more high-l states at the top and more low-l states at the bottom [47]. This admixture is smaller for the chalcogenides because of the higher p binding energy and the smaller charge transfer necessary to fill the valence band. Thus, the peaks C1 and C2 in σ_{xx} (fig. 6) are interpreted as the onset of excitations from the top of the valence band. These transitions are magneto-optically active for strong f,d admixtures and we assign peak C1 in σ_{xy} (fig. 9) to a (pd)→f transition.

Comparing our results with different photoemission studies on UAs and USe, we find in general good agreement [49,50,61]. In particular, the energy separation of high-l and low-l valence states for the uranium-pnictides has also been deduced from energy dependent UPS measurements [50]. On the other hand, in a more recent UPS study on UAs_xSe_{1-x} [54] two emission peaks, one close to E_F and one 0.7 eV below E_F have been interpreted as a final state splitting of localized 5f states and large differences in the f density of states between the chalcogenide and the pnictide have been claimed to exist. However, an examination of the experimental UPS results merely shows an increase of the peak intensity at 0.7 eV binding energy going from UAs to USe which in the light of our magneto-optical measurements reflects only an increase of the occupancy of the 6d conduction band [44].

4.2.3 Summary

In this section we have tried to point out similarities and differences in the optical and magneto-optical spectra of uranium-chalcogenides and pnictides by a systematic study of the evolution of the magneto-optical properties as a function of the As content in the pseudo-binary compound UAs_xSe_{1-x}. The characteristic features have been correlated to microscopic properties. The main results are:

i) an unambiguous identification of the interband transitions to be f→d, d→f and (pd)→f like;

ii) the first observation of a magnetic red-shift of the f→d transition energy in a metal;

iii) an negative conduction electron spin-polarization σ_d both in the chalcogenide and in the pnictide. The size of σ_d increases with decreasing number of electrons, which can satisfactorily be explained by a rigid band filling of an exchange split d conduction band; the f state,

however, is pinned at E_F.

iv) the f-magnetic moment is evidenced to be dominantely of orbital character.

4.3 Uranium Monochalcogenides and Pnictides

In the last section we have demonstrated, that the electronic structure of the uranium-chalcogenides and pnictides appears very similar in the system UAs_xSe_{1-x} from the optical and magneto-optical point of view. In this section we will show, that this observation holds in general for all UX compounds (X=S, Se, Te, P, As, Sb), but some special characteristics occur for UTe and USb.

4.3.1 Optical Properties

Because the indices of refraction n and absorption k are necessary for the calculation of σ_{xy} from the Kerr-effect, we review briefly the optical measurements of Schoenes [46] on US, USe, UTe, UAs and USb and present new data for UP.

The available single crystals of UP do not show a mirror like surface upon cleaving. Therefore the measurement of the reflected intensity at normal incidence gives poor results at higher photon energies ($\hbar\omega > 3.5$ eV), which makes a Kramers-Kronig analysis inopportune. Instead, we have measured for two different angles of incidence the ratio $R_{\parallel}/R_{\perp}$ of the reflectivity for light linealy polarized in or normal to the plane of incidence. (The method is described in [66, 67]). By means of Fresnel's equations we computed the refractive index n and the absorption index k from these data. A control measurement on UAs has shown good agreement in the 0.5-5 eV energy range with the optical constants obtained by Kramers-Kronig inversion of the absolute reflectivity.

Fig. 14 shows the absorptive diagonal conductivity σ_{1xx} for all six materials at room temperature. In this figure we have included a decomposition of σ_{1xx} into a free electron part and different Lorentzian shaped interband transitions:

$$\sigma_{1xx}(\omega) = \frac{Nne^2}{m} \frac{\gamma}{\omega^2+\gamma^2} + \sum_i f_i \frac{Ne^2}{m} \frac{\omega^2\gamma_i}{(\omega_i^2-\omega^2)^2 + \omega_i^2\gamma^2} \tag{19}$$
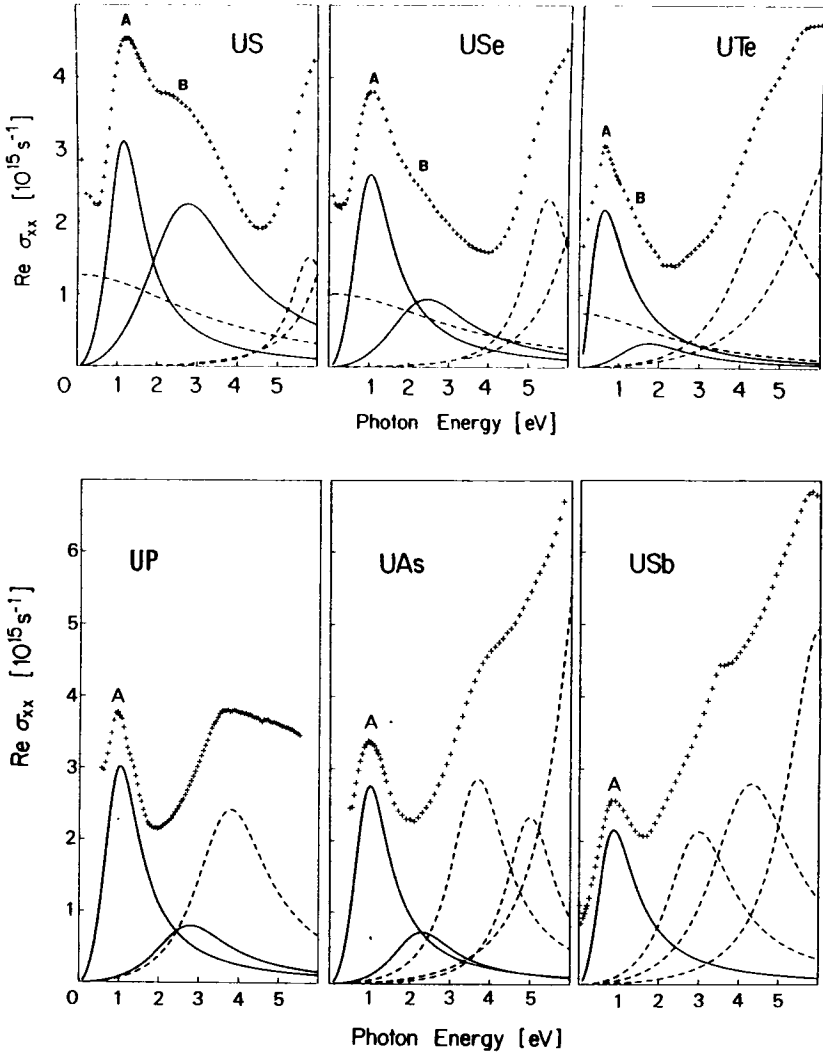
Fig. 14: Lorentz fit of the absorptive diagonal conductivity of the ura-
nium-monochalcogenides and -monopnictides in the energy range of
the f→d and d→f transitions (solid lines) at room temperature.
The fit parameters are collected in tab. 2.

In eq. (19), N is the number of molecules per cm^3 and η stands for the number of conduction electrons per formula unit. The interband fit parameters are oscillator-strength f_i, transition energy $\hbar\omega_i$ and line width $\hbar\gamma_i$. As it can easily be seen from fig. 14, an unambiguous determination of these parameters is only possible at those energies, where different transitions are clearly separated, i.e. in the energy range of the f→d and d→f transitions. Their fit values are given in tab. 2.

		US	USe	UTe	UP	UAs	USb
f→d	$\hbar\omega_A$ (±0.02) [eV]	1.15	1.0	0.6	1.05	1.0	0.9
	$\hbar\gamma_A$ (±0.05) [eV]	1.1	1.2	1.15	1.1	1.1	1.2
	f_A (±0.02)	0.85	0.9	0.9	0.9	0.9	0.9
d→f	$\hbar\omega_B$ (±0.2) [eV]	2.75	2.45	1.75	2.8	2.3	–
	$\hbar\gamma_B$ (±0.3) [eV]	2.8	2.5	2.1	2.3	1.9	–
	f_B (±0.2)	1.55	0.7	0.25	0.5	0.4	–

Tab. 2: Interband transition parameters used for the fit of σ_{1xx} in fig. 14. The values are rounded to 0.05.

Thus, from the fit of the optical data we obtain the in a sense asthonishing result, that the oscillator-strength as well as the line width of the f→d transition are equal for all the six materials whereas the transition energy decreases as expected. In particular the second result is certainly unusual, because one expects a contraction of band width and band separations [68] if for a series of materials MX, the cation M is fixed and the anion is moved down along a column of the periodic system. However, the reason of this contradiction, which occurs only for the f→d transition, may be the strong f-d hybridization, which tends to keep a certain band width, i.e. the band width is determined by hybridization effects and not by the overlap of wavefunctions. This hypothesis is corroborated by a recent calculation of the f-d radial overlap integral (eq. (15)) with LMTO-wavefunctions [69] which gives $|R_{df}|^2 = 6.6 \cdot 10^{-17}$ cm^2 for US and $5.3 \cdot 10^{-17}$ cm^2 for UTe. These numbers are about a factor of

three larger than the overlap in atomic uranium ($2.25 \cdot 10^{-17}$ cm^2 [70]) or for the f and d wavefunctions in UO ($3.1 \cdot 10^{-17}$ cm^2 [71]).

4.3.2 Magneto-optical Results

We have shown in sec. 3.2, that the Kerr-effect is proportional to the sample magnetization. Thus, to obtain a reasonable signal to noise ratio for the energy dependent measurement of θ_K and ϵ_K, one has to choose appropriate temperature and applied field conditions. US, USe and UTe are ferromagnets and hence exhibit a large magnetization at $T \ll T_C$. The applied field is necessary to obtain a one-domain sample, which is the case at B>0.5 T for field cooled samples.

In the case of hard antiferromagnetic materials like the uranium-pnictides, however, one needs a very high field to obtain a sizeable magnetization at all. For UAs, a ferrimagnetic phase can be reached in a field of 10 T (sec. 4.5). For UP, however, the magnetization and hence the Kerr-rotation is rather small even in a field of 10 T. Fig. 15 shows the temperature dependence of θ_K, which exhibits two first order phase transitions at 121 K and 21 K in excellent agreement with magnetization [37] and resistivity [72] measurements. The magnetic structure is only known for T < 21 K to be antiferromagnetic type I for applied fields up to 13T [37].

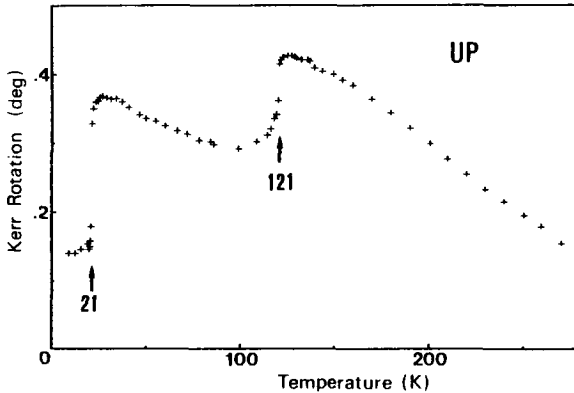Fig. 15: Temperature dependent polar Kerr-rotation of cleaved UP at B=10 T and $\hbar\omega$=1.85 eV.

In a field of 10 T, the magnetization of USb is even lower than in UP be-
cause no magnetic phase transition occurs. Instead of USb, we have there-
fore investigated the pseudo-binary compound $USb_{0.85}Te_{0.15}$ which
shows a ferromagnetic spin structure in a field of 6 T [34]. The magnetic
and crystallographic parameters of importance for the understanding of
the magneto-optical response for the investigated uranium-chalcogenides
and pnictides are summarized in tab. 3.

	US	USe	UTe	UP	UAs	$USb_{0.85}Te_{0.15}$
a [Å]	5.488	5.74	6.155	5.589	5.767	6.197
N [10^{22} cm^{-3}]	2.42	2.11	1.71	2.29	2.08	1.68
μ_{tot} [μ_B]	1.55	1.8	1.9	0.16	0.42	2.8
easy axis	<111>	<111>	<111>	<100>	<110>	<111>
μ_n [μ_B]	1.7	2.0	2.25	1.70	2.25	2.8

Tab. 3: Crystallographic [46] and magnetic data [34, 37, 40, 57, 73] for
uranium-chalcogenides and pnictides. N is the number of molecu-
les per cm^3 and a is the lattice constant. The values displayed
in the last three columns refer to the conditions of the magne-
to-optical measurement displayed in fig. 16.

The energy dependence of the complex polar Kerr-effect for (100)-cleaved
single crystals of uranium-chalcogenides and pnictides is displayed in
fig. 16. In the chalcogenide series, the shape of the Kerr-spectrum is
similar in the low energy part while at higher energies, one structure in
θ_K seems to disappear going from US to UTe. The magneto-optical respon-
se in the pnictide series is similar too, apart of a shift of the spec-
trum to lower energies with heavier anions. For the quantitative discus-
sion of the magneto-optical data, we have calculated σ_{xy}, which is dis-
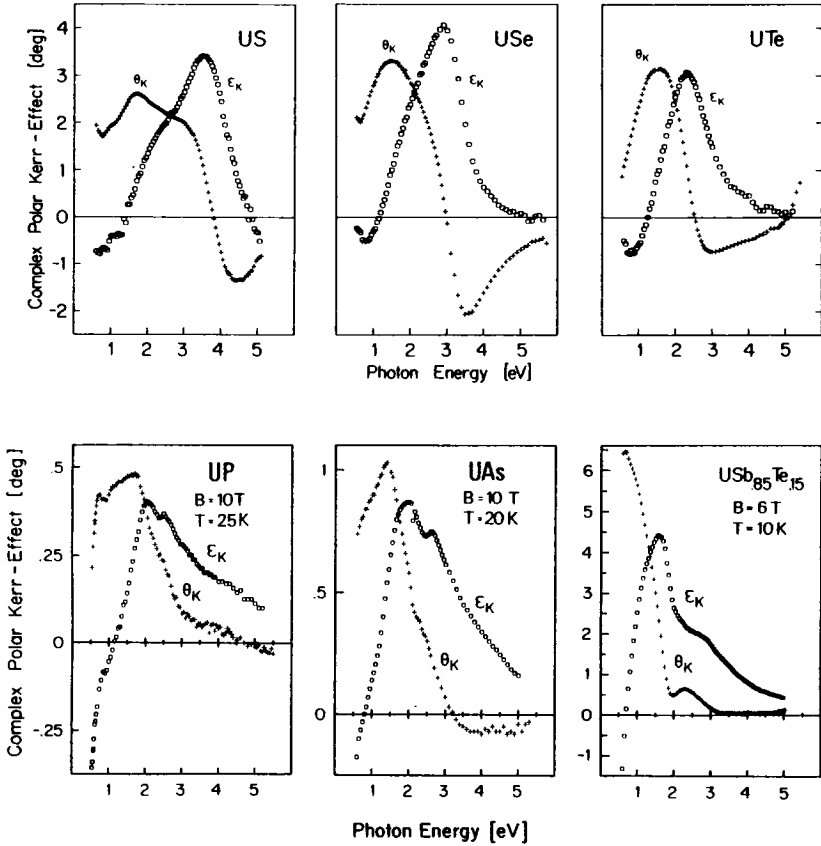played in fig. 17.

Fig. 16: Complex polar Kerr-effect of (100)-cleaved single crystals of uranium-chalcogenides and pnictides. In the case of the chalcogenides, the measurements have been performed at B=4 T and T=15 K.
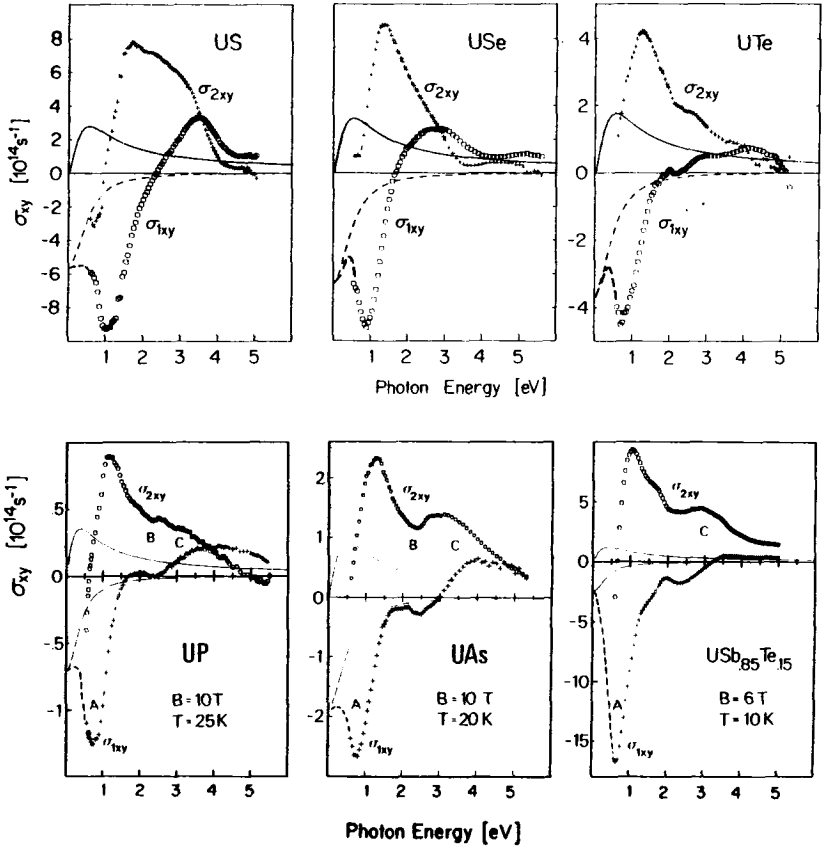
Fig. 17: The real (σ_{1xy}) and imaginary (σ_{2xy}) part of the off-diago-
nal conductivity tensor element for the uranium-chalcogenides
and pnictides as computed from the Kerr-effect and the optical
constants. The dashed line displays the extrapolation of σ_{1xy}
for $\hbar\omega < 0.5$ eV obtained by Kramers-Kronig inversion. The solid
and dash-dotted curves show the estimated free-electron contri-
bution to σ_{2xy} and σ_{1xy}, respectively. Note the different
ordinate scales.

4.3.2.1 Spin-Polarization of Conduction Electrons

The 'diamagnetic' line shape of the lowest energy transition (peak A) in σ_{xy} has already been established for UAs_xSe_{1-x} in sec. 4.2.2.2. The same argument of equal transition energies in σ_{xx} and σ_{xy} (at conditions, where magnetic energy shifts are negligible) leads to the conclusion, that the f→d transiton has the same line shape in all six compounds and allows the estimation of the free electron contribution to σ_{xy} using eq. (8). The result is shown in fig. 17 as the dashed (σ_{2xy}) and dashdotted (σ_{1xy}) lines. The most important result of this analysis of course is, that the spin-polarization is negative for all six compounds, i.e. the number of electrons with antiparallel spin moment compared to the total magnetic moment exceeds the number of those with parallel spin moment. In addition, the sign of σ_{1xy} at $\omega=0$ predicts that all six materials should exhibit the same sign of the anomalous Hall-effect (eq. (6)), which has in fact recently been observed [72, 74].

In a second step, the size of σ_d may be estimated. The spin orbit factor P_0/ev_0 (eq. (10)) increases slightly from $1.95 \cdot 10^{-16}$ sec in US to $3.3 \cdot 10^{-16}$ sec in UTe and $2.1 \cdot 10^{-16}$ sec in UP to $3.4 \cdot 10^{-16}$ sec in $USb_{0.85}Te_{0.15}$ due to the different energies of the f→d transition. Putting these numbers into eq. (8), the product of spin-polarization (in %) with the number of conduction electrons per uranium amounts to -0.46, -0.44 and -0.24 in the chalcogenide series and -0.06, -0.12 and -0.17 in the investigated pnictide series. Due to the small number of free electrons in $USb_{0.85}Te_{0.15}$, the estimated amplitude of the conduction electron curves for this compound (fig. 17) should only be taken as an upper limit.

From the atomic configurations of uranium and the chalcogenides the number of conduction electrons per uranium n is expected to be between 1 and 2. A recent calculation [75] predicts a ground state close to f^3 in the chalcogenides and a fit of the optical reflectivity and σ_{xx} for US results in 1.1 d electrons per uranium [59]. Taking this value for n, the size of σ_d comes out to be $\approx -40\%$ in US and $\approx -35\%$ in USe but only $\approx -20\%$ in UTe. This result is in favorable agreement with spin-polarized photoemission experiments [76], which have shown the same sign and approximate size of σ_d and in particular the reduced σ_d for UTe. The microscopic origin of this reduction will be discussed in sec. 4.4 in the framework of a f-d band model for the explanation of magnetic red- and blue-shifts in USb_xTe_{1-x}.

For uraniummonopnictides the number of conduction electrons per uranium
is expected to be between 0 and 1. A fit of the optical data results in
about 0.45, 0.35 and 0.2 e$^-$/U for UP, UAs and $USb_{0.85}Te_{0.15}$, respec-
tively. However, these numbers can only be taken as a crude estimate be-
cause of the reduced energy range of the reflectivity measurements (the
lower limit for the pnictides was 0.03 eV instead of 0.001 eV for US [46,
77] and USe [12]) and the obvious deviations from Drude behavior. On the
other hand, in a recent interpretation of transport properties of the
uranium-pnictides similar numbers are postulated [72]. Taking therefore
the values cited above, the spin-polarization for the field and tempera-
ture conditions mentioned in fig. 17 is found to be -15%, -30% and -100%
for UP, UAs and $USb_{0.85}Te_{0.15}$, respectively. In other words, the lo-
cal spin-polarization (sec. 4.2.2.2) amounts to -100% in all uranium-
pnictides, i.e. only one spin-polarized d subband is occupied.

4.3.2.2 The f→d Transition

The subtraction of the conduction electron contribution from the measured
σ_{xy} results in the pure interband signal. It is obvious from fig. 17,
that the lowest energy interband transition around 1 eV exhibits a 'dia-
magnetic' line shape in all six compounds and is therefore clearly iden-
tified as an f→d excitation (see also sec. 4.2.2.3). Table 4 lists the

	US	USe	UTe	UP	UAs	$USb_{0.85}Te_{0.15}$
$\hbar\omega_A$ ±2% [eV]	1.13	0.94	0.77	0.78	0.82	0.65
$\langle\sigma_{xy}\rangle$ [10^{30} sec^{-2}]	10	9.4	5.0	1.2	2.3	16
$\langle\sigma_{xy}\rangle/N\mu_{tot}$ [10^7 sec^{-2}cm$^3\mu_B^{-1}$]	2.7	2.5	1.5	2.9	2.6	3.3

Tab. 4: Observed transition energy in σ_{xy}, total weight $\langle\sigma_{xy}\rangle$ and
normalized off-diagonal oscillator strength $\langle\sigma_{xy}\rangle/N\mu_{tot}$ of
the f→d transition in the uranium-chalcogenides and -pnictides.
The field and temperature conditions are mentioned in fig. 17.
The approximate errors for $\langle\sigma_{xy}\rangle$ and $\langle\sigma_{xy}\rangle/N\mu_{tot}$ are ±10%
and ±15%, respectively.

energy, the total weight and the normalized off-diagonal oscillator strength of the f→d transition for the six investigated compounds. The transition energy decreases slightly along the chalcogenides and pnictides series but the width of the peak in σ_{1xy} remains nearly constant. Hence, the trends in σ_{xy} corroborate the results of the Lorentz-fit of σ_{xx} (tab. 2), presented in sec. 4.3.1.

A comparison of $\langle\sigma_{xy}\rangle$ and the total magnetic moment at measuring conditions indicates, that $f_{xy} \approx \langle\sigma_{xy}\rangle/N \approx \mu_{tot}$, i.e. the off-diagonal oscillator strength normalized to magnetization is approximately the same along the chalcogenides and pnictides series except for UTe. In detail, the experimental diagonal (tab. 2) and off-diagonal (tab. 4) total weigths are expressed for these five compounds by the simple equations:

$$\langle\sigma_{xx}\rangle \approx 3.3 \cdot 10^{30} \cdot N \ \left[\text{sec}^{-2}\right]$$

$$\langle\sigma_{xy}\rangle \approx 2.8 \cdot 10^{29} \cdot N \cdot \mu_{tot} \ \left[\text{sec}^{-2}\right]$$

(20)

where the units of N and μ_{tot} are 10^{22}cm^{-3} and μ_B, respectively.

To explain these values, we propose the modified atomic model mentioned in sec. 3.2, which has been successfully applied for Gd [27] and the Europium-chalcogenides [8]. The dipole matrix element is evaluated in the approximation of atomic f and d wavefunctions to be $\left|\langle b|\vec{r}|a\rangle\right|^2 = 3R_{df}^2 \approx 2\cdot10^{-16} \ \text{cm}^2$ for US, using the LMTO overlap integral calculated by Brooks [69]. Taking this value for the matrix element, eq. (16) reproduces the measured $\langle\sigma_{xx}\rangle$ if we assume an occupation of 1.4 f states. This number has to be viewed as an 'optical' occupancy which is expected to be less than the real occupancy in the case of correlated states [63]. Thus, the deviation from the expected number of 2.5 – 3 f electrons may be interpreted in terms of nonvanishing correlation effects which corroborates the model of an narrow f band in US.

One further interesting result may be obtained, if the integration in eq. (16) is dropped. In this case, the expression for the absorptive diagonal conductivity becomes

$$\sigma_{1xx} = \frac{\pi Ne^2}{\hbar} \ E_{\alpha\beta} \ \left|M_{xx}\right|^2 \ J_{\alpha\beta}$$

(21)

where $J_{\alpha\beta}$ is the joint density of states in units of states per eV.

This equation indicates, that the width of $J_{\alpha\beta}$ which is given approximately by the sum of the d and f band widths, is equal to the width $\hbar\gamma$ of σ_{1xx} for the f→d transition. The experimental value (fig. 14 and tab. 2) is about 1.1 eV in all UX and UZ compounds. A comparison with similar materials like UO_2 and EuS indicates, that the d width is expected to be >1 eV, i.e. the f band width does certainly not exceed a few tenth of an eV for the uranium-monochalcogenides and monopnictides.

The theoretical expressions eqs. (12) and (16) for the diagonal and off-diagonal weights can be combined giving:

$$\frac{\langle\sigma_{xy}\rangle}{\langle\sigma_{xx}\rangle} = \sigma_j \frac{\sum (\omega_{\alpha\beta}^- |\langle\beta|x-iy|\alpha\rangle|^2 - \omega_{\alpha\beta}^+ |\langle\beta|x+iy|\alpha\rangle|^2)/2}{\omega_{\alpha\beta} \; |\langle b|\bar{r}|a\rangle|^2} \qquad (22)$$

i.e. the ratio of $\langle\sigma_{xy}\rangle$ and $\langle\sigma_{xx}\rangle$ only depends on the orbital parts of the matrix elements and the joint spin-polarization of the initial and final state. In the framework of the microscopic model presented in sec. 3.2, the difference $\sum (\omega_{\alpha\beta}^- |\langle\beta|x-iy|\alpha\rangle|^2 - \omega_{\alpha\beta}^+ |\langle\beta|x+iy|\alpha\rangle|^2)/2$ is evaluated to be $\approx 0.63 \; R_{df}^2$ using the atomic spin orbit parameters $\zeta_f=0.18$ eV and $\zeta_d=0.15$ eV [70]. Taking a width of 1 eV for the f→d transition, the model predicts

$$\frac{\langle\sigma_{xy}\rangle}{\langle\sigma_{xx}\rangle} \approx 0.21 \; \sigma_j \qquad . \qquad (24)$$

The experimental value of this ratio for all investigated UX_xZ_{1-x} compounds except UTe is given by eq. (20) to be about $0.085\cdot\mu_{tot}$. Thus, the f spin-polarization comes out to be $\approx 60\%$ in US and increases with heavier anion to reach 100% in $USb_{0.85}Te_{0.15}$ of course within the assumption, that the spin-orbit parameters are the same for all compounds.

Apart from the spin-polarization and the energy and width of the f states, the combination of optics and magneto-optics provides additional information about the symmetry of f and d states. If electronic wavefunctions are subject of a crystalline electric field, the degeneracy of states will be lifted according to the crystal symmetry. In the case of d orbitals in a NaCl-type lattice, two energy levels with t_{2g} and e_g symmetry are expected which leads in general to a double structure of the

f→d transition. The size of the t_{2g} - e_g energy separation is expec-
ted from a simple point charge model to be ≈1.5-3 eV. Such a double
structure has in fact been observed in many compounds like the Eu- and
Tm-chalcogenides and UO_2 with an experimental t_{2g} - e_g separation of
about 2 eV. In the case of the investigated uranium compounds, however,
the magneto-optical results (fig. 16) clearly evidence the existence of
only one f→d structure, located around 1 eV, in the energy range up to
5.7 eV. The argument of a second transition beyond the upper limit of our
measurement seems to be unphysical because it implies a crystal field
splitting exceeding 5 eV. Especially for compounds with a large lattice
constant this value is by far out of the expected range. On the other
hand, a crystal field splitting in the order of 3 eV for the d states is
observed in the p→d excitation spectrum for e.g. US [46] and band struc-
ture calculations find a value of ≈3 eV for US [44]. Thus it seems to be
appropriate to interprete the absence of the f→de$_g$ transition as an ef-
fect of selections rules between crystal field split f and d states.
Fig. 18 schematically indicates by arrows the allowed transitions between
all possible crystal field levels at the Γ-point [78]. At the right side
in this figure, the possible symmetries derived from f states are dis-
played.It becomes clear that only one f→d transition is expected if the
occupied f level is of $\Gamma_{2'}$-symmetry. Hence we propose from optical and
magneto-optical spectroscopy, that the ground state of the f→d transition
is of $\Gamma_{2'}$ symmetry (or $\Gamma_{7'}$-symmetry in the double-group notation,
which includes the spin) in the six investigated compounds. In fact,
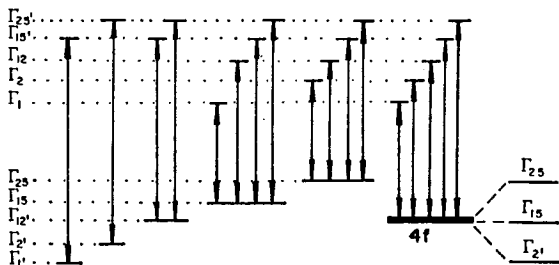various band structure calculations corroborate this finding [45, 65, 68,
79, 80].

Fig. 18: Selection rules of optical dipole transitions at Γ for elec-
tronic states in a cubic crystal field [78].

A further interesting feature of the f→d transition in uranium chalcoge-
nides and pnictides is the difference of $\hbar\omega_A$ above and below the magne-
tic ordering temperature (tabs. 2 and 4). We find a red-shift of the
whole f→d peak by 0.2 eV in UP and UAs, while for USb_xTe_{1-x} a double
structure appears with decreasing temperature. In the chalcogenide seri-
es, the magnetic red-shift is small for US and USe, but shows the oppo-
site sign for UTe. Because of the extraordinary behavior of UTe and
$USb_{0.85}Te_{0.15}$, we will study the f→d transition and its correlation
to the magnetic and electronic structure   for USb_xTe_{1-x} in the next
section. The behavior of UP and UAs, on the other hand, has already been
discussed in sec. 4.2.2.3.

At the end of this section, some remarks should be made about the reduced
magneto-optical response of UTe (tab. 4). Because $\langle\sigma_{xx}\rangle$ of UTe shows no
reduction compared with the other compounds (tab. 2), the anomaly of
$\langle\sigma_{xy}\rangle$ is certainly not due to a lower density of states. In addition it
is improbable, that the f spin polarization is reduced by a factor of 2
because of the large ferromagnetic moment. Hence, the diminution of
$\langle\sigma_{xy}\rangle$ has to be the consequence of a modified matrix element, which in
the framework of our model means, that the spin-orbit energy is reduced
by a factor of 2.

The hypothesis of a ground state with critical conditions for UTe is cor-
roborated by the observation, that the magneto-optical response of UTe
can be twofold, depending on the sample. The Kerr-spectrum shown in fig.
16, which is reproduced in the 0-3 eV energy range on the right side of
fig. 19 is of the kind which is similar to all other UX_xZ_{1-x} com-
pounds. The left part of fig. 19, however, which shows the magneto-opti-
cal spectrum for the second type of UTe, is very similar to the Kerr-ef-
fect of Tm-compounds [30]. The microscopic origins of these two characte-
ristic spectra are well understood. While the first one is caused by an
f→d interband transition, the second one is due to different plasma fre-
quencies for right and left hand circularly polarized light and the
interband transition is suppressed. The size of the Kerr-signal of $9°$ in-
dicates, that this plasma edge splitting has the extraordinary magnitude
of ≈0.1 eV.

It is important to note, that the magnetic behavior of the sample volume
probed by the Kerr-effect has been established by magneto-optics to be
equal for the two types of UTe. In both cases, the ferromagnetic ordering
temperature was found to be 104±2 K. Fig. 20 shows a magneto-optical
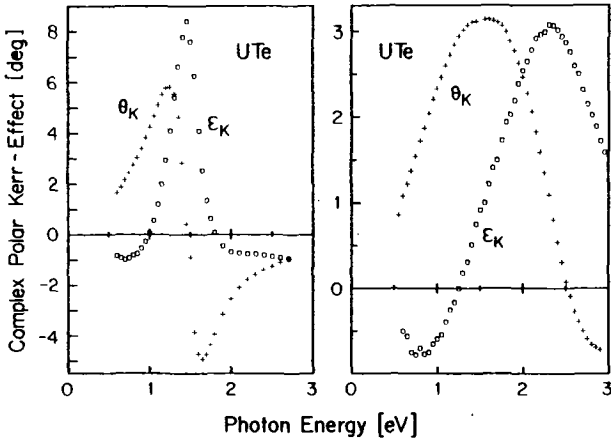hysteresis loop measurement $\theta_K(B)$ at 10 K for the second type of UTe,

Fig. 19: Polar Kerr-effect for the two different types of UTe samples at
B=4T and T=15K. Right part: f→d interband transition; left part:
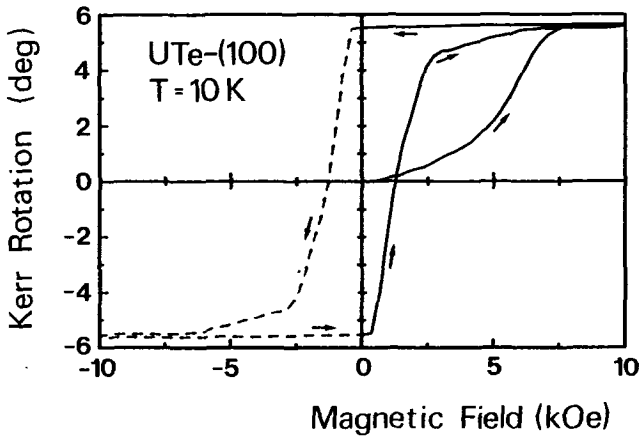plasma edge splitting.

Fig. 20: Magneto-optical determination of the magnetic hysteresis loop
for the type of UTe, which shows the characteristic features of
a plasma edge splitting.

which agrees perfectly with bulk magnetization measurements [81]. Thus we conclude, that the probed material was UTe in both cases. The characteristic differences may originate from slightly different lattice constants of the two samples, which cause drastically different f-d ground states. For the first type, the f electrons form a narrow band at E_F similar to the other UX compounds which results in a magneto-optical response typical for UX_xZ_{1-x} materials. The second type of UTe, however, may have a slightly larger lattice constant, inducing a mixed valent behavior of f-d electrons. This hypothesis is corroborated by the observation, that f→d transitions, which are clearly resolved in semiconducting $TmSe_{0.32}Te_{0.68}$, seem to be absent in mixed valent $TmSe_{0.32}Te_{0.68}$-(polished) [82]. However, the physical mechanism which suppresses the interband transition is not known yet. For a clarification of this interesting problem, the investigation of the f state properties in chemically enlarged UTe crystals are in preparation.

4.3.2.3 Excitations of p and d Electrons

Both in the series of uranium-chalcogenides and -pnictides one further dominant peak apart from the f→d transition around 1 eV is observed in σ_{xy} (fig. 17). But as we have pointed out in sec. 4.2.2.3, the microscopic origin is different for the chalcogenides and pnictides.
The center of the valence p-band in the former group of compounds is found from photoemission experiments at 5.0, 4.5 and 3.8 eV binding energy for US, USe and UTe, respectively [49, 54]. In addition, p→d transitions are known to contribute to σ_{1xx} only at $\hbar\omega > 4.5$ eV [46]. Fig. 17 evidences, that the magneto-optical signal from p excitations in these materials is less than $1 \cdot 10^{14}$ sec^{-1} at magnetic saturation, if it is present at all. Hence, only d and f electrons can be the origin of peak B in fig. 17. In sec. 4.2.2.3 it has been argued from the characteristic decrease of the oscillator strength in the UAs_xSe_{1-x} system that an interpretation in terms of an d→f transition is obvious. This model is corroborated by the strong decrease of the transition energy $\hbar\omega_B$ and oscillator strengths f_{xx} and f_{xy} going from US to UTe (tab. 5), which excludes again an interpretation in terms of an second f→d transition.
This decrease of f_{xx} as well as of f_{xy} by a factor of 5.5 from US to USe is a puzzling result. A reduction of d occupation can not account for this effect because the number of d electrons varies at maximum between 1

	US	USe	UTe
$\hbar\omega_B$ [eV]	2.75±0.1	2.4±0.2	1.75±0.3
$\langle\sigma_{xx}\rangle$ [sec^{-2}]	$13.5\cdot10^{30}$	$5.4\cdot10^{30}$	$2.1\cdot10^{30}$
$\langle\sigma_{xy}\rangle$ [sec^{-2}]	$14.5\cdot10^{29}$	$5.0\cdot10^{29}$	$2.5\cdot10^{29}$

Tab. 5: Transition energy in σ_{xy} and the diagonal and off-diagonal weigths for the d→f transition in uranium-monochalcogenides. The experimental conditions are given in figs. 14 and 17.

and 2 electrons per formula unit. Indeed, the intraband contributions to σ_{1xx} and σ_{xy} (figs. 14 and 17) have a similar size along the chalcogenides series. The decrease in oscillator strength of the d→f transition, however, may be explained by an increasing localization of the final states. For strictly localized f-states, as in many rare earth compounds, no d→f transitions have been observed at all [63]. Thus the decrease of f_{xx} and f_{xy} from US to UTe points to a substantial localization of the f states for the compounds with heavier anions.

Of course, the d→f transition is present in the light uranium-pnictides too, but it is weakened by the lower d occupation, which has been evidenced for UAs in sec. 4.2.2.3. However, even in the off-diagonal conductivity, peak B is hardly resolved because of the strong overlap with the dominant transitions A and C (fig. 17).

Structure C in σ_{xy} of the uranium-pnictides has about the same energy and similar relative weigths in the three compounds. This dominant feature in the magneto-optical spectra is also resolved in the fit of σ_{1xx} around 3.5 eV (fig. 14). A comparison with the uranium-chalcogenides evidences, that this transition is a special feature of the pnictides. Its microscopic explanation is most probably the excitation of high orbital momentum states at the top of the valence band, as has been discussed for UAs_xSe_{1-x} in sec. 4.2.2.3. Different band structure calculations find the p-band at 2.3±0.4 eV binding energy for the three materials [45, 47, 60, 75, 80], which is in good agreement with photoemission results on UAs and USb [49, 50, 52, 54].

4.3.3 Summary

In this section the variation of the magneto-optical spectrum along the chalcogenide and pnictide series have been discussed. The f states behave similar in all compounds except USb, which shows a fine structure in the f→d transition feature. This special aspect is discussed in detail in sec. 4.4. In the case of UTe, the f band width approaches a critical value which leads to a twofold magneto-optical behavior.

The conduction electrons are negatively spin-polarized in all six compounds. In the uranium-pnictides the size of the local spin-polarization σ_d reaches -100% due to the small number of d electrons, while in the chalcogenides σ_d decreases from US to UTe by a factor of 2.

In the uranium-pnictides a magnetic red-shift of the f→d transition energy in the order of 0.2 eV has been established. Together with the conduction electron polarization, this leads to the conclusion, that the f-moment is dominated by the orbital part.

Magneto-optical response of bonding d electrons has been observed only for uranium-pnictides which corroborates a similar f occupation in the chalcogenides and pnictides as it has been concluded from the f→d oscillator strength, i.e. mainly d and s electrons of uranium take part in bonding while the f occupation is near 3 in all compounds.

4.4 Magnetic Red-Shift in Uranium Compounds

We have pointed out in sec. 4.3.2.3, that the f→d transition energies measured above and below the magnetic ordering temperature do not coincidence (tabs. 2 and 4). Especially for the uranium pnictides, a red-shift in the order of 0.2 eV has been established, while in the case of UTe, a blue-shift of about 0.1 eV has been observed. This extraordinary magneto-optical effect is well known from some magnetic semiconductors [83] and has been interpreted by a coupling of the conduction band to inner shell f electrons.

4.4.1 The f-d Exchange Interaction

In 1962 Vonsovskii and Izyumov [84] proposed, that in a ferromagnetic metal the electrons move in spin-polarized subbands. These ideas have been extended to semiconductors, where the spin-dependent splitting of the

conduction band leads to a red-shift of the absorption edge [9]. In the so-called s-f or d-f model the total Hamiltonian is given by the following expression [85]

$$H = H_c + H_f + H_{df} \qquad (24)$$

where H_f describes the intra-f interactions and the conduction electron part H_c includes kinetic energy and Coulomb interaction terms. The two subsystems are coupled by a local (intra-atomic) exchange interaction H_{df}

$$H_{df} = -J_{df} \sum_i \vec{s}_i \vec{S}_i \qquad (25)$$

with the intra-atomic d-f exchange constant J_{df}. Instead of the f spin $\vec{S}$, which is of course the appropriate description for the Eu-chalcogenides ($4f^7$; $^8S_{7/2}$), the total f momentum should be used in eq. (25) for $\vec{L} \neq 0$ states, i.e. $\vec{S}_i$ should be replaced by $(g-1)\vec{J}$ where $\vec{J}$ is the total angular momentum and g the Landé factor [86].

In the framework of this theory [85,87] the energy of the conduction band center for the ↑-spin direction is given in the approximation of small exchange ($J_{df} < 1$ eV) by

$$T_\uparrow = T_0 - J_{df} \, s_\uparrow \, \langle S^z \rangle + I \langle n_\downarrow \rangle \quad . \qquad (26)$$

In this equation T_0 is the undisturbed d band center, $\langle S^z \rangle$ is the magnetization of the f system, I means the intra-atomic d-d Coulomb matrix element and $\langle n_\downarrow \rangle$ is the d band occupation with opposite spin. For the other spin direction, the sign of the second term on the right side of eq. (26) has to be changed. The maximum shift of the f→d transition in the case of an empty $d_\downarrow$-band is given by eq. (26) to be

$$J_{df} \, \langle S^z \rangle_{max} \, /2 \qquad (27)$$

and it is reduced if $\langle n_\downarrow \rangle \neq 0$.

In a more general treatment of d-f exchange [85,87], i.e. without restricting the size of J_{df}, the conduction band is shown to split into six subbands for each spin direction. Of course these quasiparticle

levels show a large overlap for small values of J_{df} thus approaching
the two subband approximation. However, the interesting point of this ge-
neralized analysis is, that the spectral weights ('reduced density of
states') of the subbands variate extremely if $\langle S^z \rangle$ approaches satura-
tion magnetization M_0, i.e. although the d band center does not show any
appriciable shift at high magnetizations, new peaks may appear. In fact,
this effect has been observed for EuS in the magnetization range between
$0.9M_0$ and M_0 [88].

It is obvious from the previous theory, that large red-shifts are expec-
ted only for ferromagnets and perhaps ferrimagnets. In the case of anti-
ferromagnets, however, a small blue-shift of the f→d energy is the common
behavior although some materials are known which also display a small
red-shift [83]. The decisive factor is the spin structure of the antifer-
romagnet which determines sign and magnitude of the local magnetic ex-
change energy [89]. But compared to ferromagnets, the size of the shift
is expected to be much smaller.

Finally it should be mentioned that the temperature dependence of the f→d
transition energy follows the short range spin correlation function as it
has been shown quantitatively by Rys et al [86]. In high fields or at low
temperatures, however, spin-correlation function and Brillouin function
will be similar.

4.4.2 The Pseudo-Binary System USb_xTe_{1-x}

As we have mentioned in sec. 4.3.2.2, red-shifts of the same size have
been observed both in ferromagnetic $USb_{0.85}Te_{0.15}$ and ferri-(antifer-
ro-)magnetic UAs and UP. We conclude further from the results presented
up to now, that the sign of the magnetic shift must change in the system
USb_xTe_{1-x} because for UTe, a blue shift has been established.

To study these different aspects of the f→d transition we have intensive-
ly investigated the system USb_xTe_{1-x}. In zero field, compounds with
$x < 0.82$ are ferromagnets, while for $x > 0.82$ ferri- or antiferromagnetic or-
dering occurs [38]. The magnetic parameters of the investigated composi-
tions are summarized in tab. 6. The lattice parameter is nearly constant
throughout the series.

x	0.9	0.85	0.8	0.5	0
$T_{C,N}$ [K]	205	204	204	201	102
μ_{tot} [μ_B]	0.91 B=4T; T=10K	2.8 B=6T; T=10K	2.58	2.24	1.91
μ_n [μ_B]	2.8	2.8	2.64	-	2.25

Tab. 6: Magnetic parameters in the system USb_xTe_{1-x}: ordering tempe-
rature T_N or T_C [38]; magnetization moment in the easy dir-
ection μ_{tot} [38,81,90]; neutron moment μ_n [34,90].

4.4.2.1 Size of Red-Shift versus Type of Magnetic Order

We will demonstrate in this section, that the dependence of the magnetic
red-shift on the type of magnetic ordering can be studied in the system
USb_xTe_{1-x} without drastic changes of other parameters like the d oc-
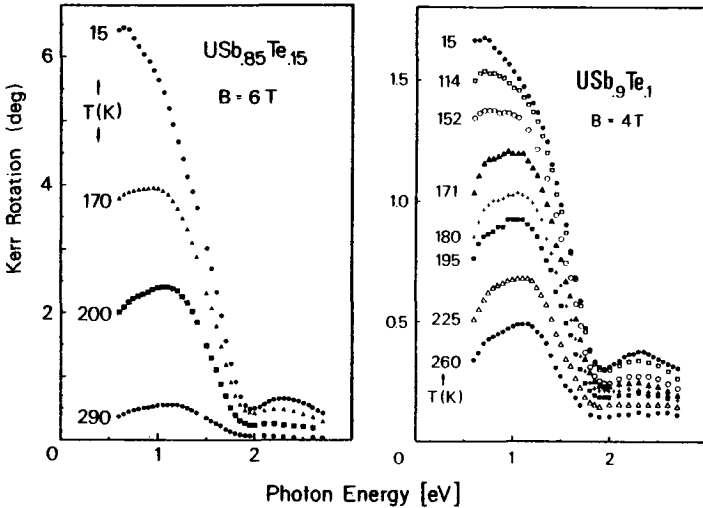cupation. Fig. 21 displays the Kerr-rotation in the f→d transition region

Fig. 21: Polar Kerr-effect of cleaved $USb_{0.9}Te_{0.1}$ and $USb_{0.85}Te_{0.15}$ at
different temperatures. At the mentioned applied fields the type
of magnetic ordering is ferri- and ferromagnetic, respectively.
Note the different ordinate scales.

of ferrimagnetic $USb_{0.9}Te_{0.1}$ and ferromagnetic $USb_{0.85}Te_{0.15}$ at different temperatures. It is obvious, that the behavior of the f→d feature is similar in both compounds. Only the size of θ_K reflects the by a factor of 4 higher magnetization in $USb_{0.85}Te_{0.15}$ compared to $USb_{0.9}Te_{0.1}$ whereas the shape and in particular the change of shape with temperature are nearly the same. In detail, the f→d transition shows a double structure in θ_K even at $T\gg T_{C,N}$ and a transfer of oscillator strength from the higher energy part to lower energies with decreasing temperature is clearly observed. This behavior may be analyzed in detail in terms of the off-diagonal conductivity. Fig. 22 displays the absorptive, off-diagonal element, normalized to its maximum value, at four temperatures. It can be seen, that the f→d feature consists of one 'paramagnetic' peak around 1.5 eV and the dominant 'diamagnetic' structure at lower energies. While the latter one displays a red-shift of about 0.15
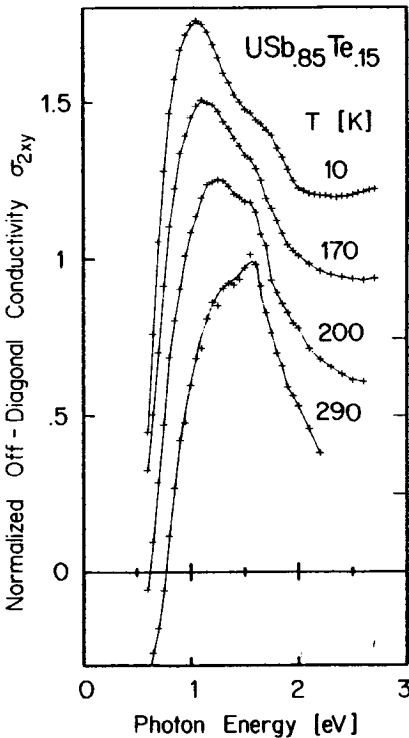

Fig. 22:
Absorptive off-diagonal conductivity of $USb_{0.85}Te_{0.15}$ at B=6 T and different temperatures. Each curve is normalized to its maximum value. For clarity, the spectra for T=200, 170 and 10 K are vertically shifted by 0.25, 0.5 and 0.75, respectively.

eV between 290K and 10K at B=6 T, the former structure shifts a little to higher energies with decreasing temperature.

According to the theory (sec. 4.4.1), the shift of the f→d transition energy as a function of temperature should be proportional to the sample magnetization in high fields and at moderate temperatures. Fig. 23 shows a plot of $\hbar\omega_A$, as determined from the peak energy in σ_{1xy}, versus temperature for $USb_{0.9}Te_{0.1}$. In the same figure, the normalized magnetization from a bulk magnetization measurement is displayed [81]. The fit of $\hbar\omega_A(T)$ is excellent and allows the determination of $\hbar\omega_A(M=0)$ to be 0.85 eV which agrees favourably with the value from reflectivity measurements of $\hbar\omega_A(M=0) = 0.87\pm0.02$ eV (tab. 2). By this way, the total shift for $USb_{0.85}Te_{0.15}$ and $USb_{0.9}Te_{0.1}$ is found to be 0.2 ± 0.02 eV.

The observed temperature dependence of the f→d transition in σ_{xy} for both uranium compounds exhibits strong similarities to the behavior of the europium chalcogenides [8]. For the latter materials the $f\rightarrow f^{n-1}dt_{2g}$ feature in the Faraday-rotation shows four peaks due to an f^{n-1} final state splitting [8]. Apart from a redistribution of oscillator strength for these structures with decreasing temperature, only the lowest energy
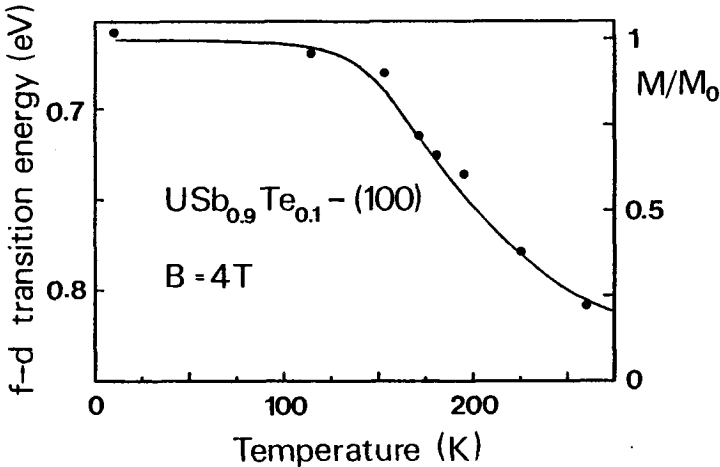

Fig. 23: f→d transition energy in σ_{xy} versus temperature for $USb_{0.9}Te_{0.1}$ at B=4 T (dots) and normalized bulk magnetization M/M_0 (solid line) for the same field.
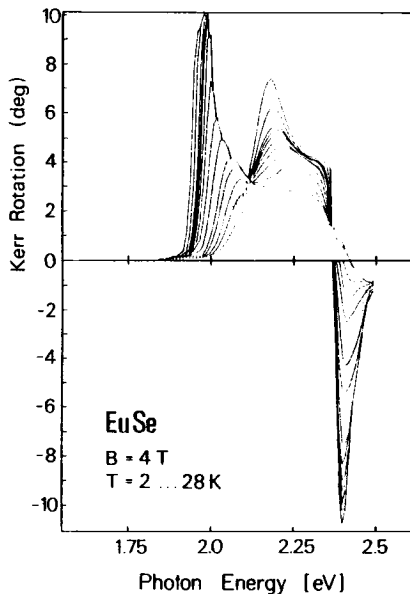
Fig. 24: Polar Kerr-rotation of cleaved EuSe at B=4 T and different tem-
peratures between 2 and 28 K.

peak shifts to the red. This characteristic behavior which has its ana-
logy in the Kerr-rotation [91] is displayed in fig. 24 for EuSe in the
ferromagnetic phase.

While the red-shift for the discussed uranium-compounds is certainly
caused by the d band, the origin of the double structure of the f→d tran-
sition may be either an initial or a final state effect. In the latter
case, atomic splittings of the $f^{n-1}d$ configuration exceed the band
broadening similar to the Eu-chalcogenides, i.e. this description leads
to a picture of localized f electrons. The alternative to this view of
the electronic structure are two transitions at different symmetry points
in the Brillouin zone, which leads to a band description. Using the ex-
perimental data presented up to now, it is not possible to favour one of
these models. However, the study of the whole system USb_xTe_{1-x} may
give additional hints which perhaps allow the decision for one model be-
cause we know already from sec. 4.3.2.2, that within this series the

double structure for x=0.85 and 0.9 changes to a single structure for x=0.

It should be mentioned, that an interpretation of the double structure in terms of a Brillouin-zone doubling, which is well known for antiferromagnets, is improbable because the additional structure should vanish if the spins are alligned by a strong external field [92, 93]. Obviously, this does not happen in $USb_{0.85}Te_{0.15}$.

4.4.2.2 Localized versus Itinerant f States in USb_xTe_{1-x}

In the previous sections it has been demonstrated, that the f→d energy shows a red-shift of about 0.2 eV in $USb_{0.9}Te_{0.1}$, while for UTe a blue-shift around 0.1 eV is observed. Thereupon we have measured the Kerr-rotation and ellipticity in the 0 - 3 eV energy range for several USb_xTe_{1-x} compounds at different temperatures. We have found, that the change from the double structure behavior in θ_K or σ_{2xy} to a single peak occurs abruptly near x=0.8. Together with this change in shape, the sign of the shift alters. This behavior is visualized distinctly by a comparison of σ_{2xy} at magnetic saturation for compounds with x=0.85 and x=0.8 (fig. 25). While for zero magnetization, the f→d
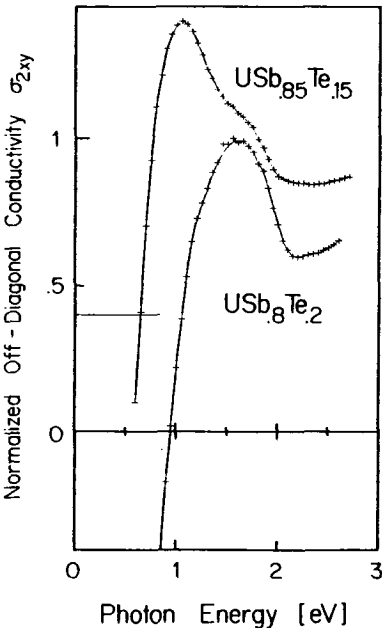

Fig. 25:
Absorptive off-diagonal conductivity σ_{2xy} normalized to its maximum values for the two compositions x=0.85 and 0.8 at magnetic saturation (B=6 T, T=10 K and B=4 T, T=10 K, respectively). For the former compound, zero is shifted vertically by 0.4.

transition occurs at 0.86±0.02 eV for both compounds, we find the reso-
nance energy at magnetic saturation for the former compound at 0.65 eV
but for the latter one at 0.95 eV. Hence, a change of the tellurium con-
centration by only 5% shifts the transition energy by as much as 50%.

Fig. 26 collects the observed total magnetic shifts in the system
USb_xTe_{1-x}. While for $x<0.8$ the resonance energy increases with magne-
tization, it lowers for compositions with $x>0.8$. The abrupt jump at $x=0.8$
is corroborated by the fact, that samples with nominal composition $x=0.8$
exhibit different shifts from sample to sample.

The distinct spectra for the compounds $x=0.8$ and $x=0.85$ certainly reflect
two drastical different f and d electronic densities of states. The
change from the situation with higher f→d transition energy to the one
with lower transition energy may also be generated by the application of
pressure although the microscopic reasons may be different. Using the
fact, that polishing of a surface may be equal to a pressure of 10-15kbar
[82, 94], fig. 27a compares the Kerr-rotation at magnetic saturation of
(100)- and (111)-polished $USb_{0.8}Te_{0.2}$ with the spectrum of a cleaved
sample.In fig. 27b, the normalized absorptive conductivity σ_{2xy} for
(100)-polished and -cleaved samples are displayed for the same tempera-
ture and field conditions. The comparison shows uneqivocally, that due to
the polishing treatment the f→d transition energy has shifted from 0.95

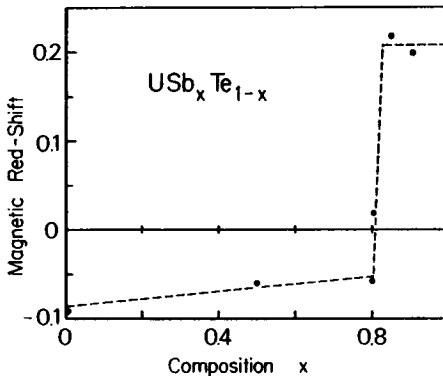Fig. 26: Observed magnetic red-shift of the f→d transition energy in
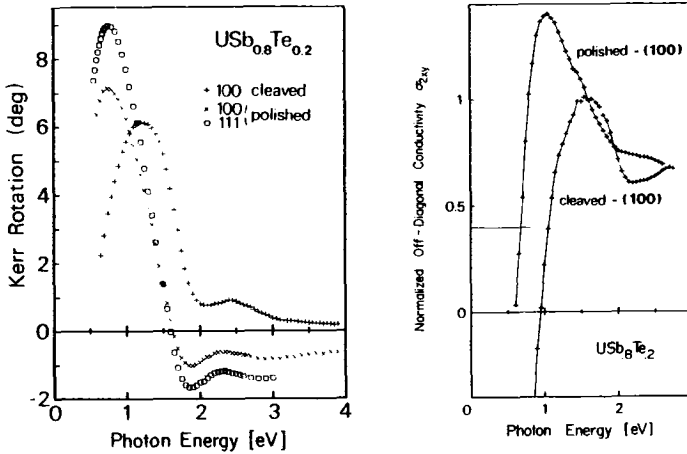USb_xTe_{1-x} versus composition x.

Fig. 27: a) Kerr-rotation of (100)- and (111)-polished compared to (100)-
cleaved crystals of $USb_{0.8}Te_{0.2}$ at magnetic saturation
(B=4T, T=10K).
b) Normalized absorptive conductivity σ_{2xy} for polished and
cleaved $USb_{0.8}Te_{0.2}$ at magnetic saturation.

to 0.67eV. The low f→d energy for the polished sample agrees well with
the one found for cleaved $USb_{0.85}Te_{0.15}$ (fig. 25) and the similarity
of the corresponding σ_{xy} spectra is obvious. However, there exists an
important difference: while for cleaved $USb_{0.85}Te_{0.15}$ the f→d energy
shifts with increasing magnetization from 0.85 to 0.65eV, this energy is
nearly independent of magnetization for polished $USb_{0.8}Te_{0.2}$.

It should be noted in this context, that no substantial change of the f→d
energy upon polishing has been observed for UAs and US (see fig. 1), i.e.
the dt_{2g} – de_g crystal field splitting seems not to increase substan-
tially and therefore it is most probably not the driving mechanism for
the lowering of the f→d transition energy upon polishing. This observa-
tion contrasts the experience with certain semiconductors [82, 94] cer-
tainly because of the partial occupation of the dt_{2g} level in the ura-
nium chalcogenides and pnictides.

A successful model of the electronic states in USb_xTe_{1-x} has to explain the following observations:

i) red- and blue shift in USb and UTe, respectively, with an abrupt change in sign at x=0.8;

ii) double structure of the f→d feature for x>0.8 and single structure for x<0.8;

iii) transition energies at zero magnetization (tab. 2) and at saturation magnetization (tab. 4);

iv) *conduction electron spin-polarizations of -100% in* $USb_{0.85}Te_{0.15}$ and only -20% in UTe.

v) pressure induced change of the f→d energy in $USb_{0.8}Te_{0.2}$.

In the following we will discuss the consequences for the model of f and d states which emerge from these observations both in a localized and an itinerant description of the f electrons.

Band model of f electrons: Within this model the occupied f-band approaches the Fermi-energy at certain symmetry points of the Brillouin zone (e.g. at L and Γ) whereas due to the strong pf hybridization it is pulled away from E_F e.g. at the X point. The d band in fcc symmetry [68], on the other hand, is lowest in energy at X and highest at the L-point within the L-Γ-X $\vec{k}$-ray. The Fermi energy for USb_xTe_{1-x} compounds with x>0.8 is placed at the bottom of the d band, while it shifts to higher energies with decreasing x due to the successive filling of the d states. The f band, however, is pinned at E_F independently of x because the number of f electrons is approximately constant. The resulting bands near E_F for UTe and USb at room temperature are displayed by the solid lines in fig. 28a and 28b. The double structure for compounds with x>0.8 is explained by two transitions at the X and the L-point. The situation for the magnetized crystals, on the other hand, is displayed by the dashed lines in fig. 28, showing a red-shift of the transition at X and a blue-shift at L.

As soon as the Fermi-energy reaches some critical value in going from USb towards UTe, the f→d transition at X suddenly will become impossible because of an occupation of the final state, leaving only one f→d peak, which shows a blue-shift with magnetization (fig. 26).

This band structure model easily explains the conduction electron spin-polarization, too. Up to some value of E_F, it is -100% due to the filling of only the lower lying spin-polarized subband. Beyond this limit it begins to decrease rapidly because then, mainly the opposite spin direc-
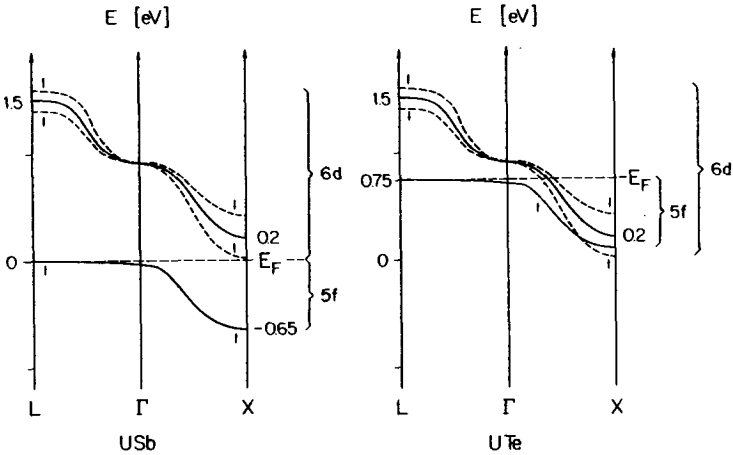
Fig. 28: f and d bands in the vicinity of E_F as proposed for the expla-
nation of the magneto-optical data of the USb_xTe_{1-x} system.
The dashed lines indicate the spin-polarized subbands at
$T \ll T_{C,N}$. The arrows display the directions of the spin-moments
for the f and d bands.

tion will be occupied. Within this description the Fermi-energy comes out
to be about 0.7eV in UTe.

The proposed general behavior of the d and f bands near E_F in the Γ-X
and Γ-L directions is corroborated by several band structure calculations
for UTe, UBi, UN and US [45, 68, 79, 80, 95]. A calculation for CeN [96],
a material which shows very similar spectroscopic features as the discus-
sed uranium compounds [97], corroborates the overall behavior of the f
and d bands. This calculated band structure is in excellent agreement
with the mentioned optical data.

We may resume, that the presented band scheme explains most of the expe-
rimental facts. However, an interpretation of the spectrum 'under pres-
sure' and the explanation of the 'diamagnetic' line shape for the lowest
energy transition for all compounds is lacking.

Model of localized f-states in USb: In this model, a localized-itinerant
transition for the f states is proposed at x=0.8 in USb_xTe_{1-x} i.e.

the f^3 state is localized in USb and itinerant in UTe. The double struc-
ture of the f→d transition for compounds with x>0.8 is explained by a fi-
nal state splitting of the f^2d^1 final state. In fact, a calculation of
the coefficients of fractional parentages in intermediate coupling gives
only two final state levels $^3H_4$ and $^3F_2$ with sufficient intensity and in
addition, the lower energy level is calculated to be a factor of three
more intensive [98]. The coupling of the 6d electron with the remaining
$5f^2$ state, which is known to be important for semiconductors [8, 10, 82],
has been neglected in this calculation.

We assume, that the localized-itinerant transition at x=0.8 is triggered
by the competition of the df-hybridization, which tends to keep the f le-
vel at E_F, and the pf-hybridizaton, which likes to pull the f-states
below E_F. The trend of the f→d energy (fig. 33) to be highest in USb
corroborates a model of localized f states in USb and is hardly in coin-
cidence with localized states in UTe and non-localized ones in USb, as
has been proposed from some photoemission data [54].

In the framework of this second model, good agreement with the finding of
localized f states in USb by specific heat [48], transport [72] and neu-
tron scattering [99] experiments is obtained. However, there is no obvi-
ous relation between the change of sign in the magnetic energy shift and
the proposed localized-itinerant transition of the f states.

Hence we may conclude, that both models have serious shortcomings. In our
opinion, however, the band model is the more unconstrained interpreta-
tion. Within this model, one may imagine also a low density of f states
at E_F if the f levels at the L and X-point are interpreted as two crys-
tal field levels forming the f band. Then, the Fermi-energy is located
just above the f state at L.

4.4.3 Discussion

In secs. 4.2 - 4.4, magnetic exchange induced variations of the f→d tran-
sition have been discussed for UP, UAs, $UAs_{0.7}Se_{0.3}$, USe and the sys-
tem USb_xTe_{1-x}. In a first approach, this effect may be understood in
the framework of the d-f exchange model, presented in sec. 4.4.1.

In the case of the uraniumpnictides, the magneto-optical response eviden-
ces a -100% local conduction electron spin-polarization, i.e. only the
subband with spin antiparallel to the total f-moment is occupied. Hence,
the third term in eq. (26) vanishes and the f-d exchange constant may be
calculated from eq. (27). However, the question arises, which value has

to be taken for the sublattice saturation moment $\langle S^z \rangle$.

In the case of a free magnetic ion of total angular momentum $\vec{J}$, the saturation moment μ_{tot} and the paramagetic moment μ_{eff} are given by $\mu_{tot} = gJ$ and $\mu_{eff} = g\sqrt{J(J+1)}$, respectively. However, this simple relationship breakes down for a solid, if strong crystal fields are present [100] which is obviously the case for the uranium chalcogenides and pnictides (fig. 5).

Because the actual angular momentum enters into the intra-atomic exchange Hamiltonian (eq. (25)), we will take gJ from the measured paramagnetic moment μ_{eff} and not from the saturation moment μ_{tot} (see fig. 5). The paramagnetic moment is nearly constant for the pnictides and results in $gJ \approx 3.25\mu_B$. Consequently, the f-d exchange parameter J_{df} comes out to be about 0.12eV for UP, UAs and USb_xTe_{1-x} with $x > 0.8$.

Going from the pnictides to the chalcogenides, the increasing occupation of the d band will reduce the red-shift, as predicted in the d-f model. Thus, the model is adequate for the application to the compounds with light anions, while in the case of USb_xTe_{1-x} the observed effects are determined by the band structure and therefore the simple model is overstressed.

It should be mentioned, that an interpretation of the observed magnetic changes of the f→d transition energy by magnetostriction is inadequate. Data of the lattice constant a of UTe versus magnetization reveal a small decrease of a in the order of $\Delta a/a = 1.5 \cdot 10^{-3}$ [101]. This value would lead via an increase of the d crystal field splitting to a red shift in the order of < 0.01 eV [102], i.e. it leads to a shift which has the opposite sign and which is one order of magnitude to small. In the case of UP [101], the experimental value of $\Delta a/a$ is lower by a factor of 30 compared to UTe and thus it can not explain the magneto-optical observations, too. At this point of the discussion, some explanations should be given for the antiferromagnetic compounds regarding the so called 'local' conduction electron spin-polarization and the unexpected observation, that the size of the magnetic shift seems to be proportional to the sublattice magnetization while the Kerr-rotation itself is proportional to the bulk magnetization.

Let us consider an antiferromagnetic structure composed of ferromagnetic planes stacked e.g. in the sequence +-+-. Within these planes, the spin-polarized band structure equals that of a ferromagnet displayed in fig. 28. Along the $\vec{k}$-direction perpendicular to these planes, however, the spin-polarized subbands of f and d states have to cross each other to

achieve the antiferromagnetic ordering. The spin-polarized d and f densi-
ties of states for two adjacent planes with opposite total moment is vi-
sualized in fig. 29a. It becomes clear, that within each plane, the size
of the magnetic shift is determined by the sublattice magnetization and
the sign of the shift is the same in both sublattices for a f→d transi-
tion conserving the spin. This explanation holds as long, as the optical
transitions do not occur at Brillouin-zone symmetries inbetween opposite-
ly magnetized ferromagnetic planes. The sign of the Kerr-rotation, on the
other hand, is of course opposite for the transitions in differently mag-
netized planes and therefore, θ_K sums to zero (fig. 29b). If a magnetic
field is applied, θ_K will be proportional to the introduced net magne-
tization.

The same conclusion of course is valid for the magneto-optically deter-
mined conduction electron spin-polarization.

Hence we may conclude, that the observed optical transitions predominan-
tely occur within the ferromagnetic planes for the uranium pnictides.
This model explains in addition, that no additional transitions caused by
a magnetic Brillouin-zone doubling can be expected because this doubling
occurs only along the antiferromagnetic stacking direction.

The mentioned possibility of a magnetic red-shift for an antiferromagne-
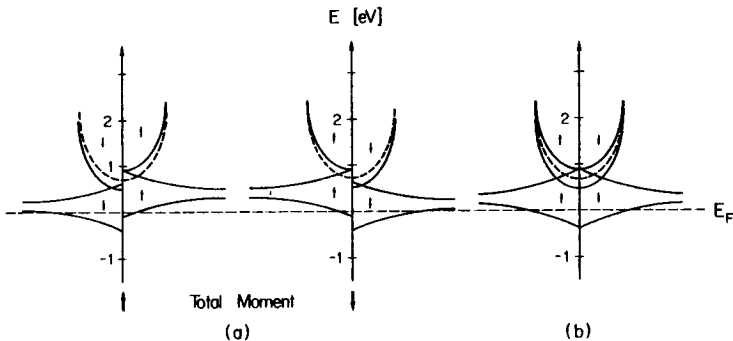tic material in zero applied field poses the question, how this effect in

Fig. 29: Scetch of the spin-polarized sublattice (a) and total (b) densi-
ty of states for f and d electrons in the uranium pnictides. The
arrows indicate the direction of the spin-moments.

general may be determined experimentally. The use of magneto-optics has
the disadvantage to require relatively high applied fields to obtain a
net magnetization. For zero field measurements, the determination of the
optical reflectivity or the absorption constant would be appropriate, be-
cause these properties do not depend on the macroscopic moment.

Unfortunately, an easy measurement of the f→d absorption edge is impos-
sible because of the metallic properties of all the uranium compounds. To
get an idea, what are the expected differences for measurements above and
below the magnetic ordering temperature, we have calculated the influence
of a f→d red-shift on the reflectivity R and the absorption constant K
for UAs. The solid lines in fig. 30 display the calculated spectra of R
and K at room temperature obtained by a six oscillator fit of the measu-
red R up to 12 eV. The effect of a 0.2 eV red-shift of the f→d transition
energy, ·keeping all other oscillators unchanged, is visualized by the
dashed lines. The essential change in the reflectivity spectrum is a 5%
increase in magnitude near $\hbar\omega_A$, indicating that the measurement of R is
certainly not straightforward for this purpose.

The direct determination of the absorption constant, i.e. the optical
density of a thin film seems to be more appropriate as it becomes clear
from fig. 30b. However, also in the optical density, the 0.2 eV shift of
$\hbar\omega_A$ from 1.0 eV to 0.8 eV manifests itself in a modification of K in
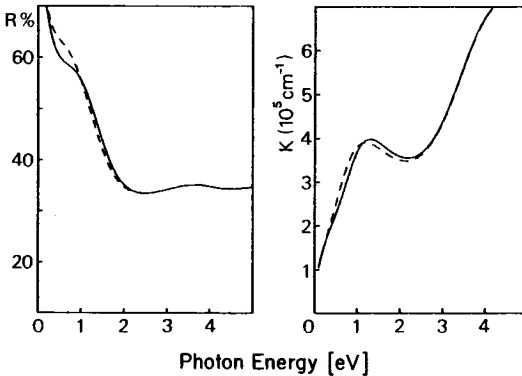the 0.5 - 2.5 eV energy range with varying horizontal shifts.

Fig. 30: Calculated reflectivity (a) and absorption constant (b) of UAs,
using an f→d transition energy of 1.0 eV (solid curves) and of
0.8 eV (dashed curves), respectively.

4.5 Magnetic Phase Diagram of UAs

Among the UX-compounds, UAs is certainly the compound which exhibits the most complex magnetic behaviour [34]. To demonstrate magneto-optics as a powerful tool for the investigation of magnetic phase transitions, we have reexamined the magnetic phase diagram of UAs in applied fields up to 10T. In fig. 31 the computer graph of the measured temperature dependence of the Kerr-rotation is reproduced for a (001)-cleaved single crystal with the applied magnetic field along (100) as a parameter. Around $T_N =$ 124.5K one observes at medium fields the appearence of an intermediate phase with higher magnetization than the surrounding paramagnetic and antiferromagnetic (type I) structures. This intermediate phase has been identified by neutron scattering to be single - $\vec{k}$ ferrimagnetic with a (++-) stacking of (001) ferromagnetic planes [34]. The triple point of coexisting paramagnetic, antiferromagnetic and ferrimagnetic phases is found at B=3T and T=124.5K. For B < 9T, fig. 31 exhibits at T ≃ 62K the phase transition to the double-$\vec{k}$ antiferromagnetic type IA structure. This transition is accompanied by a 10% decrease in magnetization which is due to the jump of the magnetic moments from a (001) to a (110) direction [34]. At B = 9.2T and T = 61.5K we find the triple point of two antiferromagnetic phases (type I and IA) and another ferrimagnetic phase with a double-$\vec{k}$ structure. For comparison, the field-temperature plot from magnetization and neutron scattering experiments [34] is displayed in fig. 32.

Besides the described transitions, which have been observed on several cleaved UAs single crystals, one sample showed at 10T between 53K and 62K one further magnetic structure displaying a strong hysteresis as can be recognized in fig. 7c. The magnetic moment at 10T in this additional phase, which was also not found by neutron scattering in all investigated samples [34], is estimated from our magneto-optical data to be $0.53\mu_B/U$. This value corresponds to the magnetization expected theoretically for the 2k-ferrimagnetic structure [34]. The reduced experimental value of $0.42\mu_B/U$ found for T<53K is explained [34] by defects in the stacking sequence of ferromagnetic sheets. The introduction of stacking defects is accompanied by a change in magnetization but the wave vector remains unchanged in agreement with the neutron experiments. The observation of the same size of the Kerr-rotation for both kinds of UAs crystals at 10T and T<40K indicates that only the crystals with the additional
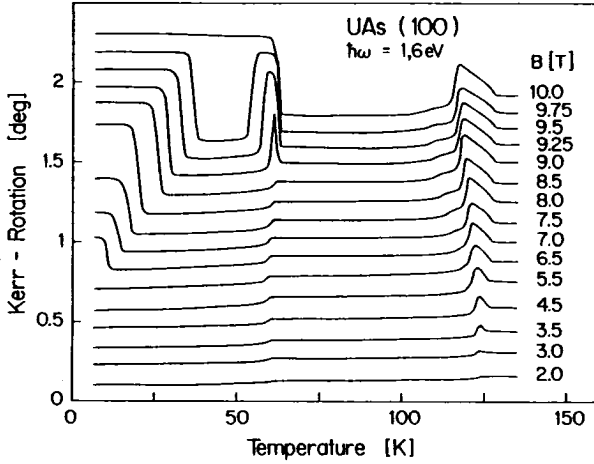
Fig. 31: Temperature dependence of θ_K measured on a cleaved UAs single crystal in fields up to 10 T and decreasing temperature. Consecutive curves are shifted by 0.1° for clarity.
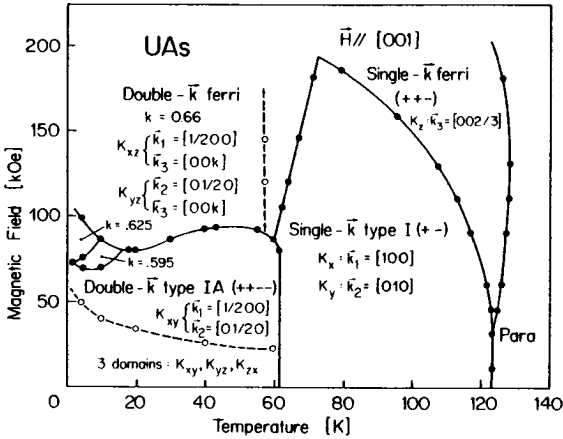

Fig. 32: The magnetic phase diagram of UAs as derived from magnetization and neutron scattering experiments [34].

phase between 54K and 62K at 10T possess a 2$\vec{k}$ ferrimagnetic structure without stacking faults. Our observation of dramatic changes of the magnetic phase diagram on polishing (fig. 7c) suggests that also the different magnetic behaviour of the two kinds of UAs single crystals reflects the large sensitivity of the magnetic properties of this material to internal strain and stress.

In fig. 7c we have added the field cooled temperature dependence of θ_K at 10 T measured on a polished surface. We observe, that T_N as well as the size of the rotation in the ferrimagnetic phases remain unchanged compared with the cleaved sample, but θ_K (or the magnetization) increases quite strongly in the antiferromagnetic and paramagnetic regions. These changes of the magnetic phase diagram have to be related to the deformation of the regular lattice by the polishing process. Phase transitions from the semiconducting to the metallic state in certain semiconductors, which need about 6-15kbar hydrostatic pressure, are known to occur also on polishing [82, 94]. On the other hand magnetization measurements at hydrostatic pressure in fields up to 7T on UAs have shown that only minor variations of the transition temperatures occur up to 8kbar [103] whereas the magnetization of the antiferromagnetic phases was shown to be independent of pressure. Thus in the case of UAs the effect of polishing can not simply be correlated with the application of hydrostatic pressure but more complicated phenomena such as alterations of exchange energies have to be evoked.

5. THE VALENCE OF URANIUM IN $U_xY_{1-x}Sb$

5.1 Introduction

In the uranium pnictide series, the spatial overlap of the 5f wavefunctions decreases with increasing size of the anion. However, due to strong crystal field and hybridization effects, the f-states form a narrow band even in USb as we have recognized in the last chapter. Diluting the uranium sublattice in USb by nonmagnetic ions like Th or Y further increases the spatial separation of the magnetic ions and thus perhaps provides the possibility to study an increasing localization of the 5f electrons. Dilution with trivalent yttrium having the atomic configuration $3d^1 4s^2$

decreases the total number of 5f electrons whereas the d occupation re-
mains nearly unchanged. Dilution with thorium, on the other hand, varies
the number of both the 5f and 6d electrons due to the atomic configura-
tion $[Rn]6d^2 7s^2$ of Th. Therefore, the former way is the appropriate me-
thod for the study of the pure effect of spatial separation on the f band
and to check the band structure proposed for USb in the last chapter.

A second stimulation for the magneto-optical study of the pseudo-binary
system $U_x Y_{1-x} Sb$ is the interpretation of electrical resistivity,opti-
cal, magnetic and lattice constant data in terms of a valence transition
[11] from a localized $5f^2$ state for $x<0.15$ to an intermediate valent
$5f^{3-\eta}$ state for $x>0.15$. In particular, magneto-optics may allow the de-
termination of the $f^3 \to f^2 d$ transition energy $\hbar\omega_A$ as a function of x with
a much higher resolution compared to the normal reflectivity and thus may
check the major conclusion from the optical data of a continuous decrease
of $\hbar\omega_A$ with decreasing x down to $\hbar\omega_A = 0$ at $x=0.15$.

The physical properties of this system are quite well investigated. For
all compositions x, a metallic conductivity is reported [11]. The magne-
tic order [34] is of type I antiferromagnetism with a triple-$\bar{k}$ structure
down to $x=0.55$ and changes at this composition directly to ferromagne-
tism. At concentrations below $x=0.2$ a paramagnetic behavior has been ob-
served [34].

5.2 Results and Discussion

We have investigated magneto-optically the three compositions $x=0.7$, 0.4
and 0.15 of $U_x Y_{1-x} Sb$. The temperature dependences of θ_K indicate
for the three compounds an antiferromagnetic, ferromagnetic and paramag-
netic behavior, respectively, as it is expected from the magnetic data
collected in tab. 7.

x	0.7	0.4	0.15
magnetic order	AF I	F	P
$T_{C,N}$ [K]	181	102	0
μ_{tot} [μ_B/U]	0.7	1.71	0.34
	B=7T; T=181K	B=4T; T=10K	B=7T; T=10K

Tab. 7: Magnetic data of the investigated $U_x Y_{1-x} Sb$ compounds [34, 81].

The energy dependence of the complex Kerr-effect, displayed in fig. 33, shows for all three compounds a sharply structured behavior at the low energy side of the spectrum, similar to all other uranium chalcogenides and pnictides. With increasing substitution of U by Y, this f→d feature narrows substantially. Fig. 34 displays the off-diagonal conductivity as calculated from the Kerr-effect and the optical constants of ref. 11. Similar to the spectrum of $USb_{0.85}Te_{0.15}$ shown in fig. 17, we observe a double structure for the f→d transition with a 'diamagnetic' peak at the low energy side and a 'paramagnetic' structure at higher energies. The resolution of this two peaks becomes better with increasing dilution due to the narrowing of the two lines. In particular for $U_{0.15}Y_{0.85}Sb$, the two peaks are located at 0.5 and 1.2eV, respectively, indicating that the f→d transition energy has not yet shifted to zero for x=0.15.

Fig. 35 compares the energy of the 'diamagnetic' structure in the two systems USb_xTe_{1-x} and $U_xY_{1-x}Sb$ in the magnetically ordered and in the paramagnetic state. Obviously the transition energy is highest for USb and decreases towards UTe and YSb. However, the physical reasons of this drop are different in the two pseudo-binary systems. Going from UTe to USb, the d occupation is reduced by approximately 1 electron per formula unit which results in a reduction of the Fermi-energy. According to fig. 28, the f-states at the L-point are pinned at E_F and thus $\hbar\omega_A$ increases. Going from USb to YSb, on the other hand, does not change E_F relative to the d band. However, the reduction of $\hbar\omega_A$ in this series reflects the decreasing strength of pf-hybridization. According to fig. 28, the lowest energy f→d peak in $U_xY_{1-x}Sb$ corresponds to a transition at the X-point. Compared to a hypothetical energy level scheme without pf hybridization, the f level is pulled away from E_F due to the interaction with p wavefunctions, while the p band is pushed towards E_F. Diluting Y in USb now has the same effect as pushing down the valence band because the energy gained from pf-mixing decreases. Consequently the f states move closer to the Fermi-level. Such an effect has already been infered for diluted CeSb [104].

Hence we conclude, that the band structure proposed for USb in fig. 28 still holds for $U_xY_{1-x}Sb$ but with a decreasing f binding energy at X with dilution. This interpretation is in agreement with an UPS-result on $U_{0.5}Y_{0.5}Sb$, finding the same shape of the energy distribution curve as for USb [54]. The conclusion of a vanishing $\hbar\omega_A$ at x=0.15 drawn from the diagonal conductivity [11], on the other hand, appears to be incorrect.
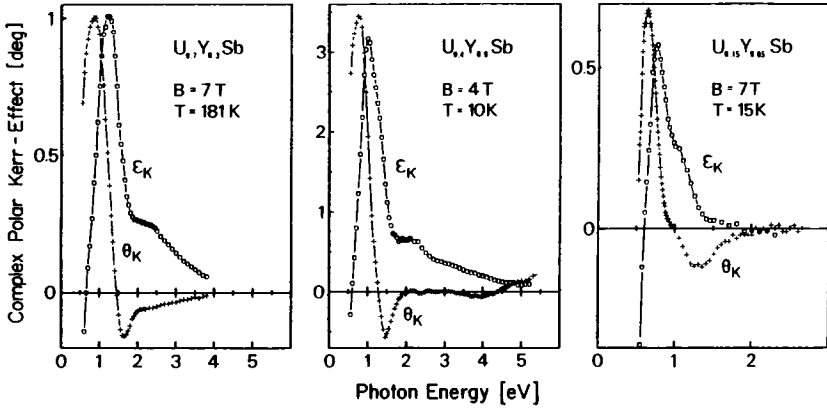
Fig. 33: Energy dependent polar Kerr-rotation and ellipticity of (100)-
cleaved single crystals of $U_xY_{1-x}Sb$ with x=0.7, 0.4 and
0.15. Note the different ordinate scales and the expanded energy
scale for x=0.15.

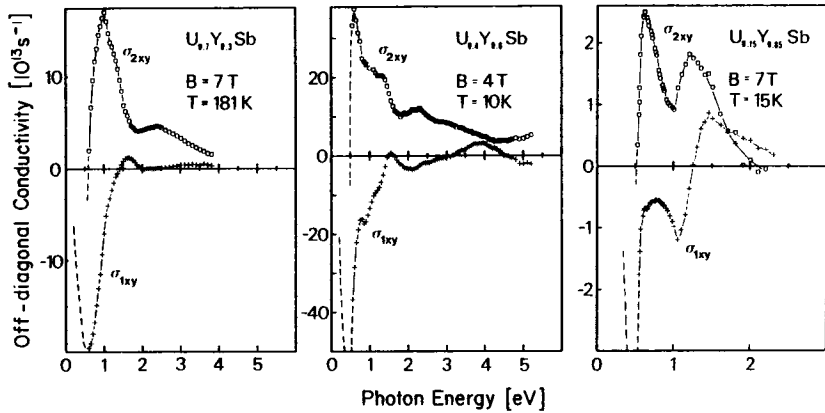Fig. 34: Absorptive (σ_{2xy}) and dispersive (σ_{1xy}) part of the off-dia-
gonal conductivity for the three $U_xY_{1-x}Sb$ compounds. The
dashed line displays the extrapolation of σ_{xy} for $\hbar\omega < 0.5eV$ ob-
tained by Kramers-Kronig inversion (sec. 3.1). Note the diffe-
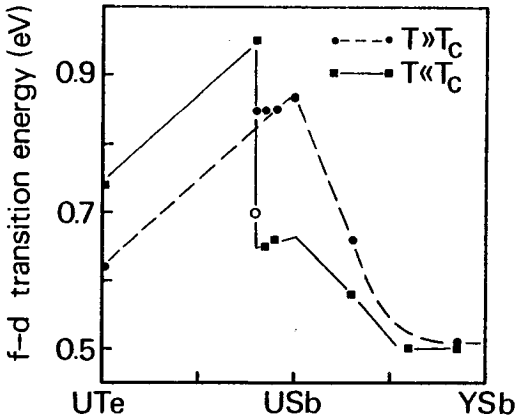rent ordinate scales and the expanded energy scale for x=0.15.

Fig. 35: Energy of the 'diamagnetic' part of the f→d transition in the pseudo-binary systems USb_xTe_{1-x} and $U_xY_{1-x}Sb$ in the magnetically ordered and disordered state, respectively. The open circle displays the f→d energy for polished $USb_{0.8}Te_{0.2}$ (sec. 4.4.2.2).

It is not surprizing, that the f→d transition has not been detected unambiguously in the diagonal conductivity for compounds with x<0.15 because its amplitude in σ_{1xx} for $U_{0.15}Y_{0.85}Sb$ is only 15% of the amplitude in USb, i.e it amounts to only $0.3 \cdot 10^{15}$ sec^{-1}. In general a signal of this size is hardly resolved in the optical reflectivity at low energies because of the dominating conduction electron contribution (even if the number of free electrons is small) and the overlap with strong valence band contributions in the refractive index. This situation in $U_xY_{1-x}Sb$ is a nice example to demonstrate the superiority of magneto-optics for the identification of weak excitations of magnetic electrons. With the knowledge of $\hbar\omega_A \approx 0.55$ eV for the f→d transition in $U_{0.15}Y_{0.85}Sb$ from the magneto-optical spectra, the corresponding peak in σ_{1xx} of ref. 11 can easily be identified.

The high energy structure of the f→d transition around 1.25eV is well resolved in the magneto-optical spectra of the three $U_xY_{1-x}Sb$ compounds and compares well with the same feature in $USb_{0.85}Te_{0.15}$. According

to the energy level scheme for USb (fig. 28), it is attributed to an f→d transition at the L-point. In the diagonal conductivity of ref. 11 for the compounds with small uranium concentration, we find a weak shoulder at an energy of 1.25eV, too, while this structure is lost in the high background for compounds with x>0.3 [11].

The total weight of the whole f→d transition in $U_xY_{1-x}Sb$ is found to be roughly proportional to the magnetic moment and the uranium concentration. This result again makes a valence transition in the composition range x>0.15 very unlikely.

The main result of the present magneto-optical study is, that the proposed itinerant model for the f states in USb_xTe_{1-x} with an occupation slightly less than three works also to explain the magneto-optical behavior for all investigated compositions of $U_xY_{1-x}Sb$. Within this model, the f→d transition consists of two excitations at the X and L points in the Brillouin-zone. The main influence of the dilution of the magnetic ion is a reduction of the pf-mixing at the X-point which results in a decrease of the f→d transition energy down to 0.5 eV in $U_{0.15}Y_{0.85}Sb$. Thus, the present results strongly support an f occupation near three down to a dilution of x=0.15.

6. THE TERNARY COMPOUNDS UAsSe AND ThAsSe

6.1 Introduction

In the last two sections an comprehensive magneto-optical study of rock-salt-structure uranium compounds has been presented regarding the density of states a few eV around E_F, the f-d exchange and the spin-polarization of these states. The f electrons are found to be almost itinerant with a band occupation near 3. Due to this itinerant behavior, the f→d transition exhibits large diagonal and off-diagonal oscillator strengths and shows a simple 'diamagnetic' line-shape in the magneto-optical spectrum. On the other hand, the magneto-optical response of the localized $5f^2$ state of UO_2 displays a pronounced final state splitting of the f→d feature into two structures separated by ≈1 eV [10]. This double structure indicates a strong interaction of the excited electron with the remaining $5f^{n-1}$ state and in fact the spectrum is understood perfectly by atomic theory treating the $5f^1 6d^1$ excited state in UO_2 as a whole. Of course now the question raises, whether metallic uranium compounds exist, for which the magnetic f electrons are localized in a $5f^2$ or a $5f^3$ configuration. This situation may be present in the ternary compounds UZX (and also UZ_2) with Z=P, As, Sb and X=S, Se, Te, which are reported to have a localized $5f^2$ magnetic ground state from magnetic data [105], photoemission data [106, 107] and by crystallographic considerations [108]. These proposals have stimulated the optical and magneto-optical investigation of UAsSe and the isostructural compound ThAsSe, which are presented in the following.

Both materials crystallize in the tetragonal PbFCl crystal structure with similar lattice parameters a and c (UAsSe: a=3.986Å, c=8.384Å; ThAsSe: a=4.081Å, c=8.562Å [108]). The PbFCl structure is composed of layers of cation and anion, which in UAsSe, for instance, are stacked in the sequence As–U–Se–Se–U–As along the c-axis. A random distribution of As and Se atoms on the two different lattice sites has been excluded by neutron scattering and the investigation of $UAs_{2-x}Se_x$ solid solutions [109]. The crystallographic unit cell of the PbFCl structure is shown in fig. 36a and the coordination polyhedron around the uranium ion is displayed in fig. 36b. The distances between the cations and anions, marked in fig. 36b by R_i, are collected in tab. 8. For comparison, the inter-
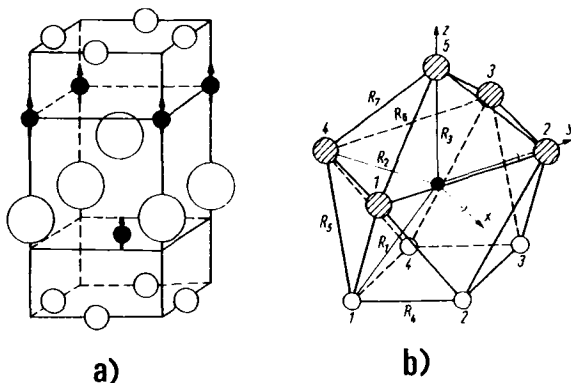
a)   b)

Fig. 36: a) The crystallographic and magnetic unit cell of UAsSe and
ThAsSe. Black circles: U or Th; small empty circles: As; large
empty circles: Se.
b) The coordination around the uranium ion (black circle) in the
PbFCl type crystal structure.

atomic distances for the rocksalt structure compound UAs are juxtaposed.
The bonding conditions in these layered compounds are by far more complex
than those of the NaCl structure because of the different interatomic
distances (tab. 8). In particular, strong anion-anion bonds are suggested
by the small As-As separation.

atom	neighbour	coordination number (PbFCl-structure)	distance (Å) UAsSe	UAs	distance in fig. 35
U	U	4	3.986	4.078	
	As	4	3.022	2.884	R_1
	Se I	4	3.937		R_2
	Se II	1	3.027		R_3
As	As	4	2.818	4.078	R_4
	Se I	4	3.684		R_5
Se I	Se I	4	3.986		R_6
Se I	Se II	4	2.969		R_7

Tab. 8: Interatomic nearest neighbours distances in UAsSe [108, 109] and
in UAs.

Magnetization [105] and neutron scattering [109] measurements have re-
vealed ferromagnetic ordering in UAsSe below T_C = 109 K [110] with a
saturation moment of μ_{tot} = 1.36μ_B and a neutron moment of μ_n = 1.5
μ_B. The magnetic structure is collinear with ferromagnetic layers per-
pendicular to the c-axis (fig. 36a). ThAsSe, on the other hand, is dia-
magnetic [108].

6.2 Results and Discussion

We have measured the room temperature reflectivity in the 0.03-12 eV
energy range of UAsSe and ThAsSe. The measurements have been performed
under high vacuum conditions on in situ cleaved single crystals. Details
are described elsewhere [46].
For high energies, the reflectivity spectra (fig. 37) for both compounds
are similar but they exhibit marked differences at ħω<4 eV. While for
ThAsSe the reflectivity curve shows a Drude behavior, a strong interband
transition around 1 eV is observed for UAsSe similar to the uranium mono-
pnictides and especially to UAs [46]. Using standard extrapolations at
the low and high energy sides of the measurement [46], the spectra have
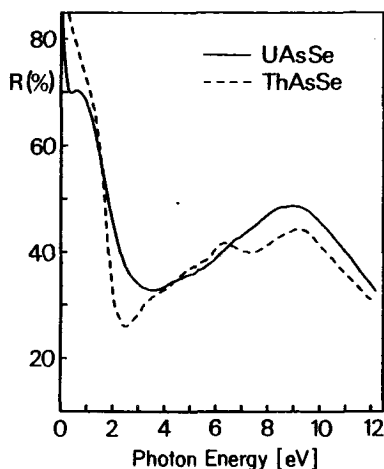been Kramers-Kronig transformed to derive the optical constants. The ab-

Fig. 37: Near normal incidence reflectivities of UAsSe and ThAsSe cleaved
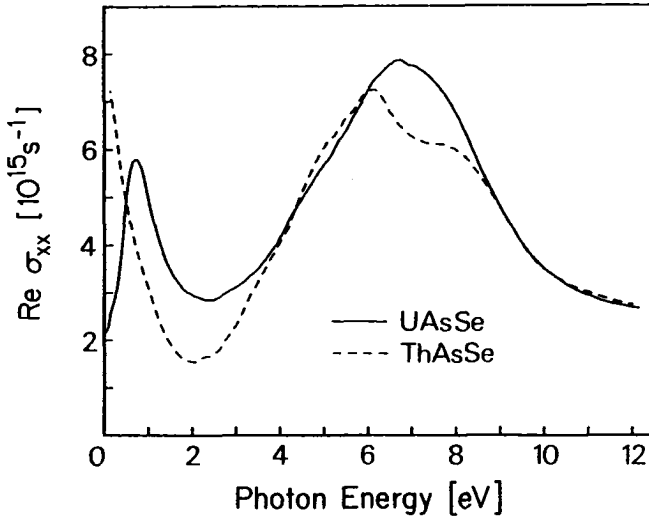single crystals at room temperature.

Fig. 38: The absorptive part of the diagonal conductivity for UAsSe and
ThAsSe at room temperature.

sorptive diagonal conductivity is displayed in fig. 38. It should be men-
tioned, that the conductivity tensor may be written as in eq. (2) also
for a tetragonal lattice, if the c-axis is perpendicular to the sample
surface. But in contrast to cubic symmetry, $\sigma_{xx} \neq \sigma_{zz}$ even for B=0 be-
cause of the two different lattice parameters a and c. For the configura-
tion of a light propagation parallel to the c-axis, the optical measure-
ments probe the conductivity within planes perpendicular to the c-axis.
To separate the 'magnetic' from the 'nonmagnetic' electrons, we have
measured in addition the polar Kerr-rotation and ellipticity of UAsSe at
magnetic saturation (fig. 39a). The complex off-diagonal conductivity
σ_{xy}, calculated by eq. (3) from the Kerr-effect and the optical con-
stants is displayed in fig. 39b. A comparison of the magneto-optical re-
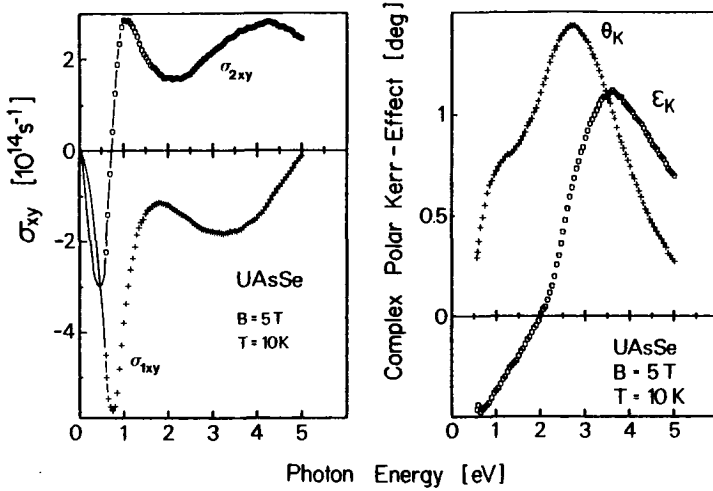sponse σ_{xy} for UAsSe and UAs (fig. 17) again visualizes large simi-
larities.

Fig. 39: a) Complex polar Kerr-effect of cleaved UAsSe at magnetic satu-
ration (B=5 T and T=10 K).

b) Complex off-diagonal conductivity at magnetic saturation as
calculated from the polar Kerr-effect and the optical constants.
The extrapolation for $\hbar\omega<0.5$ eV is estimated by Kramers-Kronig
transformation (sec. 3.1).

6.2.1 f- and d-States

A comparison of σ_{xx} and σ_{xy} for UAsSe suggests an interpretation of
the lowest energy interband transition in terms of an f→d excitation be-
cause of the strong and narrow line both in the diagonal and the off-dia-
gonal conductivity. This assignment is corroborated by the absence of any
sharp interband feature in the spectrum of ThAsSe.

A Lorentz-fit (eq. (19)) of the f→d peak in σ_{1xx} at room temperature
reveals $\hbar\omega_A$ = 0.74±0.02 eV, $\hbar\gamma$=1.1 eV, f_{xx} = 2.35 and $\langle\sigma_{xx}\rangle\simeq$
$13\cdot10^{30}$ sec^{-2}. The informations from σ_{xy} for the same transition at
magnetic saturation are $\hbar\omega_A$ = 0.74 eV and $\langle\sigma_{xy}\rangle$ = $5.8\cdot10^{29}$ sec^{-2},
which combines to $\langle\sigma_{xy}\rangle/\langle\sigma_{xx}\rangle$=0.045. Neither in σ_{xx} nor in σ_{xy}
any additional structure of the f→d transition is observed, which could
point to a final state coupling of a localized f system. From these re-

sults the following conclusions about the f density of states and spin-polarization may be drawn: i) The f electrons form a narrow band at E_F, which is occupied by approximately three electrons. Correlation effects play a minor role, which is indicated by the absence of final state effects and by the large value of f_{xx}. ii) The f spin-polarization is lower than in the uranium monochalcogenides and -pnictices, reaching a value of ≈25% at magnetic saturation. This result is based on the assumption of atomic spin-orbit parameters (sec. 4.3.2.2) and the atomic model presented in sec. 3.2.2.

Consequently it may be stated, that the f electrons are well described in a purely itinerant picture at least within the crystal planes perpendicular to the c-axis. This model is corroborated by the observation of a rather high γ-term in the electronic specific heat for UAsSe of 41mJ/mole·K^2 [110]. For UAs, in comparison, the same size of γ is observed (γ = 53mJ/mole·K^2 [48]) whereas it reaches only 0.5 mJ/mole·K^2 [111] for ThAs.

In contrast to UAsSe, the low energy conductivity of ThAsSe is dominated by the conduction electrons (fig. 38). In the Drude theory of free carries, which is expected to hold for s and d electrons of Th, the conductivity is given by:

$$\sigma_{1xx}(\omega) = \frac{\omega_p^2}{4\pi} \frac{\gamma^2}{\omega^2 + \gamma^2} \tag{28}$$

Therefore, from a plot of $1/\sigma_{1xx}$ versus $(\hbar\omega)^2$ one may obtain the size of ω_p^2 and γ. In fact, fig. 40 visualizes Drude-behavior for ThAsSe in the energy range between 0.25 and 1.5 eV. The parameters of the linear fit in this figure are the uncoupled plasma frequency $\hbar\omega_p$=7.15 eV and $\hbar\gamma$=1.0 eV. From the definition $\omega_p^2 = 4\pi Ne^2/m^*$ and the assumption m=m*, we compute a conduction electron concentration of $3.7 \cdot 10^{22}$ cm^{-3}, i.e. about 2.6 free electrons per formula unit for ThAsSe.

The number of charge carriers in UAsSe, on the other hand, is estimated to be less than 0.3 electrons per formula unit by a fit of σ_{1xx} after subtraction of the f→d contribution.

It becomes clear from these results, that the bonding is probable not identical in UAsSe and ThAsSe in spite of the similar lattice parameters, if the assumption m=m* holds for the conduction band in ThAsSe. While for the latter compound the charge transfer from cation to anion is only
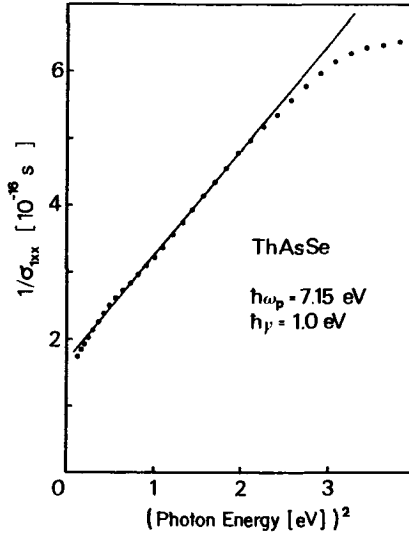
Fig. 40: Drude fit of the optical conductivity of ThAsSe.

1.3 electrons, 2.7 electrons of uranium contribute to bonding in UAsSe.
These values are substantially lower than the 5 electrons, required to
fill up the p bands of As and Se. Consequently, strong anion-anion bon-
ding may be expected. Table 8 suggests, that mainly As-As and SeI-SeII
bonds in the planes perpendicular to the c-axis may occur because these
distances are only slightly larger than twice the atomic radii. This ex-
planation works well for UAsSe, but it fails to account for the different
bonding in ThAsSe, which has a larger unit cell than UAsSe. It is note-
worthy to mention, that the number of d and s conduction electrons in
UP_2, which exhibits a still larger unit cell, is found from transport
measurements to be ≈2 electrons per formula unit [112].

6.2.2 The Valence Band

We have found in the last section, that the electronic density of states
at E_F for UAsSe and ThAsSe is completely different. On the other hand,
it is evident from figs. 37 and 38, that the optical spectra are quanti-
tatively more similar at photon energies above ≈4 eV. In this latter
energy range, the diagonal conductivity of the Th-compound is only a

little more structured. This broad absorption band, centered at 6.9 eV, is assigned to the charge transfer transtion of p valence electrons of As and Se into empty d states of Th or U. It is interesting to note, that no pronounced crystal field splitting is resolved in UAsSe although several peaks could be present for tetragonal crystal field symmetry, which is actually the case for ThAsSe (for tetragonal symmetry, both the t_{2g} and the e_g crystal-field level in cubic symmetry split into two subbands). This behavior of the two compounds may be caused by the different occupation of the d conduction band. Due to the larger number of overlapping p→d transitions in UAsSe, all structures may be smeared out.

The dominant structure at 4.3 eV in the off-diagonal conductivity of UAsSe (fig. 39b) corresponds to the weak shoulder in σ_{1xx} at the onset of valence band excitations. A very similar optical and magneto-optical response has been already discussed for UAs (sec. 4.2.2.3). Thus, it is obvious to assign this feature similar as for UAs to the excitation of bonding pd-electrons from the top of the valence band into spin-polarized f states, which explains the strong magneto-optical signal. The two valence band structures at 4.3 eV and 6.9 eV for UAsSe, therefore, reflect two different bonding states of anion p electrons with uranium d and s states, respectively.

6.3 Summary

In contrast to the expected localized behavior of the 5f electrons in UAsSe we found evidence for a f band at the Fermi energy, occupied by nearly three electrons. Despite the similar lattice parameters of ThAsSe compared to UAsSe, these two compounds show different cation-anion bonds most probably due to strong f-p hybridization. In fig. 41, we have combined the findings from optical and magneto-optical spectroscopies in empirical energy level schemes for UAsSe and ThAsSe. In spite of the relatively high d density at E_F, the diamagnetism of ThAsSe can be explained by the diamagnetism of the inner shells, exceeding the Pauli-paramagnetism of the d states.

It should be noted, that the d band in UAsSe displays no exchange splitting as is evidenced by the same f→d transition energy in σ_{xx} and σ_{xy}. This observation contrasts with the behavior of the uranium pnictides, where we have found exchange splittings in the order of 0.2eV, although the f and d densities of states near E_F seem to be similar in UAs and UAsSe.
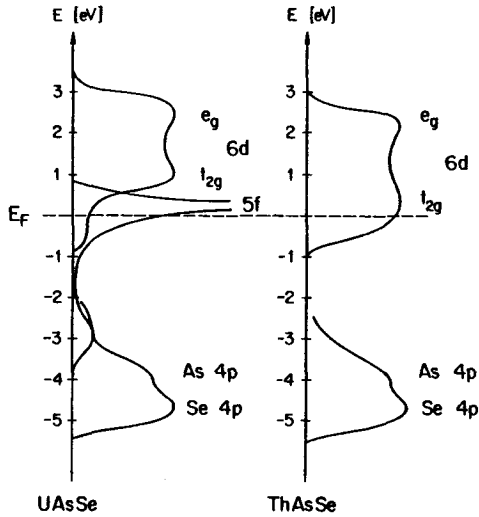
Fig. 41: Empirical energy level schemes for UAsSe and ThAsSe as derived from optical and magneto-optical spectroscopies.

7. Th$_3$P$_4$-STRUCTURE COMPOUNDS

7.1 Introduction

U$_3$P$_4$ and U$_3$As$_4$ crystallize in the Th$_3$P$_4$-type bcc structure with four formula units per crystallographic unit cell. The two compounds order ferromagnetically at 138 and 198K with a saturation magnetization of 1.39 and 1.83μ_B/U, respectively [113]. Unusually large magnetic [114, 115], magnetostrictive [116] and resistivity [117] anisotropy with respect to the (111)-direction, which is the easy axis of magnetization, have been reported. However, the magnetic moments on the uranium sites are not oriented along (111) but a noncollinear magnetic structure has been established [113]. Anisotropic pf-mixing has been introduced [118, 119] to explain the three axial structure with the observed tilting of the magnetic moment from the (111)-direction by about 20° within (110)-planes. The size of the pf-mixing energy for the two compounds was estimated to be

about 1eV [118,119]. And in fact, a careful analysis of optical data for
Th_3P_4, Th_3As_4, U_3P_4 and U_3As_4 [120] strongly supports a mixing energy in
this order of magnitude, which is assumed to be the driving force for the
U-compounds to be metallic in contrast to the corresponding semiconduc-
ting Th-compounds. One conclusion from these optical data was, that the
main effect of the pf-mixing is a shifting up of the p valence band by
0.85eV and pushing down the f states by the same amount of energy.
The optical conductivity σ_{1xx} was found to be dominated by strong exci-
tations of the valence p electrons into the fourfold crystal field split
d band superposed by a free carrier part at low energies. No f→d transi-
tions could be identified. Consequently, the starting point of the mag-
neto-optical investigation of these compounds was the question for the f
binding energy. However, as we will see in the following, the observed
magneto-optical spectra differ completely from the typical f→d response
of all the materials discussed in the preceeding chapters and it will be
demonstrated that it is in fact not caused by f→d transtions.

7.2 Experimental Results and Discussion

The polar Kerr-effect of (112)-polished U_3P_4 and U_3As_4 crystals at magne-
tic saturation (B=4T, T=15K) is displayed in fig. 42. These spectra are

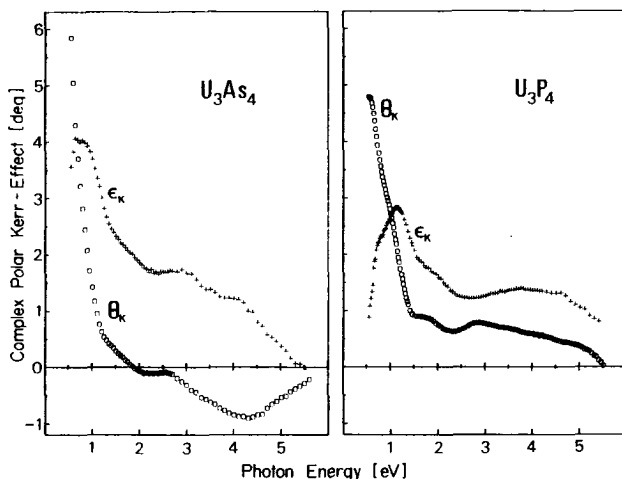Fig. 42: Polar Kerr-effect of (112)-polished U_3P_4 and U_3As_4 at magnetic
saturation (B=4T, T=15K).

characterized by an extremely large gradient of θ_K at low energies with a θ_K reaching absolute values of $6°$ and a more or less flat behavior above ≈ 1.5eV. Although these curves show some similarities with the Kerr-effect of the uranium monopnictides, the off-diagonal conductivity in fig. 43 clearly indicates a different behavior. The absorptive part of σ_{xy} displays for both materials a general ω^{-1} decrease superposed by some weak structures. This general decrease strongly points to a dominant intraband contribution, although the possibility of an interband transition at an energy less than 0.5eV can not be excluded at this point of the analysis. However, if the magneto-optical feature would be caused by an interband transition, there should be a peak of at least $1.8 \cdot 10^{15}$ sec^{-1} amplitude in σ_{1xx} at the resonance energy, i.e. this transition would dominate σ_{1xx} at $\hbar\omega < 1$eV which is actually not observed [120]. Further, performing Kramers-Kronig transformations of σ_{2xy} into σ_{1xy} and vice versa (sec. 3.1) either with an extrapolation for an intra- or for an interband transition excludes the latter possibility and yields an extrapolation for $\hbar\omega < 0.5$eV which is displayed in fig. 43. Hence we find a
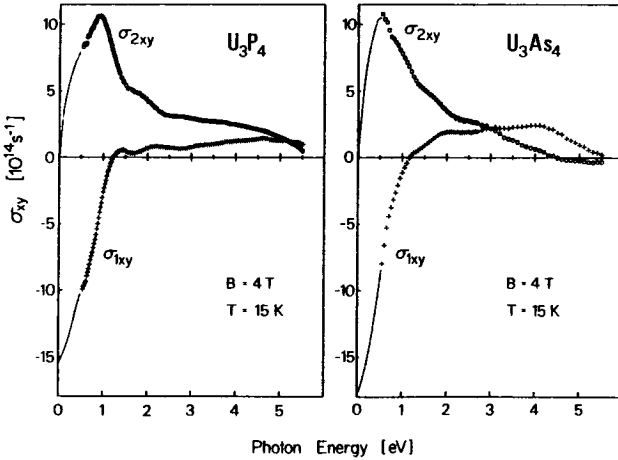

Fig. 43: Off-diagonal conductivity of U_3P_4 and U_3As_4 at magnetic satura-tion, calculated from the polar Kerr-effect and the optical data of ref. 120. The low energy extrapolation has been calculated by Kramers-Kronig inversion.

predominant free carrier contribution to the magneto-optical response in U_3P_4 and U_3As_4 in contrast to all other uranium compounds, discussed in the preceeding chapters.

At zero energy, the extrapolation gives values for $\sigma_{1xy}(0)$ in the order of $-18 \cdot 10^{14}$ sec^{-1}. These numbers may be used as a further check of the extrapolation because they imply a positive Hall-resistivity of an extremal size. If the magneto-optical spectrum is governed by interband transitions, on the other hand, $\sigma_{1xy}(0)$ would be expected to be much smaller because only free carriers contribute to $\sigma_{1xy}(0)$. Using the relation between σ_{1xx}, σ_{1xy} and ρ_H (eq. (6)), we derive from our measurements a ratio $\sigma_{1xy}(0)/\sigma_{1xx}(0) = \rho_H/\rho_0$ of $+1/1.8$ and $+1/2.9$ for U_3As_4 and U_3P_4, respectively. These results are in favorable agreement with transport measurements [121] giving $+1/2.3$ and $+1/2.8$ for the two compounds with absolute values of ρ_H in the order of $200\mu\Omega$cm at $T \ll T_C$. Thus, this comparison with transport data evidences that the magneto-optical spectrum is in fact determined by the ω^{-1} dependent term in σ_{xy} (eq. (9)) and the important result of a negative charge carrier spin-polarization emerges from the sign of σ_{xy}.

Of course the question now arises, what are the microscopic origins of this large intraband effect in particular if it is noticed, that for other ferromagnetic materials like the uranium chalcogenides, the ratio ρ_H/ρ_0 is at least one order of magnitude smaller [72]. To derive the parameters of eq. (9), we have performed a fit of the line-shape and the size of σ_{xy}, taking the ratio $\omega_p^2/4\pi\gamma$ from $\sigma_{1xx}(0)$. The spin-orbit term (eq. (10)) has been assumed to be the same as in the UX compounds, i.e. we take 1eV for both $\hbar\omega_{ab}$ and $\hbar\omega_{so}$. The main results of this fit are:

i) the charge carriers are totally spin-polarized and their moment is antiparallel to the f-moment, i.e. $\sigma_d = -100\%$;

ii) the unscreened plasma frequencies are 4 and 4.7eV for U_3As_4 and U_3P_4, respectively, which yields a number of 0.6 and 0.75 charge carriers per uranium within the assumption m=m*. These values are by far larger than the carrier densities derived from de-Haas-van-Alphen measurements [122] and point to undetected orbits in those experiments as the authors did intimate.

The weak structures in σ_{2xy} of both compounds (fig. 43) indicate, that apart from the prevailing intraband part, magneto-optical signals from interband transitions are present. To suppress the ω^{-1} dependence, it is convenient to discuss $\omega\sigma_{2xy}$, which is displayed in fig. 44 for U_3P_4.
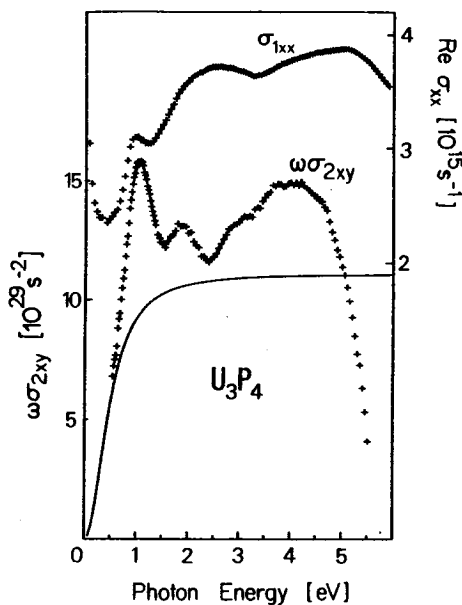
Fig. 44: Experimental values of $\omega\sigma_{2xy}$ for U_3P_4 at magnetic saturation. The area under the solid line is the estimated intraband contribution, derived from a fit of σ_{xy}. At the top of this figure, the absorptive diagonal conductivity from ref. 120 is displayed for comparison.

The solid line in this figure shows the free carrier contribution as derived from the fit of σ_{xy}, which becomes energy independent in $\omega\sigma_{2xy}$ for $\hbar\omega \gg \hbar\gamma$. For comparison with normal optics, we have added in this figure the absorptive diagonal conductivity σ_{1xx} [120]. It becomes clear, that each peak in σ_{1xx} corresponds to a structure in $\omega\sigma_{2xy}$, i.e. no unresolved transitions in σ_{1xx} can be identified by magneto-optics.

The detailed analysis of σ_{1xx} for U and Th tetrapnictides has revealed an assignment of the four lowest energy structures in fig. 44 to p excitations into the crystal field split d band. In the context of this investigation, the structures observed in $\omega\sigma_{2xy}$ correspond to the same transitions. This picture is supported by the relatively small total weights $\langle\sigma_{xy}\rangle$ for a ferromagnetic 5f material, reaching $\approx 2.5 \cdot 10^{29}$ sec^{-2} for the lowest energy peak and $\approx 6 \cdot 10^{28}$ sec^{-2} for each of the other struc-

tures. The peak at 5eV, however, which has been tentatively assigned to a
f→d transition, seems also to be due to a p excitation, because the mag-
neto-optical signal is as weak as for the other transitions and because
there is no reason from selection rules, that f excitations into the lo-
wer lying d crystal field levels should not occur.

Hence we are left with the situation, that no f→d transitions are obser-
ved in the magneto-optical spectra and therefore the nature of the f
states in Th_3P_4-structure compounds is still a subject of speculations.
However, it can not be excluded, that the f→d transitions are energeti-
cally degenerated with the p→d transitions, i.e. the huge peaks in σ_{1xx}
display mainly p-excitations whereas the sharp structures in $\omega\sigma_{2xy}$ cor-
respond merely to f→d transitions at the same energy.

8. SOME ASPECTS OF THE TECHNICAL APPLICATION OF MAGNETO-OPTICS

To realize the importance of magnetic storage technologies in the today's
industrial market one has to notice that the fabrication of magnetic sto-
rage products already exceeds the semiconductor output.

For longitudinal recording (i.e. in plane magnetization like tapes, hard-
discs, floppy-discs etc.) the physical limits of bit-density and access-
time seem to be reached [123]. In particular, serious mechanical diffi-
culties arose. For example, the flying hight of the recording head had to
be reduced down to less than 0.2µm to achieve the highest bit densities
of a few Mbit/cm^2 in longitudinal recording. Parallel to the reduction of
the gap between recording head and material, the size of the recording
head itself was miniaturized down to a few µm side length.

To achieve an additional progress in storage density, vertical recording
(i.e. magnetization perpendicular to the surface of the storage material)
is intensively studied today on a research level. With this type of re-
cording, the bit density may be further increased by a factor of three.
However, the important mechanical difficulties remain and new trouble
comes up e.g. due to the stray field of the recording head [123]. To
avoid these problems, several techniques of optical recording have been
developed in the last decade. They allow bit densities of several 10^7bit/
cm^2, determined by the wavelength of the used laser. One of the very few
erasable techniques takes advantage of the polar magneto-optical effects,
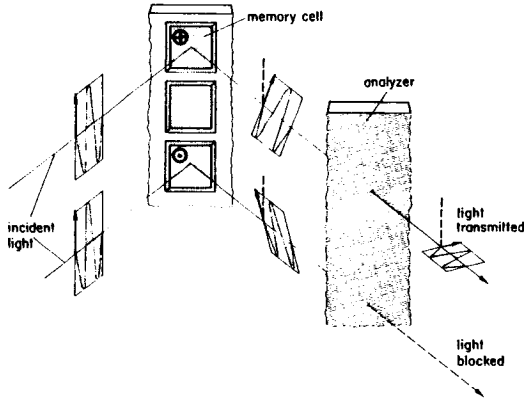i.e. the Faraday-effect in transmission or the polar Kerr-effect in re-

Fig. 45: Viewing of magnetic domains using the polar Kerr-effect and po-
larization optics.

flection. Fig. 45 shows a typical setup for the latter configuration. The
linear polarization of the incident light which is reflected from do-
mains with magnetization parallel or antiparallel to the direction of
light propagation is rotated by θ_K and $-\theta_K$, respectively. Hence,
using an analyser perpendicular to the one polarization, the figure of
merit η for the read-out process is defined by

$$\eta = R \sin^2 2\theta_K \qquad (29)$$

where R is the reflectivity of the storage material. A similar equation
holds for the Faraday configuration, but with R replaced by the transmit-
ted light intensity e^{-Kd} (where K is the absorption constant and d is
the thickness of the storage material) and of course θ_K replaced by the
Faraday-rotation θ_F. To achieve a high η and hence to render possible a
high data rate, large magneto-optical effects are required.
But first let us discuss which of the two polar magneto-optical effects
dominates for a given material with optical indices n and k and with a
magneto-optical activity σ_{xy}. The complex polar Kerr-effect is deter-
mined by [124]

$$\phi_K = \theta_K + i\epsilon_K = -i\epsilon_{xy}/\sqrt{\epsilon_{xx}(\epsilon_{xx}-1)} \qquad (30)$$

where σ_{ij} and the dielectric tensor ϵ_{ij} are connected by $\epsilon_{ij}=\delta_{ij}-i4\pi\sigma_{ij}/\omega$ with the Kronecker-Delta δ_{ij}. Using the same optical functions, the complex Faraday rotation is given by [124]

$$\phi_F = \theta_F + i\epsilon_F = -(\pi d/\lambda)\epsilon_{xy}/\sqrt{\epsilon_{xx}} \qquad . \qquad (31)$$

The combination of these equations results in

$$\frac{\phi_F}{\phi_K} = \frac{\pi d}{\lambda}\left|(\epsilon_{xx} - 1)\right| = \frac{2\pi d}{c}\left|\sigma_{xx}\right| \qquad . \qquad (32)$$

This interesting result postulates, that the relative size of Faraday and Kerr-effect simply is proportional to the diagonal conductivity $\left|\sigma_{xx}\right| = \left|\sigma_{1xx}+i\sigma_{2xx}\right|$. Taking for the Faraday configuration a transmittance of 37% (i.e. d=1/K), which is in the order of typical reflectivities, eq. (32) has been computed as a function of n and k and is displayed in fig. 46. The quite surprising result is, that the Faraday effect exceeds the
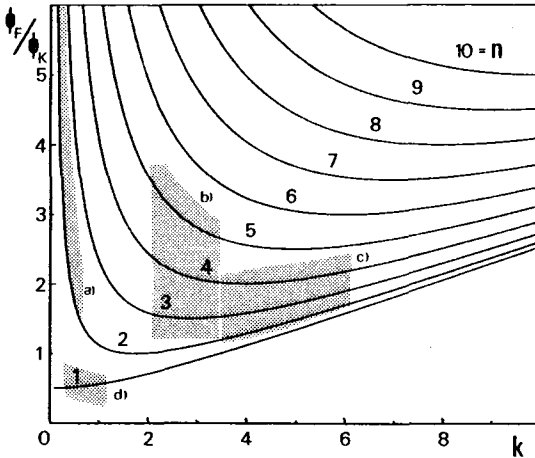
Fig. 46: Ratio of the total Faraday and Kerr-signals for a material with optical constants n and k. The area of fundamental absorption in the n-k plane is indicated for: a) f→d transition in Eu-chalcogenides [66]; b) f→d transition in U-chalcogenides; c) d excitations in Fe, Co, Ni [125, 126]; d) plasma-edge splitting [30].

Kerr-effect for nearly all physical combinations of n and k. In particular, in the case of typical magneto-optical active interband transitions in 3d, 4f and 5f materials, the ratio $|\phi_F/\phi_K|$ is about 2. However, taking photon energies in the gap of magnetic semiconductors, this ratio may be orders of magnitude larger (e.g. YIG). The only known magneto-optical effect which results in a dominant Kerr-rotation is the plasma-edge splitting of the conduction electrons [30].

For these reasons, mainly transparent thin films are used for storage applicatins. If a reflection configuration is required by reasons of the design (e.g. erasable compact disc), double Faraday-rotation rather than single Kerr-rotaton is applied [123].

To elucidate the strength of the magneto-optical activity in the fundamental absorption regime of the known magnetic materials, let us compare the polar Kerr-rotation. In the group of 3d and 4f metals and metallic compounds, the typical rotation is 0.5^o or less [27, 125-128]. Exceptions are some compounds with extraordinary electronic structure (e.g. half-metallic ferromagnets), where θ_K may reach 1.2^o [129]. The largest rotations up to now have been reported for magnetic semiconductors with θ_K up to 6°, which have, however, very low Curie-temperatures [130-132]. In the present work, on the other hand, new materials with ordering temperatures up to 210K have been reported, showing single Kerr-rotations up to 9° at 65% reflectivity. In addition it has been shown that the maximum Kerr-rotation may be adjusted to a given photon energy by varying the composition of the compounds. Fig. 47 displays in example the Kerr-rotation in (100)-direction of the system USb_xTe_{1-x} for different x (in (111)-direction, the rotation is larger by a factor of 1.45 (fig. 27)). The peak position shifts between 1.7 and 0.5eV with Te-concentration.

In fig. 48, we have collected the largest values of the 'figure of merit' η versus energy for the investigated 5f materials. For comparison, η-values of some 3d and 4f compounds which have been considered for application are included. This collection shows, that the 'figure of merit' of the present uranium compounds exceeds those of all other materials known up to now by at least one order of magnitude. The only restriction for a successful application in storage devices may be, that the Curie temperatures of about 200K are below room temperature. In future, this shortcoming may perhaps be overcome by an appropriate alloying although the magnetic moment on the uranium sites in the known systems with $T_C>300K$ decreases to very low values. However, a specific search for such systems has not yet been done.
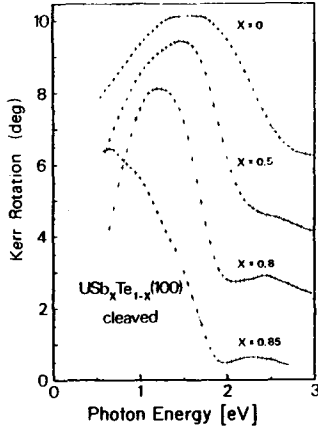
Fig. 47: Polar Kerr-rotation of four different (100)-oriented cleaved USb$_x$Te$_{1-x}$ single crystals at magnetic saturation. For clarity, the curves with x=0.8, 0.5 and 0 are vertically shifted by 2, 4 and 7 degrees, respectively.
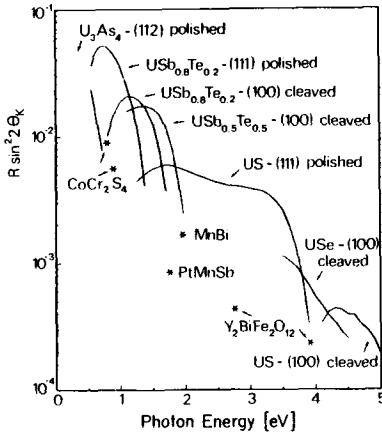

Fig. 48: Read-Out efficiency Rsin^{2}2θ$_K$ versus photon energy of some uranium compounds at magnetic saturation. For comparison, we have added the values for CoCr$_2$S$_4$ [130], MnBi [133], PtMnSb [129] and Y$_2$BiFe$_2$O$_{12}$ [134].

9. CONCLUDING REMARKS

It has been demonstrated during this work, that the investigated metallic uranium compounds may be classified in two groups of distinct magneto-optical response of the 5f electrons.

The materials of the first class including uranium-monochalcogenides, monopnictides and pseudo-binaries between the chalcogenides and pnictides but also diluted uranium in a nonmagnetic NaCl-structure matrix and certain ternary compounds display a strong magneto-optical response proportional to the density of uranium ions and to the magnetic moment per uranium. The ground state for these compounds has been evidenced to be a narrow f band occupied by nearly three electrons. The 'diamagnetic' line shaped signal of the f→d transition in σ_{xy} is well understood in size and shape by a band model.

For the second class of the investigated magnetic uranium compounds like those with a Th_3P_4 crystal structure or certain intermetallics like UIr, the magneto-optical signal from interband transitions was found to be too small for an unambiguous identification of f-excitations. However it may be stated, that the Kerr-response of the 5f electrons is reduced by at least a factor of 50 compared to the first group of materials, if it is present at all. Concerning the reasons of this unexpected behavior we can only speculate. The magneto-optical signal may be reduced either by a small radial overlap integral for localized states or by a singlet crystal field ground state or by the fact, that the moment on the uranium sites contributes only little to the total moment as it is well known for UFe_2. A further study of uranium intermetallics seems to be a promising field for new and fascinating results.

For uranium systems with almost trivalent uranium,   the off-diagonal conductivity reaches values up to $\sigma_{xy}/\sigma_{xx} \approx 0.35$, which approaches the theoretical limit of 2/3 and is considerably larger than in 3d and 4f metals with a ratio of typically 10^{-3}. Nay it may be stated, that the observed magneto-optical effects nearly reach the largest possible values in principle. The reason is, that on the one hand, σ_{xy} is proportional to the total magnetic moment, which becomes larger for more localized states, but on the other hand, σ_{xy} also is proportional to the radial overlap integral, which is known to decrease strongly with localization. Hence the investigated compounds display an almost optimal degree of itinerancy regarding extremal Kerr-signals.

REFERENCES

1) E. Kisker, K. Schröder, M. Campagna and W. Gudat, Rhys. Rev. Lett. $\underline{52}$ (1984) 2285

2) J. Hubbard, J. Appl. Phys. 52 (1981) 1654

3) V. Korenmann and R.E. Prange, Rhys. Rev. $\underline{B20}$ (1979) 4698 and references therein

4) R. Linke, J.L. Moran-Lopez and K.H. Bennemann, Phys. Rev. $\underline{B30}$ (1984) 315

5) T. Moriya, J. Magn. Magn. Mat. $\underline{31-34}$ (1983) 10

6) Handbook of Physics and Chemistry of the Actinides, A.J. Freeman, G.H. Lander, eds., North Holland, Amsterdam 1984

7) M. S. S. Brooks and P. J. Kelly, Phys. Rev. Lett. $\underline{51}$ (1983) 1708

8) J. Schoenes, Z. Physik $\underline{B20}$ (1975) 345

9) P. Wachter, in 'Handbook of Physics and Chemistry of Rare Earth', K.A. Gschneider, jr. and L. Eyring, eds., North Holland, Amsterdam 1979

10) W. Reim and J. Schoenes, Solid State Commun. $\underline{39}$ (1981) 1101

11) B. Frick, J. Schoenes, F. Hulliger and O. Vogt, Solid State Commun. $\underline{49}$ (1984) 1133

12) J. Schoenes, in 'Handbook of Physics and Chemistry', A. J. Freeman, G. H. Lander, eds., North Holland, Amsterdam 1984

13) W. Reim, J. Schoenes and O. Vogt, Phys. Rev. $\underline{B29}$ (1984) 3252

14) G. Metzger, P. Pluvinage and R. Torquet, Ann. Phys. $\underline{10}$ (1965) 5

15) S. E. Schnatterly, Phys. Rev. $\underline{183}$ (1969) 664

16) P. S. Theocaris and E. E. Gdoutos, 'Matrix Theory of Photoelasticity', Springer Verlag, Berlin 1979

17) H. LeGall and J.P. Jamet, phys. stat. sol. $\underline{b46}$ (1971) 467

18) D.Y. Smith, J. Opt. Soc. Am. $\underline{66}$ (1976) 454

19) The fact, that current and field are real quantities requires: $\sigma_{ij}(-\omega) = \sigma_{ij}*(\omega)$. See e.g.: S.D. Smith in "Optical Properties of Solids", S. Nudelman and S.S. Mitra, eds., Plenum Press 1969, chap.4

20) J.F. Dillon, jr., in 'Proc. Intern. School of Physics' Enrico Fermi, A. Paoletti, ed., North Holland, Amsterdam 1978

21) G.B. Scott, D.E. Lacklison, H.I. Ralph and J.L. Page, Phys. Rev. $\underline{B12}$ (1975) 2562

22) H. R. Hulme, Proc. Roy. Soc. (London) $\underline{A135}$ (1932) 237

23) P. N. Argyres, Phys. Rev. $\underline{97}$ (1955) 334

24) B. R. Cooper, Phys. Rev. $\underline{139}$ (1965) 1504

25) A. N. Voloshinskii and G. A. Bdotin, Fiz. metallov i metallovedeni 17 (1964) 481

26) H. S. Bennett and E. A. Stern, Phys. Rev. 137 (1965) 448

27) J. L. Erskine and E. A. Stern, Phys. Rev. B8 (1973) 1239

28) P. J. Stephens, J. Chem. Phys. 52 (1970) 3489

29) C. Kittel, Phys. Rev. 83 (1951) 208

30) W. Reim, O. E. Hüsser, J. Schoenes, E. Kaldis, P. Wachter and K. Seiler, J. Appl. Phys. 55 (1984) 2155

31) E. A. Stern, Phys. Rev. Lett. 15 (1965) 62

32) D. J. Lam and A. T. Aldred, in 'The Actinides: Electronic Structure and Related Properties', A. J. Freeman and J. B. Darby, jr., eds., Academic Press, New York 1974, vol. 1

33) G. Busch, O. Vogt, A. Delapalme and G. H. Lander, J. Phys.C 12 (1979) 1391

34) J. Rossat-Mignod, P. Burlet, S. Quézel, O. Vogt and H. Bartholin, Proc. Crystalline Electric Field Effects in f-Electron Magnetism, Guertin, R.P., Suski, W. and Zolnierek, Z. eds., Plenum Publishing Corp. 1982, p. 501

35) D. L. Tillwick and P. de V. du Plessis, J. Magn. Magn. Mat. 3 (1976) 319

36) P. de V. du Plessis, A. T. Aldred and G. H. Lander, J. Magn. Magn. Mat. 20 (1980) 236

37) O. Vogt, P. Wachter and H. Bartholin, Physica 102B (1980) 226

38) P. Burlet, S. Quézel, J. Rossat-Mignod, O. Vogt and G. H. Lander, Physica 102B (1980) 271

39) R. Troc, J. Solid State Chem. 13 (1975) 14

40) O. Vogt, Physica 102B (1980) 206

41) L. Heaton, M. H. Müller, K. D. Anderson and D. D. Zanberis, J. Phys. Chem. Solids 30 (1969) 453

42) F. A. Wedgwood and M. Kuznietz, J. Phys. C5 (1972) 3012

43) Proc. Intern. Symp. Actinides, Zürich 1980, Physica 102 B

44) J. Schoenes, O. Vogt and C. Keller, Solid State Commun. 32 (1979) 873

45) J. Kübler, EPS conference 1983 and to be published

46) J. Schoenes, Physics Reports 66 (1980) 187

47) M. S. S. Brooks and D. Glötzel, Physica 102B (1980) 51

48) H. Rudigier, Ch. Fierz, H. R. Ott and O. Vogt, Solid State Commun. 47 (1983) 803 and H. Rudigier, ETH-thesis Nr. 7489, Zürich 1984

49) Y. Baer, Physica 102B (1980) 104

50) F. Greuter, E. Hauser, P. Oelhafen, H. J. Güntherodt, B. Reihl and O. Vogt, Physica 102B (1980) 117

51) R. Baptist, M. Belakhovsky, M. S. S. Brooks, R. Pinchaux, Y. Baer and O. Vogt, Physica 102B (1980) 63

52) R. Baptist, J. Naegele and Y. Baer, J. Phys. C 4 (1979) 40

53) B. Reihl, M. Erbudak and F. Greuter, J. Magn. Magn. Mat. 13 (1979) 132

54) B. Reihl, M. Martensson and O. Vogt, J. Appl. Phys. 53 (1982) 2008

55) O. Vogt and H. Bartholin, J. Magn. Magn. Mat. 29 (1982) 291

56) G. H. Lander, M. H. Müller and J. F. Reddy, Phys. Rev. B6 (1972) 1880

57) G. Busch, O. Vogt and H. Bartholin, J. Phys. (Paris) Colloq. 40, C4(1979) 64

58) G. Busch and O. Vogt, J. Less-Common Metals 62 (1978) 335

59) W. Reim, J. Schoenes and O. Vogt, Solid State Commun. 47 (1983) 597

60) M. S. S. Brooks, private communication

61) F. Greuter, W. Eib, M. Erbudak, F. Meier and B. Reihl, J. Appl. Phys. 50 (1979) 7483

62) M.-P. Stoll, Phys. stat. sol. 22 (1967) 163

63) For strictly localized f electrons i.e. UO_2, the calculation results in an f occupancy which is too small by a factor of 10. See J. Schoenes, J. Phys. (Paris) Colloq. 5 (1980) 31; and in: Proc. NATO Summer Institute on Moment Formation in Solids, W. J. L. Buyers, ed., Plenum Press, New York 1984

64) J. Schoenes and P. Wachter, Phys. Rev. B9 (1974) 3097

65) P. Weinberger and R. Podloucky, Phys. Rev. B22 (1980) 645

66) G. Güntherodt and P. Wachter, Phys. Lett. 29A (1969) 660

67) D.M. Kolb, J. Opt. Soc. Am. 62 (1972) 599

68) H. L. Davis, in 'The Actinides: Electronic Structure and related Properties', A. J. Freeman and J. B. Darby, jr., eds., Academic Press, New York 1974, vol. 2

69) M. S. S. Brooks, private communication

70) F. Herman and S. Skillman, 'Atomic Structure Calculations', Prentice Hall 1963

71) P. J. Kelly, Thesis at the European Institute for Transuranium Elements, Karsruhe 1980

72) J. Schoenes, B. Frick and O. Vogt, to appear in Phys. Rev. B, 1984

73) P. Burlet, S. Quézel, J. Rossat-Mignod and R. Horyn, 12èmes Journées des Actinides, Orsay, France 1982, unpublished

74) B. Frick, private communication

75) M. S. S. Brooks, J. Phys. F 14 (1984) 653

76) M. Erbudak and F. Meier, Physica 102B (1980) 134

77) J. Schoenes and P. Brüesch, Solid State Commun. 38 (1981) 151 and unpublished results

78) K. Lendi, Phys. Cond. Mat. 17 (1974) 189

79) M. S. S. Brooks, J. Phys. F 14 (1984) 857

80) P. Weinberger, R. Podloucky and A. Neckel, J. Magn. Magn. Mat. 29 (1982) 247

81) O. Vogt, private communication

82) J. Schoenes, O. E. Hüsser, W. Reim, E. Kaldis and P. Wachter, Proc. of the 4th Intern. Conf. on Valence Fluctuations, Köln 1984

83) B. Batlogg, E. Kaldis, A. Schlegel and P. Wachter, Phys. Rev. B12 (1975) 3940

84) S.V. Vonsovskii and Y.A. Izyunov, Usp. Fiz. Nauk 77 (1962) 377

85) W. Nolting, J. Phys. C 11 (1978) 1427

86) F. Rys, J. S. Helman and W. Baltensperger, Phys. kondens. Materie 6 (1967) 105

87) W. Nolting, phys. stat. sol. (b) 79 (1977) 573

88) J. Schoenes and W. Nolting, J. Appl. Phys. 49 (1978) 1466

89) J. Schoenes, Physics Reports 63 (1980) 301

90) A. Delapalme, G. Busch, O. Vogt and G. H. Lander, J. Phys. (Paris) 40,C4 (1979) 74

91) W. Reim, O.E. Hüsser and J. Schoenes, to be published

92) J. Schoenes and P. Wachter, Physica 86-88B (1977) 125

93) J. Schoenes, J. Magn. Magn. Mat. 11 (1979) 102

94) It is possible to introduce a semiconductor-metal transition e.g. in SmS (at 6kbar) and $Tm_{0.68}Eu_{0.32}Se$ (17kbar) by polishing. V.P. Zhuze, A.V. Golubkov, E.V. Goucharova, T.I. Komarova and V.M. Sergeeva, Fiz. Tverd. Tela (Leningrad) 6 (1964) 268 (Sov. Phys. (solid state) 6 (1964) 213); and H. Boppart, private commun.

95) M.S.S. Brooks, J. Phys. F 14 (1984) 639

96) W.E. Pickett and B.M. Klein, J. Less Com. Met. 93 (1983) 219

97) J. Schoenes, in 'Proc. of the NATO Summer Institute on Moment Formation in Solids', W.J.L. Buyers, ed., Plenum Press, New York 1984

98) N. Beatham, P.A. Cox, A.F. Orchard and I.P. Grant, Cham. Phys. Lett. 63 (1979) 69

99) G.H. Lander and W.G. Stirling, Phys. Rev. B 21 (1980) 436

100) S.-K. Chan, J. Phys. Chem. Solids 32 (1971) 1111

101) P. Erdös and J.M. Robinson, 'The Physics of Actinide Compounds', Plenum Press, New York 1983, p.20 and 33

102) P. Wachter, Solid State Commun. 7 (1969) 693

103) J. Rossat-Mignod, P. Burlet, H. Bartholin, R. Tchapoutian, O. Vogt C. Vettier and R. Lagnier, Physica 102B (1980) 177

104) H. Bartholin, J.M. Effantin, P. Burlet, j. Rossat-Mignod and O. Vogt, Proc. Crystalline Electric Field Effects in f-Electron Magnetism, R.P. Guertin, W. Suski and Z. zolnierek, eds., Penum Press, New York 1982

105) C. Bazan and A. Zygmunt, phys. stat. sol. a12 (1972) 649

106) J. Brunner, M. Erbudak and F. Hulliger, Solid State Commun. 38 (1981) 841

107) J. Brunner, M. Erbudak and F. Hulliger, Proc. 11émes Journées des Actinides, Jesolo 1981, Italy

108) F. Hulliger, J. Less Common Metals 16 (1968) 113

109) J. Leciejewicz and A. Zygmunt, phys. stat. sol. a 13 (1972) 657

110) A. Blaise, R. Lagnier, A. Wojakowski, A. Zygmunt and M.J. Martimer, J. Low Temp. Physics 41 (1980) 61

111) A. Blaise, R. Troc, R. Lagnier and M.J. Martimer, J. Low Temp. Phys. 38 (1980) 79

112) Z. Henkie and W. Trzebiatowski, phys. stat. sol. 35 (1969) 827

113) P. Burlet, J. Rossat-Mignod, R. Troc and Z. Henkie, Solid State Commun. 39 (1981) 745

114) C.F. Buhrer, J. Phys. Chem. Solids 30 (1969) 1273

115) W. Trzebiatowski, Z. Henkie, K.P. Bielov, A.S. Dmitrievskii, R.Z. Levitin and Y.F. Popov, Zh. Exper. Teor. Fiz. 61 (1971) 1522

116) K.P. Bielov, Z. Henkie, D.S. Dimitrievsky, R.Z. Levitin and W. Trzebiatowski, Zh. Eksp. Teor. Fiz. 64 (1973) 1351

117) Z. Henkie, Physica 102B (1980) 329

118) K. Takegahara, A. Yanase and T. Kasuya, Proc. IV Intern. Conf. Crystal Field and Struct. Effects in f-Electron Systems, Warschau 1981

119) T. Suzuki, S. Takagi, N. Niitsuma, K. Takegahara, T. Kasuya, A. Yanase, T. Sakakibara, M. Date, P.J. Markowski and Z. Henkie, Proc. Intern. Symp. High Field Magnetism, M. Date, ed., North Holland, Amsterdam 1982

120) J. Schoenes, M. Küng, R. Hauert and Z. Henkie, Solid State Commun. 47 (1983) 23

121) Z. Henkie, Bull. Acad. Polan. Sci., Ser. Sci.-Chim. 20 (1972) 531

122) Z. Henkie, W.R. Johanson, A.J. Arko, G.W. Crabtree and C. Bazan, Phys. Rev. B28 (1983) 4198

123) Proc. of the 12th International Magnetics Conference, INTERMAG, Hamburg 1984; to be published in IEEE Trans-Mag, Sep. 1984

124) F.J. Kahn, P.S. Pershan and J.P. Remeika, Phys. Rev. 186 (1969) 891

125) H. Burkhard and J. Jaumann, Z. Physik 235 (1970) 1

126) G.S. Krinchik, in 'Optical Properties and Electronic Structure of Metals and Alloys', F. Abeles, ed., North Holland, Amsterdam 1966

127) X.X. Zhang, J. Schoenes, W. Reim and P. Wachter, J. Phys. C16 (1983) 6055

128) P.G. van Engen, thesis at the technical university of Delft, 1983; and K.H.J. Buschow, P.G. van Engen and J. Jongebreur, J. Magn. Magn. Mat. 38 (1983) 1

129) P.G. van Engen, K.H.J. Buschow, R. Jongebreur and M. Erman, Appl. Phys. Lett. 42 (1983) 202

130) R.K. Ahrenkiel and T.J. Coburn, Appl. Phys. Lett. 22 (1973) 340

131) W. Jung, J. Appl. Phys. 36 (1965) 2422

132) J.C. Suits and K. Lee, J. Appl. Phys. 42 (1971) 3258

133) K. Egaskira and T. Yamada, J. Appl. Phys. 45 (1974) 3643

134) S. Wittekoek, T.J.A. Popuma, J.M. Robertson and P.F. Bongers, Phys. Rev. B 12 (1975) 2777

PUBLICATIONS

1. W. Reim, J. Schoenes
   Evidenz für jj-Kopplung beim f-d Uebergang in UO_2
   Verhandl. DPG 16, 275 (1981)

2. W. Reim, J. Schoenes
   Magneto-Optical Study of the $5f^2 \rightarrow 5f^1 6d^1$ Transition in UO_2
   Solid State Commun. 39, 1101 (1981)

3. W. Reim, J. Schoenes
   Importance of Final State Coupling in the $5f \rightarrow 6d$ Excitation of UO_2
   "Actinides 81", p. 76 (1981)

4. W. Reim, J. Schoenes
   Magneto-Optische Untersuchungen an UO_2 Filmen
   Helv. Phys. Acta 54, 238 (1981)

5. X. Zhang, W. Reim, J. Schoenes, P. Wachter
   Characteristics of Magneto-Optical Spectra and 3d-Localized States in Pure and Substituted Magnetite
   Helv. Phys. Acta 54, 378 (1981)

6. W. Reim, J. Schoenes
   Messungen des Magneto-Optischen Kerr-Effekts an US
   Verhandl. DPG (VI), 17, 828 (1982)

7. W. Reim, J. Schoenes, O. Vogt
   Magneto-Optischer Kerr-Effekt an UAs und US Einkristallen
   Helv. Phys. Acta 55, 144 (1982)

8. W. Reim, J. Schoenes, O. Vogt
   Magneto-Optik und elektronische Struktur der Uranchalkogenide
   Helv. Phys. Acta 55, 543 (1982)

9. W. Reim, J. Schoenes, O. Vogt
   Magneto-Optical Response of f- and d-States in Uraniummonosulfide
   Solid State Commun. 47, 567 (1983)

10. X.X. Zhang, J. Schoenes, W. Reim, P. Wachter
    Evidence for $3d^n \rightarrow 3d^{n-1} 4s$ Transitions in Magnetite and in Lithium and Magnesium Ferrites
    J. Phys. C: Solid State Phys. 16, 6055 (1983)

11. O.E. Hüsser, E. Kaldis, W. Reim, J. Schoenes und P. Wachter
    Austauschinduzierte Plasmakantenaufspaltung der Tm-Chalcogenide
    Helv. Phys. Acta 56, 613 (1983)

12. W. Reim, J. Schoenes
    Neue Kerr-Rotatoren mit der grössten "figure of merit"
    Helv. Phys. Acta 56, 616 (1983)

13. W. Reim, J. Schoenes, O. Vogt
    Magnetische Rotverschiebung des f-d Uebergangs in
    $USb_{0.9}Te_{0.1}$
    Helv. Phys. Acta $\underline{57}$ (1984) 227

14. W. Reim, O.E. Hüsser, J. Schoenes, E. Kaldis, P. Wachter,
    K. Seiler
    First Magneto-Optical Observation of an Exchange Induced
    Plasma Edge Splitting
    J. Appl. Phys. $\underline{55}$, 2155 (1984)

15. W. Reim, J. Schoenes, O. Vogt
    Magneto-Optics and Electronic Structure of Uranium Mono-
    chalcogenides
    J. Appl. Phys. $\underline{55}$, 1853 (1984)

16. W. Reim, J. Schoenes, O. Vogt
    Magneto-Optical Investigation of the Electronic and Magnet-
    ic Structure of UAs_xSe_{1-x}
    Phys. Rev. $\underline{B29}$, 3252 (1984)

17. W. Reim, J. Schoenes and O. Vogt
    Magnetic Exchange and Spin-Polarization in Uranium-Mono-
    pnictides
    Proc. 14èmes Journées des Actinides, Davos, Switzerland,
    1984, p.34

18. W. Reim, J. Schoenes and P. Wachter
    New High-Efficiency Kerr-Rotators
    IEEE Transactions on Magnetics $\underline{20}$, 1045 (1984)

19. W. Reim, J. Schoenes and O. Vogt
    Der f→d Uebergang in USb_xTe_{1-x}
    Helv. Phys. Acta $\underline{57}$, 492 (1984)

20. J. Schoenes, O.E. Hüsser, W. Reim, E. Kaldis and P. Wachter
    Magneto-Optics of Semiconducting, Intermediate Valent and
    Metallic Tm-Chalcogenides
    Proc. of the 4th Intern. Conf. on Valence Fluctuations,
    Köln, 1984 in: J. Magn. Magn. Mat. 47&48, ... (1985)

21. W. Reim, J. Schoenes and F. Hulliger
    Optics and Magneto-Optics of UAsSe
    submitted to Physica B, 1985

ORAL PRESENTATIONS

1. Evidenz für jj-Kopplung beim $f \to d$ Uebergang in UO_2
   Spring meeting of the German Physical Society, Münster,
   West Germany
   10.3.1981

2. Characteristics of Magneto-Optical Spectra and 3d-Localized
   States in Pure and Substituted Magnetite
   Fall meeting of the Swiss Physical Society, Davos, Switzer-
   land
   24.9.1981

3. Magneto-Optische Untersuchungen der elektronischen Struktur
   von reinem und substituiertem Magnetit
   Tagung über "Optische Eigenschaften magnetisch geordneter
   Materialien", Bad Honnef, Germany
   21.10.1981

4. Messungen des magneto-optischen Kerr-Effekts an US
   Spring meeting of the German Physical Society, Münster,
   West Germany
   1.4.1982

5. Kerr-effect and Dielectric Tensor Elements of Magnetite and
   other Transition Metal Compounds: Evidence of Final State
   Coupling
   EUCHEM Conference on Magnetic Circular Dichroism and Rela-
   ted Magneto-Optical Techniques, Leuven, Belgium
   29.9.1982

6. Magneto-Optik und elektronische Struktur der Uranmonochal-
   kogenide
   Fall meeting of the Swiss Physical Society, Basel, Switzer-
   land
   7.10.1982

7. Neue Kerr-Rotatoren mit der grössten 'figure of merit'
   Spring meeting of the Swiss Physical Society, Fribourg,
   Switzerland
   24.3.1983

8. Magneto-Optical Investigation of Uranium-Monopnictides
   3rd General Conference of the Condensed Matter Division of
   the EPS, Lausanne, Switzerland
   29.3.1983

9. Magnetische Rotverschiebung des $f \to d$ Uebergangs in
   $USb_{0.9}Te_{0.1}$
   Fall meeting of the Swiss Physical Society, Delémont, Swit-
   zerland
   14.10.1983

10. Magneto-optics of 4f and 5f materials: Basic research and potential applications
    Seminar at IBM Yorktown Heights, New York, USA
    4.11.1983

11. Magneto-Optics and Electronic Structure of Uranium-monochalcogenides
    29th Conference on Magnetism and Magnetic Materials, Pitts-bourgh, Pennsylvania, USA
    9.11.1983

12. First Magneto-Optical Observation of an Exchange Induced Plasma Edge Splitting
    29th Conference on Magnetism and Magnetic Materials, Pitts-bourgh, Pennsylvania, USA
    9.11.1983

13. Magnetic Exchange and Spin-Polarization in Uranium-Mono-pnictides
    14èmes Journées des Actinides, Davos, Switzerland
    2.4.1984

14. New High-Efficiency Kerr-Rotators
    22nd International Magnetics Conference (INTERMAG),
    Hamburg, West Germany
    13.4.1984

15. Optics and Magneto-Optics of UAsSe
    International Conference on Rare Earth and Actinide
    Intermetallics (REACIM),
    St. Pölten, Austria
    5.9.1984

16. Magneto-Optical Response of d and f Systems: Basic Research and Potential Applications
    Seminar at IBM Rüschlikon, Rüschlikon, Switzerland
    19.9.1984

17. Der polare Kerr-Effekt von Uranverbindungen
    Seminar at Laboratorium für Festkörperphysik, ETH Zürich,
    Switzerland
    29.11.1984

DANK

CURRICULUM VITAE

1956, Nov. 12th : Born at Lohne, West Germany.

April 1963 –   : Primary school and gymnasium at Lohne and Vechta,
     Mai 1975   West Germany.

October 1975 – : Study of mathematics and physics at ETH Zürich,
   October 1980   Switzerland. Special emphasis on curses in atomic
     and solid state physics and group theory.
     Diploma work with PD Dr. J. Schoenes (group of
     Prof. Dr. P. Wachter) on magneto-optical properties
     of UO_2 thin films.

November 1980 – : Thesis supervised by PD Dr. J. Schoenes within the
   September 1984   group of Prof. Dr. P. Wachter.

Scientific work:

- Investigation of 3d, 4f and 5f materials like ferrites,
  Thulium-chalcogenides and Uranium-pnictides.
- Magneto-optics at low temperatures (2K) and high
  magnetic fields (10T).
- Different methods of optical measurements.
- UHV technique.
- Thin film preparation by different methods.
- Atomic models including crystal-field, spin-orbit and
  final state coupling effects for different systems
  like Fe_3O_4, $TmSe_{0.65}Te_{0.35}$ and UO_2.
- Calculation of transition matrix elements.

Teaching

Partizipation in the theoretical and practical
education of students at ETH Zürich.